Volume 70A
Number 3
May–June 1966

Physics and Chemistry

U.S. DEPARTMENT OF COMMERCE

SECTION A

JOURNAL OF RESEARCH

NATIONAL BUREAU OF STANDARDS

Journal of Research

of the

National Bureau of Standards

A. Physics and Chemistry

May–June • 1966

VOLUME • 70A

NUMBER • 3

Editor: C. W. Beckett

Associate Editors: D. D. Wagman
J. M. Richardson

Publication dates:
Feb. 1, Apr. 1, June 1, Aug. 1, Oct. 1, Dec. 1, 1966

JOURNAL OF RESEARCH

The National Bureau of Standards Journal of Research reports research and development in the fields of activity shown at right. Also included from time to time are survey articles on topics closely related to the Bureau's scientific and technical program.

The Journal is published in three separate sections as follows:

A. Physics and Chemistry

Contains papers of interest primarily to scientists working in these fields. Issued six times a year. Annual subscription: domestic, $5.00; foreign, $6.00. Single copy, $1.00.

B. Mathematics and Mathematical Physics

Presents studies and compilations designed mainly for the mathematician and the theoretical physicist. Issued quarterly. Annual subscription: domestic, $2.25; foreign, $2.75. Single copy, 75c.

C. Engineering and Instrumentation

Reports research and development results of interest chiefly to the engineer and the applied scientist. Issued quarterly. Annual subscription: domestic, $2.75; foreign, $3.50. Single copy, 75c.

The National Bureau of Standards is a principal focal point in the Federal Government for assuring maximum application of the physical and engineering sciences to the advancement of technology in industry and commerce. Its responsibilities include development and maintenance of the national standards of measurement, and the provision of means for making measurements consistent with those standards; determination of physical constants and properties of materials; development of methods for testing materials, mechanisms, and structures, and making such tests as may be necessary, particularly for government agencies; cooperation in the establishment of standard practices for incorporation in codes and specifications; advisory service to government agencies on scientific and technical problems; invention and development of devices to serve special needs of the Government; assistance to industry, business and consumers in the development and acceptance of commercial standards and simplified trade practice recommendations; administration of programs in cooperation with United States business groups and standards organizations for the development of international standards of practice; and maintenance of a clearinghouse for the collection and dissemination of scientific, technical and engineering information. The scope of the Bureau's activities is suggested in the following listing of its three Institutes and their organizational units.

Institute for Basic Standards. Applied Mathematics. Electricity. Metrology. Mechanics. Heat. Atomic Physics. Physical Chemistry. Laboratory Astrophysics.* Radiation Physics. Radio Standards Laboratory.* Radio Standards Physics & Radio Standards Engineering. Office of Standard Reference Data.

Institute for Materials Research. Analytical Chemistry. Polymers. Metallurgy. Inorganic Materials. Reactor Radiations. Cryogenics.* Materials Evaluation Laboratory. Office of Standard Reference Materials.

Institute for Applied Technology. Building Research. Information Technology. Performance Test Development. Electronic Instrumentation. Textile and Apparel Technology Center. Technical Analysis. Office of Weights and Measures. Office of Engineering Standards. Office of Invention and Innovation. Office of Technical Resources. Clearinghouse for Federal Scientific and Technical Information.**

*Located at Boulder, Colo., 80301.
**Located at 5285 Port Royal Road, Springfield, Va., 22151.

U.S. DEPARTMENT OF COMMERCE
John T. Connor, Secretary

NATIONAL BUREAU OF STANDARDS
A. V. Astin, Director

Order all publications from the Superintendent of Documents
U.S. Government Printing Office, Washington, D.C., 20402

Use of funds for printing this publication approved by the Director of the Bureau of the Budget (June 19, 1961).

JOURNAL OF RESEARCH of the National Bureau of Standards — A. Physics and Chemistry
Vol. 70A, No. 3, May–June 1966

Thermal Relaxation and Brillouin Scattering in Liquids

Raymond D. Mountain

Institute for Basic Standards, National Bureau of Standards, Washington, D.C.

(February 21, 1966)

Weak coupling of internal degrees of freedom of molecules to the translational degrees of freedom of a fluid results in additional modes of motion for density fluctuations. These new modes affect the spectral distribution of light scattered by density fluctuations so that the Landau-Placzek ratio is not satisfied. The case of thermal relaxation with a single relaxation time is worked out in detail. Formulas for the spectral distribution of the scattered light, for the ratio of the intensities of the central (Rayleigh) to the Brillouin components and for the phonon velocity are derived and applied to carbon disulfide and carbon tetrachloride. The data for carbon tetrachloride are shown to be inconsistent with the single relaxation time model for thermal relaxation.

Key Words: Brillouin scattering, density fluctuations in liquids, light scattering in liquids, Rayleigh scattering, spectral distribution of scattered light, thermal relaxation, volume viscosity.

1. Introduction

In this paper we are concerned with density fluctuations in a fluid in which internal degrees of freedom of the molecules are weakly coupled to the translational degrees of freedom of the fluid. Thermal relaxation is an example of the type of processes we have in mind. Problems of this type are of interest because it is now possible to experimentally probe the frequency spectrum of density fluctuations with light scattering experiments using a laser as the light source [1].[1] The coupling of internal degrees of freedom to the translational motion means that the decay of density fluctuations will proceed by more ways than the three "normal modes" usually considered. This is reflected in the spectral distribution of light scattered by density fluctuations. In this paper we investigate a relatively simple case involving thermal relaxation with a single relaxation time. The existence of the additional mode is shown and the effect of this mode on the spectrum of the scattered light is examined in detail.

Light scattering experiments provide a Fourier analysis of the density variations in a fluid. The variation of the intensity of the scattered light with the scattering angle θ (and therefore with the *change* in the wave vector of the scattered light) Fourier decompose the spatial dependence of the fluctuations while the *shifts* in the frequency of the scattered light decompose the time dependence of the fluctuations [2]. Such experiments enable us to study collective motions in the fluid without seriously disturbing the fluid. On the other hand, it is also possible to use light scattering measurements in conjunction with a model for the fluctuations to measure several of the bulk properties of the fluid. For example, the sound velocity and the sound absorption coefficient can be obtained by measuring the shift in frequency and the width of the Brillouin lines.

In some circumstances it is possible to obtain from light scattering experiments information about the structure of the correlation functions whose time integrals are the transport coefficients [3]. An example of this type provides the basis for the calculations we present.

This paper consists of three parts. In the first part we review the relationship between density fluctuations and light scattering. The phenomenological approach of Einstein and Smoluchow-

[1] Figures in brackets indicate the literature references at the end of this paper.

ski [4] is discussed and compared with the formulation of scattering problems of Van Hove [5]. The generalized structure factor $\mathcal{S}(k, \omega)$ is introduced and some of its properties are described.

The second part of the paper consists of a detailed analysis of the frequency spectrum of density fluctuations in a fluid in which thermal relaxation of vibrational degrees of freedom can occur. Particular emphasis is placed on single relaxation time processes. The results for single relaxation time processes are summarized at the end so that readers not wishing to go through the details of the calculation will not lose heart.

The third part of the paper consists of a comparison of available experimental data with the analysis of the density fluctuations. The primary example is concerned with CS_2, a substance whose internal degrees of freedom relax with a single relaxation time. We also demonstrate that the data for CCl_4 are not in agreement with the predictions for a single relaxation time.

2. Light Scattering Formalism

2.1. Phenomenological Theory of Einstein-Smoluchowski

The random thermal motion of molecules in a fluid produces fluctuations in the density and also in the orientation of molecules in volumes small compared to the wavelength of the incident light. These fluctuations result in local variations in the dielectric constant and therefore scatter light. We are concerned in this paper only with fluctuations in the density. Orientation fluctuations result in the depolarization of the scattered light making it possible to experimentally separate the scattering by density fluctuations, which is fully polarized, from the scattering by orientation fluctuations [6].

The intensity of the scattered light is

$$I(\mathbf{R}, \omega) = I_0 \left[\frac{N k_i^4}{16\pi^2 R^2}\right] \sin^2 \varphi \langle [\epsilon(k, \omega)]^2 \rangle. \tag{1}$$

In eq (1) incident plane polarized light of intensity I_0 and wave vector $\mathbf{k}_i$ is scattered at the origin and is observed at $\mathbf{R}$. There are N molecules in the scattering volume. The angle between the electric vector of the incident wave and $\mathbf{R}$ is φ; $\epsilon(k, \omega)$ is the Fourier component of the fluctuation in the dielectric constant. The *shift* in the angular frequency of the scattered light is ω and the *change* in the wave vector in the medium of the scattered light is $\mathbf{k}$; since only the direction of $\mathbf{k}$ changes

$$k = 2nk_i \sin \theta/2. \tag{2}$$

The index of refraction of the scattering fluid is n and the scattering angle is θ. The angular brackets $\langle \ldots \rangle$ indicate an ensemble average over the initial states of the system.

Direct calculation of $\epsilon(k, \omega)$ is avoided by assuming that fluctuations in the dielectric constant are due to fluctuations in the density and the temperature;

$$\Delta\epsilon = (\partial\epsilon/\partial\rho)_T \Delta\rho + (\partial\epsilon/\partial T)_\rho \Delta T. \tag{3}$$

The contribution of the temperature fluctuations is ignored; we assume that $(\partial\epsilon/\partial\rho)_T \gg (\partial\epsilon/\partial T)\rho$. Equation (1) is now reduced to

$$I(\mathbf{R}, \omega) = I_0 \left[\frac{N k_i^4}{16\pi^2 R^2}\right] \sin^2 \varphi (\partial\epsilon/\partial\rho)_T^2 \langle [\rho(k, \omega)]^2 \rangle \tag{4}$$

where $\rho(k, \omega)$ is a Fourier component of the density fluctuation. The problem is now one of

calculating $\rho(k, \omega)$ from the appropriate kinetic model of the fluid. For dense fluids the appropriate model is described by the linearized hydrodynamic equations of irreversible thermodynamics.

We should note that $(\partial\epsilon/\partial\rho)_T$ has been assumed to be independent of the *shift* in the frequency of the scattered light, ω. If this is not the case it is probably also true that the separation of $\Delta\epsilon$ into a thermodynamic derivative times a fluctuation term is not a meaningful procedure. Of course the value of $(\partial\epsilon/\partial\rho)_T$ may vary somewhat as the frequency of the incident light changes, reflecting the frequency dependence of the dielectric constant.

2.2. Molecular Theory

Before we undertake the calculation of $\rho(k, \omega)$ we review the light scattering formalism obtained by adapting Van Hove's neutron scattering paper [5] to light scattering. Komarov and Fisher [7] have shown that the intensity of light scattered from a fluid of N molecules of effective polarizability α is

$$I(\mathbf{R}, \omega) = I_0 \left[\frac{N\alpha^2 k_i^4}{2\pi R^2}\right] \sin^2 \varphi \, \mathcal{S}(k, \omega). \tag{5}$$

The important change from eq (4) is to replace the mean square fluctuation $\langle [\rho(k, \omega)]^2 \rangle$ by the generalized structure factor $\mathcal{S}(k, \omega)$ which is the space and time Fourier transform of the two-body correlation function. The correlation function is defined by Van Hove to be

$$G(\mathbf{r}, t) = N^{-1} \left\langle \sum_{l, j=1}^{N} \int d\mathbf{r}' \delta[\mathbf{r} + \mathbf{r}_l(0) - \mathbf{r}'] \delta[\mathbf{r}' - \mathbf{r}_j(t)] \right\rangle. \tag{6}$$

For long times and sufficiently large r, $G(\mathbf{r}, t)$ reduces to the autocorrelated density

$$G(r, t) = N^{-1} \int d\mathbf{r}' \langle \rho[\mathbf{r}' - \mathbf{r}(0), 0] \rho(\mathbf{r}', t) \rangle. \tag{7}$$

Equation (7) is appropriate to light scattering in fluids [8]. Care must be taken to use

$$\mathcal{S}(k, \omega) = \int d\mathbf{r} \int dt e^{i\mathbf{k}\cdot\mathbf{r}} e^{-i\omega t} G(r, t) \tag{8}$$

only to describe the fully polarized part of the scattered light. The inclusion of angular correlations, which result in depolarization, is a more complicated problem than the one we consider here [9].

In this paper we are concerned with $\mathcal{S}(k, \omega)$ as defined by eqs (7) and (8);

$$\mathcal{S}(k, \omega) = \langle \rho(k, \omega) \rho(-k) \rangle. \tag{9}$$

Thus eqs (4) and (5) predict the same frequency distribution for light scattered by density fluctuations. A useful property of $\mathcal{S}(k, \omega)$ is the sum rule

$$S(k) = \frac{1}{2\pi} \int_{-\infty}^{\infty} d\omega \, \mathcal{S}(k, \omega) = \langle \rho(k) \rho(-k) \rangle. \tag{10}$$

$S(k)$ is the ordinary structure factor. Finally, we note that $\mathcal{S}(k, \omega)$ is an even function of ω at high temperatures; that is $\hbar\omega/k_B T \ll 1$ where k_B is Boltzman's constant and T is the absolute temperature. In this paper we assume that the inequality is satisfied.

3. Density Fluctuations When the Internal Modes Decay With a Single Relaxation Time

We are concerned with the calculation of $\mathcal{S}(k, \omega)$ for a fluid whose molecules possess internal degrees of freedom which are weakly coupled to the translational modes of the fluid. Further we shall suppose that the transfer of energy from the internal degrees to the translational degrees of freedom is described by a single relaxation time process [10, 11].

The procedure to be used is to solve the linearized hydrodynamic equations for $\rho(k, \omega)$ in terms of an initial fluctuation $\rho(k)$ [5]. The use of initial values facilitates calculation of the average over initial states indicated by $\langle \ldots \rangle$.

An equivalent procedure is the hydrodynamic fluctuation theory of Landau and Lifshitz [12]. This method has been used by Rytov to discuss fluctuations in a viscoelastic medium [13].

The linearized hydrodynamic equations for the system are the continuity equation

$$\partial \rho_1/\partial t + \rho_0 \operatorname{div} \mathbf{v} = 0, \tag{11}$$

the longitudinal part of the Navier-Stokes equation (suitably modified to allow for a frequency dependent bulk viscosity)

$$\rho_0 \frac{\partial \mathbf{v}}{\partial t} = -\left(\frac{c_0^2}{\gamma}\right) \operatorname{grad} \rho_1 - \left(\frac{c_0^2 \beta \rho_0}{\gamma}\right) \operatorname{grad} T_1 + \left(\frac{4}{3}\eta_s + \eta_v\right) \operatorname{grad} \operatorname{div} \mathbf{v} + \int_0^t \eta'(t-t') \operatorname{grad} \operatorname{div} \mathbf{v}(t')dt', \tag{12}$$

and the energy transport equation.

$$\rho_0 c_v (\partial T_1/\partial t) - [c_v(\gamma - 1)/\beta](\partial \rho_1/\partial t) - \lambda \nabla^2 T_1 = 0. \tag{13}$$

Here $\rho = \rho_0 + \rho_1$ is the number density, $T = T_0 + T_1$ is the temperature; ρ_0 and T_0 being the equilibrium values. The shear viscosity is η_s, the bulk or volume viscosity consists of a frequency independent part η_v and frequency dependent part which is the Fourier transform of $\eta'(t)$. The low frequency (adiabatic) sound speed is c_0, the thermal expansion coefficient is β, the thermal conductivity is λ and the ratio of the specific heat at constant pressure c_p to the specific heat at constant volume c_v is denoted by γ.

The analysis proceeds as in reference 8. First the Fourier (space) and Laplace (time) transforms are taken of eqs (11), (12), and (13). Then we solve for

$$\rho(k, s) = \int_v d\mathbf{r} e^{-i\mathbf{k}\cdot\mathbf{r}} \int_0^\infty dt e^{-st} \rho_1(r, t) \tag{14}$$

in terms of the initial value

$$\rho(k) = \int_v d\mathbf{r} e^{-i\mathbf{k}\cdot\mathbf{r}} \rho(r, 0) \tag{15}$$

The result is

$$\frac{\rho(k, s)}{\rho(k)} = \frac{F(s)}{G(s)} \tag{16}$$

where

$$F(s)=s^2+s[ak^2+b_0k^2+b'(s)k^2]+ab_0k^4+ab'(s)k^4+c_0^2k^2(1-1/\gamma) \tag{17}$$

and

$$G(s)=s^3+s^2[ak^2+b_0k^2+b'(s)k^2]+s[c_0^2k^2+ab_0k^4+ab'(s)k^4]+c_0^2ak^4/\gamma. \tag{18}$$

The quantities

$$\begin{aligned} a&=\lambda/\rho_0c_v \\ b&=(4/3\eta_s+\eta_n)/\rho_0 \\ b'(s)&=\frac{1}{\rho_0}\int_0^\infty e^{-st}\eta'(t)dt \end{aligned} \tag{19}$$

have been introduced to simplify the notation. Equation 19 for $b'(s)$ applies to any frequency dependent bulk viscosity. We will be concerned with $b'(s)$ for a single relaxation time process;

$$b'(s)=b_1/(1+s\tau) \tag{20}$$

where τ is the relaxation time.

The dispersion equation is

$$G(s)=0 \tag{21}$$

and is used in ultrasonics with s replaced by $i\omega$. It is known from ultrasonics [10] that

$$b_1=(c_\infty^2-c_0^2)\tau \tag{22}$$

where c_∞ is the infinite frequency sound speed. In thermal relaxation [11]

$$b_1=\left[\frac{(c_p-c_v)c_I}{(c_v-c_I)c_p}\right]c_0^2\tau,$$

where c_I is the specific heat of the vibrational degrees of freedom.

To compute $\mathcal{S}(k,\omega)$ we first observe that

$$\rho(k,\omega)=2\ \mathrm{Re}\int_0^\infty dte^{-i\omega t}\rho(k,t) \tag{23}$$

where $\rho(k,t)$ is the inverse Laplace transform of $\rho(k,s)$. It follows that

$$\begin{aligned} \mathcal{S}(k,\omega)&=\langle\rho(k)\rho(-k)\rangle\ \{2\ \mathrm{Re}\ F(i\omega)/G(i\omega)\} \\ &=\langle\rho(k)\rho(-k)\rangle\sigma(k,\omega). \end{aligned} \tag{24}$$

An exact expression for $\sigma(k,\omega)$ may be readily obtained by replacing s by $i\omega$ in eq (16) and taking twice the real part. The resulting expression is quite involved; direct substitution leads to

$$\sigma(k,\omega)=2[N_1D_1+N_2D_2]/[D_1^2+D_2^2] \tag{25}$$

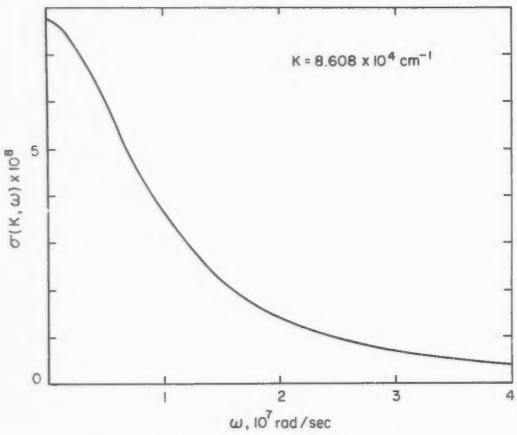

FIGURE 1. *The central component of* $\sigma(k, \omega)$ *for scattering in* CS_2 *at 20 °C as a function of* ω.
When a He-Ne laser is the source, $k = 8.608 \times 10^4$ cm^{-1} corresponds to scattering at 30°

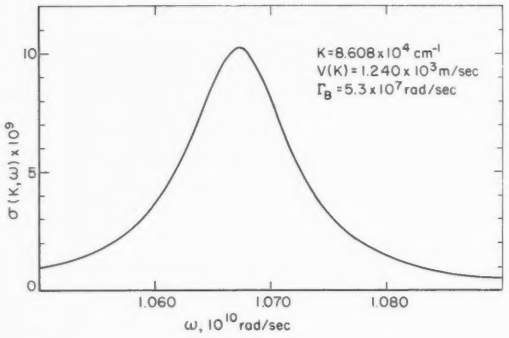

FIGURE 2. *The phonon component of* $\sigma(k, \omega)$ *for scattering in* CS_2 *at 20 °C as a function of* ω.
When a He-Ne laser is the source $k = 8.608 \times 10^4$ cm^{-1} corresponds to scattering at 30°

where

$$N_1 = -\omega^2 + ab_0k^4 + c_0^2k^2(1 - 1/\gamma) + (ab_1k^4 + b_1k^2\omega^2\tau)/(1 + \omega^2\tau^2),$$

$$N_2 = \omega[ak^2 + b_0k^2 + (b_1k^2 - ab_1k^4\tau)/(1 + \omega^2\tau^2)],$$

$$D_1 = -\omega^2(ak^2 + b_0k^2) + c_0^2ak^4/\gamma + (ab_1k^4\omega^2\tau - \omega^2b_1k^2)/(1 + \omega^2\tau^2) \tag{26}$$

and

$$D_2 = \omega[-\omega^2 + c_0^2k^2 + ab_0k^4 + (b_1k^2\omega^2\tau + ab_1k^4)/(1 + \omega^2\tau^2)]. \tag{27}$$

Now we have an exact expression for the frequency distribution of the scattered light. If we wish to be able to interpret this in terms of the properties of the material, we must develop a way to pick out the significant portions of $\sigma(k, \omega)$ for different values of ω. We have evaluated $\sigma(k, \omega)$ for a representative set of material parameters and $k = 8.608 \times 10^4$; the results are shown in figure 1 and figure 2. This corresponds to $\theta = 30°$ for scattering in CS_2 using a He-Ne laser. To obtain as much useful information as possible from such a pattern it is necessary to write eq (25) as a sum of terms which are individually important only over a restricted range of frequencies ω. The denominator does not obviously factor so an indirect approach is needed. One method is to pick out the important terms, say for small ω and to discard the rest. Another approach, one used profitably in reference 8, is to approximately compute the inverse Laplace transform of $\rho(k, s)$ and then to compute $\rho(k, \omega)$ by means of eq (23). The virtue of this method is that algebraic expressions for the modes of motion of the density fluctuations are obtained. The difficulty of course is to obtain good approximate solutions to the dispersion equation, eq (21). We shall make use of both approaches to investigate the properties of $\sigma(k, \omega)$.

4. Properties of $\sigma(k, \omega)$

In this section we are concerned with the construction of a good approximation to $\sigma(k, \omega)$ which will permit interpretation of spectral distribution curves in terms of the properties of the

scattering fluid. The results of this section are contained in eqs (43), (45), and (46), and are listed, for convenience, in subsection 4.6.

4.1. Approximate Solution of the Dispersion Equation

When $b'(s)$ is given by eq (20), the transform for the density, eq (16), is

$$\frac{\rho(k, s)}{\rho(k)} = \frac{F_1(s)}{G_1(s)}$$

where

$$F_1(s) = (1 + s\tau)s^2 + s[(1 + s\tau)(ak^2 + b_0k^2) + b_1k^2] + (1 + s\tau)[ab_0k^4 + c_0^2k^2(1 - 1/\gamma)] + ab_1k^4 \tag{28}$$

and

$$G_1(s) = \tau s^4 + s^3[1 + \tau(ak^2 + bk^2)] + s^2[ak^2 + b_0k^2 + b_1k^2 + \tau(c_0^2k^2 + ab_0k^4)]$$
$$+ s[c_0^2k^2 + ab_0k^4 + ab_1k^4 + \tau(c_0^2ak^4/\gamma)] + c_0^2ak^4/\gamma. \tag{29}$$

The first step in computing $\rho(k, t)$ is to obtain approximate roots of

$$G_1(s) = 0. \tag{30}$$

It is convenient to introduce the dimensionless quantities

$$\begin{aligned} Y &= s/c_0k \\ \alpha &= ak^2/c_0k \\ \beta_0 &= b_0k^2/c_0k \\ \beta_1 &= b_1k^2/c_0k \\ D &= c_0k\tau \end{aligned} \tag{31}$$

into eq (30) with the result

$$DY^4 + Y^3[1 + D(\alpha + \beta_0)] + Y^2[\alpha + \beta_0 + \beta_1 + D(1 + \alpha\beta_0)] + Y[1 + \alpha\beta_0 + \alpha\beta_1 + D\alpha/\gamma] + \alpha/\gamma = 0. \tag{32}$$

For interesting values of the change in the wave vector, k,

$$D \approx 1, \qquad \beta_1 \approx 1$$

while

$$\alpha \ll 1, \qquad \beta_0 \ll 1.$$

First we look for solutions of eq (31) which are of order unity. The relevant parts of eq (31) are

$$DY^4+Y^3+(D+\beta_1)Y^2+Y\simeq 0; \tag{33}$$

we have neglected terms of order α and α^2. One root of eq (33) is zero so we also must examine eq (32) for solutions of order α. The dominant terms are then

$$Y+\alpha/\gamma\simeq 0. \tag{34}$$

Here terms of order α^2 and smaller have been dropped. The solution to eq (34) is

$$Y=-\alpha/\gamma \tag{35}$$

or

$$s=-\lambda k^2/\rho_0 c_p$$

which also appears in classical theory.

When the $Y=0$ term is removed from eq (33) we have

$$Y^3+Y^2/D+\left[\frac{D+\beta_1}{D}\right]Y+\frac{1}{D}=0. \tag{36}$$

The formal factoring of eq (36) is

$$(Y+A)(Y^2+BY+C)=0. \tag{37}$$

Two solutions are

$$Y=-B/2\pm iC^{1/2}[1-B^2/4C]^{1/2} \tag{38}$$

which correspond to the phonon modes. The third solution,

$$Y=-A$$

yields a second nonpropagating mode. In order that damping occur, it is necessary that $A>0$ be satisfied. For phonons to exist it is necessary that $B^2/4C\ll 1$ so

$$Y\simeq -B/2\pm iC^{1/2}. \tag{38'}$$

Comparison of eqs (36) and (37) shows that

$$AC=1/D$$

therefore

$$Y=-1/CD. \tag{39'}$$

Now multiply eqs (38') and (39') by c_0k to obtain

$$s=\Gamma_B\pm ivk;\ vk=c_0kC^{1/2} \tag{40}$$

and

$$s = -c_0^2/v^2\tau.$$

The lifetime of the phonons is $(\Gamma_B)^{-1}$ and their speed is v. These are as yet unspecified quantities to be extracted from the exact expression of $\sigma(k, \omega)$. Before we do this we shall obtain an approximate formula for $\sigma(k, \omega)$.

4.2. Calculation of $\sigma(k, \omega)$

We take $G_1(s)$ to be

$$G_1(s) = \tau(s + ak^2/\gamma)(s + \Gamma_B - ivk)(s + \Gamma_B + ivk)(s + c_0^2/v^2\tau). \tag{41}$$

Combining eqs (28) and (41) it is a straight forward process to obtain the inverse Laplace transform of $\rho(k, s)$. Ignoring small terms, we obtain

$$\frac{\rho(k, t)}{\rho(k)} = (1 - 1/\gamma)e^{-\lambda k^2 t/\rho_0 c_p} + \left[\frac{(c_\infty^2 - c_0^2)k^2 - (v^2/c_0^2 - 1)(c_0^4/v^4\tau^2 + c_0^2k^2(1 - 1/\gamma))}{c_0^4/v^4\tau^2 + v^2k^2}\right] e - c_0^2 t/v^2\tau$$

$$+ \left[\frac{[1 - c_0^2/v^2(1 - 1/\gamma)](v^2k^2 + c_0^2/v^2\tau^2) - (c_\infty^2 - c_0^2)k^2}{v^2k^2 + c_0^4/v^4\tau^2}\right] \times e^{-\Gamma_B t}\cos(vkt). \tag{42}$$

Next we apply the operation indicated in eqs (23) and (24) to obtain

$$\sigma'(k, \omega) \simeq (1 - 1/\gamma)\left[\frac{2\lambda k^2/\rho_0 c_p}{(\lambda k^2/\rho_0 c_p)^2 + \omega^2}\right]$$

$$+ \left[\frac{(c_\infty^2 - c_0^2)k^2 - (v^2/c_0^2 - 1)(c_0^4/v^4\tau^2 + c_0^2k^2(1 - 1/\gamma))}{c_0^4/v^4\tau^2 + v^2k^2}\right]\left[\frac{2c_0^2/v^2\tau}{c_0^4/v^4\tau^2 + \omega^2}\right]$$

$$+ \left[\frac{[1 - c_0^2/v^2(1 - 1/\gamma)][v^2k^2 + c_0^2/v^2\tau^2] - (c_\infty^2 - c_0^2)k^2}{c_0^4/v^4\tau^2 + v^2k^2}\right]$$

$$\times \left[\frac{\Gamma_B}{\Gamma_B^2 + (\omega - vk)^2} + \frac{\Gamma_B}{\Gamma_B^2 + (\omega + vk)^2}\right]. \tag{43}$$

The prime means that σ' is an approximation to $\sigma(k, \omega)$, which is given by eq (25).

The first term in eq (43) corresponds to decay of a fluctuation by a thermal diffusion process. We refer to it as the thermal mode. The second term also represents a nonpropagating type of decay which is coupled to the internal degrees of freedom of the molecules. The last term represents the phonon modes. Equation (43) is derived on the assumption that $(ak^2/\gamma)\tau$ is much less than one. If this is not the case, eq (43) is a poor representation of the nonpropagating modes.

4.3. Determination of $v(k)$ and Γ_B

Thus far the phonon speed v and width Γ_B are undetermined quantities. In this subsection we remedy this by comparing the phonon terms of eq (43) with the significant parts of $\sigma(k, \omega)$, eq (25), when $\omega \sim vk$.

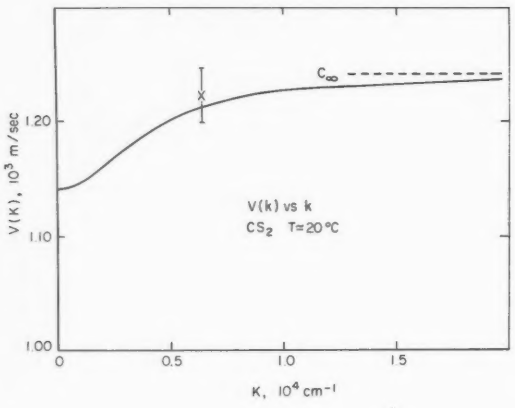

FIGURE 3. *The phonon velocity* v(k) *as a function of the wave vector* k *for* CS_2 *at 20°C.*
The experimental point (x) is taken from reference 18. Equation (45) and parameters from table 1 were used to construct this curve.

The direct evaluation of $\sigma(k, \omega)$ shows that the phonon peak coincides with the vanishing of the imaginary part of the dispersion relation,

$$D_2(\omega) = 0. \tag{44}$$

The positive root of eq (44) determines the phonon frequency $v(k)k$. Neglecting the term involving the thermal diffusivity, a, eq (44) is

$$-\omega^2 + c_0^2 k^2 + b_1 k^2 \omega^2 \tau/(1+\omega^2\tau^2) = 0.$$

The solution is

$$(\omega\tau)^2 = (v(k)k\tau)^2 = 1/2[(c_\infty k\tau)^2 - 1] + 1/2[(1 - c_\infty^2 k^2\tau^2)^2 + 4c_0^2 k^2\tau^2]^{1/2}. \tag{45}$$

From eq (45) we see that as $k \to 0$, $v(k) \to c_0$ and as $k \to \infty$, $v(k) \to c_\infty$. The variation of $v(k)$ with k is indicated in figure 3

The width Γ_B is obtained by observing that if $D_2(v(k)k) = 0$, $D_1(v(k)k) = -2[v(k)k]^2\Gamma_B$. The minus sign is necessary so that $\Gamma_B > 0$ be satisfied. Direct substitution in eq (26) yields

$$2\Gamma_B = ak^2 + b_0k^2 - \left(\frac{c_0^2}{v^2}\right)\left(\frac{ak^2}{\gamma}\right) + \left[\frac{b_1k^2}{1+v^2k^2\tau^2}\right](1 - ak^2\tau). \tag{46}$$

It should be noted that the width due to the relaxation is not simply added to the classical absorption term $ak^2(1-1/\gamma) + b_0k^2$. In practice this difference may not be significant, although for CS_2 it amounts to about 5 percent of Γ_B.

The method used to obtain $v(k)$ and Γ_B should be applicable to more complicated situations although it would be advisable to examine $D_1(\omega)$ and $D_2(\omega)$ numerically and to verify that $D_2(v(k)k)=0$ for each new situation.

4.4. Comparison With the Exact Expression

The approximate frequency distribution contained in eq (43) has been compared numerically with the exact expression, eq (25). This is illustrated in figure 4 where the percent deviation of the approximate expression from the exact one is shown as a function of frequency. The parameters are the ones used to obtain figure 1. The deviation in the central components is probably due to a small error in the width of the thermal diffusion mode. A decrease of 1 percent in that width would eliminate most of the difference between $\sigma(k, \omega)$ and $\sigma'(k, \omega)$. The deviation in the phonon

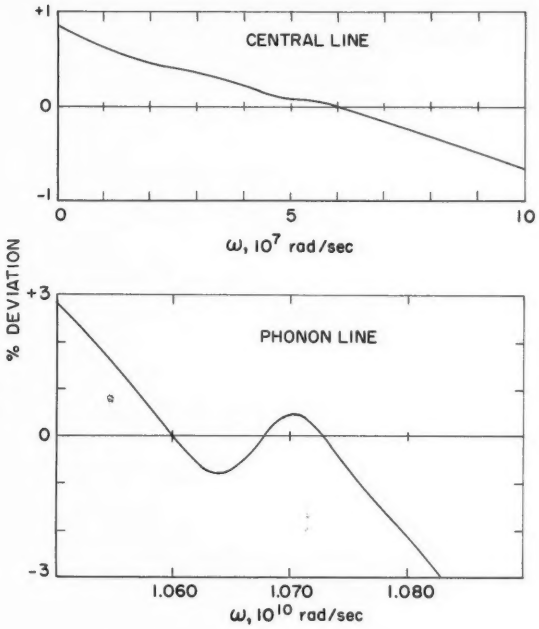

FIGURE 4. *The percent deviation* $[(\sigma-\sigma')/\sigma]$ *100 of the approximate frequency distribution,* $\sigma'(\mathrm{k}, \omega)$, *from the exact distribution,* $\sigma(\mathrm{k}, \omega)$, *is shown as a function of frequency* ω.
The parameters are those of CS_2 at 20 °C and $k = 8.608 \times 10^4$ cm^{-1}.

component indicates that the maxima of the exact and approximate expressions do not quite coincide. This results in the oscillating deviation shown in figure 4. Deviations greater than 1 percent occur when the magnitude of $\sigma'(k, \omega)$ has fallen to less than 1 percent of its maximum value $\sigma'(k, 0)$. The sum rule, eq (10), is satisfied by the approximate expression $\sigma'(k, \omega)$ to within 1 percent using this set of parameters.

It is, of course, possible to improve the accuracy of $\sigma'(k, \omega)$ by obtaining more accurate solutions to the dispersion equation. This would involve using the solutions we have found, eqs (35) and (40), as the starting point of an iteration of the dispersion equation. The resulting formula for $\sigma'(k, \omega)$ would be much more complicated than eq (43).

4.5. Intensity Ratio

The ratio of the intensity of the unshifted (central) components of the scattered light to the intensity of the Brillouin components is a quantity which is readily obtained experimentally. This ratio, $\mathscr{I} = I_c/2I_B$, is easily obtained from eq (43) by integrating the individual terms:

$$\mathscr{I} = \frac{(1-1/\gamma)+\dfrac{(c_\infty^2-c_0^2)k^2-(v^2/c_0^2-1)[(c_0^4/v^4\tau^2)+c_0^2k^2(1-1/\gamma)]}{c_0^4/v^4\tau^2+v^2k^2}}{\dfrac{[1-c_0^2/v^2(1-1/\gamma)]\,[v^2k^2+c_0^2/v^2\tau^2]-(c_\infty^2-c_0^2)k^2}{c_0^4/v^4\tau^2+v^2k^2}}. \tag{47}$$

At low phonon frequencies $vk\tau \ll 1$ this reduces to the Landau-Placzek result

$$\mathscr{I} = \gamma - 1. \tag{48}$$

At large phonon frequencies ($vk\tau \gg 1$) a more involved expression than eq (48) is obtained;

$$\mathscr{I} = (\gamma-1)[1+\{\gamma/(\gamma-1)\}\{(c_\infty^2-c_0^2)/c_0^2\}]. \tag{49}$$

The high frequency limit, eq (49) was obtained earlier by Rytov [13].

The ratio of intensities $\mathscr{I}$, given by eq (47) agrees within 1 percent of $\mathscr{I}$ obtained by numerical integration of the exact expression for $\sigma(k, \omega)$. From an experimental point of view, eq (47) should be taken to be an upper bound on $\mathscr{I}$. This is because it may be difficult to detect all of the light scattered by the second nonpropagating mode; the difficulty arises from the large width of this component.

4.6. Summary of the Properties of $\sigma(k, \omega)$

In the previous paragraphs we have shown that $\sigma(k, \omega)$, the frequency distribution function, may be approximately represented as a sum of four Lorentzian curves;

$$\sigma'(k,\omega)=(1-1/\gamma)\left[\frac{2\lambda k^2/\rho_0 c_p}{(\lambda k^2/\rho_0 c_p)^2+\omega^2}\right]$$
$$+\left[\frac{(c_\infty^2-c_0^2)k^2-(v^2/c_0^2-1)(c_0^4/v^4\tau^2+c_0^2k^2(1-1/\gamma))}{c_0^4/v^4\tau^2+v^2k^2}\right]\times\left[\frac{2c_0^2/v^2\tau}{(c_0^2/v^2\tau)^2+\omega^2}\right] \quad (43)$$

$$+\left[\frac{[1-c_0^2/v^2(1-1/\gamma)]\,[v^2k^2+c_0^2/v^2\tau^2]-(c_\infty^2-c_0^2)k^2}{c_0^4/v^4\tau^2+v^2k^2}\right]$$
$$\times\left[\frac{\Gamma_B}{\Gamma_B^2+(\omega-vk)^2}+\frac{\Gamma_B}{\Gamma_B^2+(\omega+vk)^2}\right] \quad (44)$$

where the phonon speed $v(k)$ satisfies

$$[v(k)k\tau]^2=1/2\,[(c_\infty k\tau)^2-1]+1/2\,[(1-c_\infty^2k^2\tau^2)^2+4c_0^2k^2\tau^2\,]^{1/2} \quad (45)$$

and the phonon width is

$$2\Gamma_B=ak^2+b_0k^2-\left(\frac{c_0^2}{v^2}\right)\left(\frac{ak^2}{\gamma}\right)+\left(\frac{b_1k^2}{1+[v(k)k\tau)\,]^2}\right)(1-ak^2\tau). \quad (46)$$

The ratio of the central components to that of the Brillouin lines is, in the high frequency limit $(v(k)\rightarrow c_\infty)$

$$\mathscr{I}=(\gamma-1)[1+\{\gamma/(\gamma-1)\}\,\{(c_\infty^2-c_0^2)/c_0^2\}]. \quad (49)$$

5. Comparison With Experiment

5.1. CS_2

In the previous sections, various points have been illustrated by using parameters appropriate to carbon disulfide (CS_2). For example, Figures 1, 2, and 3 show $\sigma\ (k, \omega)$ and $v\ (k)$ for CS_2 as predicted by egs (25) and (45). Comparison with experiment is limited to the phonon speed and to $\mathscr{I}$, the ratio of the intensities of the central and Brillouin components.

The parameters for CS_2 at approximately 20 °C are listed in table 1. Several measurements of the phonon speed are listed in table 2. To within the precision with which τ and k are known, eq (45) predicts that $v\ (k)$ lies within the experimental uncertainty in each case.

TABLE 1. *Material parameters:* CS_2 *at 20 °C*

Parameter	Value	Reference
a	1.95×10^{-3} cm²/sec	6
b_0	3.84×10^{-3} cm²/sec	14
b_1	4.76 cm²/sec	10
c_0	1.142×10^5 cm/sec	10
τ	2.04×10^{-9} sec	10
n	1.675	6
ρ_0	1.262 gm/cm³	6
γ	1.55	10

TABLE 2. *Phonon velocity and intensity ratio;* CS_2

Reference	Experimental		Calculated	
	Velocity	$\mathscr{I}$	Velocity	$\mathscr{I}$
	m/sec		*m/sec*	
15	1235	—	1241	0.83
16	1241	0.77	1241	.83
17	1250	.71	1241	.83
6	1265	.93	1241	.83
18	1223	—	1212	.69

The experimental velocities have been reduced to 20 °C using $dv/dT = -3.2$ m/sec-deg [6]. The velocities were calculated using eq (45). $\mathscr{I}$ values were calculated using eq (47). The material parameters were taken from table 1 and **k**, the wave vector, was determined from information in the references.

Three of the references contain measurements of $\mathscr{I}$. Here the agreement is not as close. The value of $\mathscr{I}$ predicted by eq (49) is 0.83. That the agreement with the phonon velocity is better than the agreement with $\mathscr{I}$ is not surprising. The limited sensitivity of the detectors used in these measurements makes it difficult to obtain accurate determinations of $\mathscr{I}$. The presence of the "second" nonpropagating mode aggravates the situation; unless the detector is quite sensitive, much of the light in that mode would be lost in the noise of the detector.

5.2. CCl_4

Sufficient data exist for carbon tetrachloride (CCl_4) to warrant comparison with the prediction of the single relaxation time theory. This comparison indicates that only a part of the energy of the internal degrees of freedom relaxes with a time on the order of $10^{-10} - 10^{-11}$ sec. Presumably the remainder of the energy relaxes more rapidly than can be detected by light scattering experiments.

The parameters for CCl_4 at approximately 20 °C are listed in table 3. Four measurements of the phonon speed obtained from Brillouin scattering measurements and one acoustic measurement of the speed of sound in CCl_4 are listed in table 4. The calculated velocities in table 4 are based on the assumption that only 75 percent of the internal specific heat is involved in the relaxation process and that $\tau = 5.12 \times 10^{-11}$ sec. This value for τ is consistent with the acoustic measurement. The agreement between the measured and calculated values of $\mathscr{I}$ is poor. This is not unexpected if another relaxation time exists for CCl_4. This would imply the existence of another nonpropagating mode which would make $\mathscr{I}$ larger than the prediction of eq (47).

Also, for CCl_4, there is a measurement of the width of the Brillouin line. Experimentally $\Gamma_B \approx 4 \times 10^9$ rad/sec while eq (46) predicts $\Gamma_B \approx 5 \times 10^9$ rad/sec if 3/4 of the internal specific heat is involved in the relaxation process.

TABLE 3. *Material parameters:* CCl_4 *at 20 °C*

Parameter	Value	Reference
a	1.78×10^{-3} cm²/sec	6
b_0	5.98×10^{-3} cm²/sec	14
b_1	3.59×10^{-2} cm²/sec	10
c_0	9.20×10^4 cm/sec	10
τ	5.12×10^{-11} sec	
n	1.472	6
ρ_0	1.594 gm/cm²	6
γ	1.46	10

The relaxation time τ was estimated from acoustic measurements [19].

TABLE 4. *Phonon velocity and intensity ratio;* CCl_4

Reference	Experimental		Calculated	
	Velocity	$\mathscr{I}$	Velocity	$\mathscr{I}$
	m/sec		*m/sec*	
6	1040	1.10	1024	0.77
16	988	0.75	990	.62
17	1000	.72	990	.62
20	1002	—	990	.62
19	972 — acoustic measurement			

The experimental velocities have been reduced to 20 °C using $dv/dT = -3.1$ m/sec − deg [6]. The velocities were calculated using eq (45). $\mathscr{I}$ values were calculated using eq (47). The material parameters were taken from table 3 and **k**, the wave vector, was determined from information in the references.

In a previous publication [21] we stated that more than one relaxation time exists in CCl_4 and therefore the single relaxation time theory did not apply. Although the available data are insufficient to fully verify this statement, the phonon speed comparison suggests that this statement is correct.

6. References

[1] G. B. Benedek and N. C. Ford, Conference on Phenomena in the Neighborhood of Critical Points held at the National Bureau of Standards, Washington, D.C., April 5–8, 1965.
[2] L. D. Landau and E. M. Lifshitz. Electrodynamics of Continuous Media, ch. 14 (Addison-Wesley Publishing Company, Reading, Mass., 1960).
[3] M. S. Green, J. Chem. Phys. **22,** 398 (1954).
[4] A. Einstein, Ann. Physik **33,** 1275 (1910).
M. V. Smoluchowski, Ann. Physik **25,** 205 (1908).
[5] L. van Hove, Phys. Rev. **95,** 249 (1954).
[6] I. L. Fabelinskii, Uspekhi Fiz. Nauk. **63,** 355 (1957).
[Translated in Advances in Physical Sciences **63,** 474 (1957)].
[7] L. I. Komarov and I. Z. Fisher, Soviet Physics JETP **16,** 1358 (1963).
[8] R. D. Mountain, Rev. Mod. Phys. **38,** 205 (1966).
[9] R. Pecora and W. A. Steele, J. Chem. Phys. **42,** 1872 (1965).
[10] Karl F. Herzfeld and T. A. Litovitz, Absorption and Dispersion of Ultrasonic Waves (Academic Press, New York, 1959).
[11] Robert Zwanzig, J. Chem. Phys. **43,** 714 (1965).
[12] L. D. Landau and E. M. Lifshitz, Fluid Mechanics, ch. 17 (Academic Press, Reading, Mass., 1959).
[13] S. M. Rytov, Soviet Physics JETP **6,** 130, 401, 513 (1958).
[14] Handbook of Chemistry and Physics 37 Edition, p. 2014 (Chemical Rubber Company, Cleveland, Ohio, 1955).
[15] R. Y. Chiao and B. P. Stoicheff, J. Opt. Soc. Am. **54,** 1286 (1964).
[16] D. H. Rank, Edward M. Kiess, Uwe Fink and T. A. Wiggins, J. Opt. Soc. Am. **55,** 925 (1965).
[17] H. Z. Cummins and R. W. Gammon, J. Chem. Phys. **44,** 2785 (1966).
[18] D. A. Jennings and H. Takuma, Appl. Phys. Letters **5,** 241 (1964).
[19] E. S. Stewart and J. S. Stewart, Phys. Rev. Letters **13,** 437 (1964).
[20] G. B. Benedek, J. B. Lastovka, K. Fritsch, and T. Greytak, J. Opt. Soc. Am. **54,** 1284 (1964).
[21] R. D. Mountain, J. Chem. Phys. **44,** 832 (1966).

(Paper 70A3–396)

JOURNAL OF RESEARCH of the National Bureau of Standards—A. Physics and Chemistry
Vol. 70A, No. 3, May-June 1966

Density of Polyethylene Crystals Grown From Solution

Gordon M. Martin and Elio Passaglia

Institute for Materials Research, National Bureau of Standards, Washington, D.C.

(February 9, 1966)

The density of Marlex 50 polyethylene crystals grown from a 0.75 percent solution in *p*-xylene at 70 °C was measured by a pycnometric method. Difficulties in making the measurements to the necessary accuracy are discussed. The values obtained were close to 0.98 g/cm³ at 30 °C and significantly less than the crystallographic density of 1.00 g/cm³. Several possible explanations of this density deficiency are mentioned.

Key Words: Crystals, density, polymer, *p*-xylene, polyethylene, pycnometer, density deficiency, weighing method.

1. Introduction

The measured density of a crystalline polymer is usually less than that calculated from the density of its unit cell. This reduced density has been attributed to the amorphous regions in a two phase amorphous-crystalline model or to defects and "mispacking" of folds in adjacent lamella in a chain-folded crystalline model. Crystals of polymers grown from dilute solution appear to have many of the characteristics of single crystals of nonpolymeric materials, and there has been special interest in their densities.

The density of polyethylene crystals grown from solution has been measured by a centrifuge method [1, 2],[1] a gradient tube method [1], and a pycnometer method [1, 3]. Values around 0.97 g/cm³ have been obtained by all these methods for crystals formed at 70 °C [1, 2] as compared to the crystallographic density of nearly 1.00 g/cm.³ However, values of about 1.00 g/cm³ have been obtained by a pycnometer method for the density of the crystals [3].

Although the density gradient tube method is subject to some uncertainty [4], the centrifuge method, in which the density of a buoying liquid is adjusted to be equal to that of the crystals, appears to be as valid as pycnometric methods. It is clear that a discrepancy exists. The present work was undertaken to provide another pycnometric measurement of the density of polyethylene crystals.

2. Experimental Procedure

To prepare the crystals, Marlex 50[2] polyethylene (with a weight average molecular weight of 130,000) was first dissolved in xylene at 145 °C, allowed to crystallize at 80 °C, and rinsed with xylene at 80 °C to remove low molecular weight fractions or other material. The polymer was dried under vacuum at room temperature. Enough of this treated polyethylene to make a 0.75 percent solution was dissolved in distilled *p*-xylene at 145 °C and allowed to crystallize for a week at 70 °C. Micrographs of some typical crystals are shown in figures 1 and 2.

The pycnometers used, which had a nominal volume of 50 cm³, were made from Pyrex glass as illustrated in figure 3. They were annealed and the standard taper joints were ground together by hand using fine emery in water. They were filled by a hypodermic syringe with a needle which was inserted through the capillary tube. The pycnometers could be emptied either by using the hypodermic syringe or by turning upside down and connecting to an aspirator. This was somewhat inconvenient, but the single, carefully fitted joint which could be dried before assembly reduced the rate of evaporation of an enclosed liquid.

The pycnometers were cleaned with a sulfuric acid and sodium dichromate solution, rinsed several times with distilled water, and dried overnight at 120 °C. After cleaning they were always handled with forceps or rubber gloves.

[1] Figures in brackets indicate the literature references at the end of this paper.

[2] A commerical material is identified in this paper in order to adequately specify the experimental procedure. Such identification does not imply recommendation or endorsement by the National Bureau of Standards.

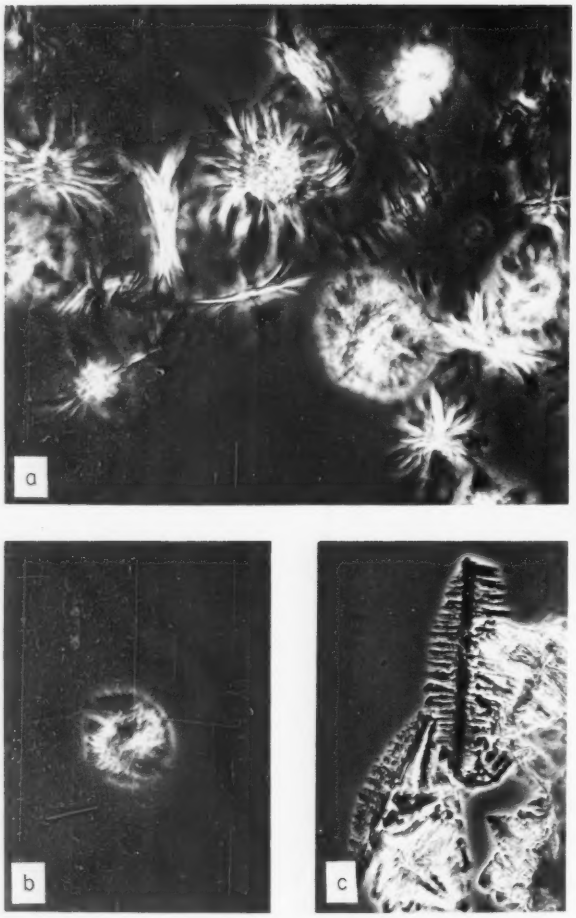

FIGURE 1. *Optical phase contrast micrographs of the type of crystal aggregates in the preparation;* × *155 (a) Dendrites and axialites in suspension in xylene. Note distinct splaying of layers in some crystals. (b) Axialite in suspension in xylene. (c) Dendrites after drying.*

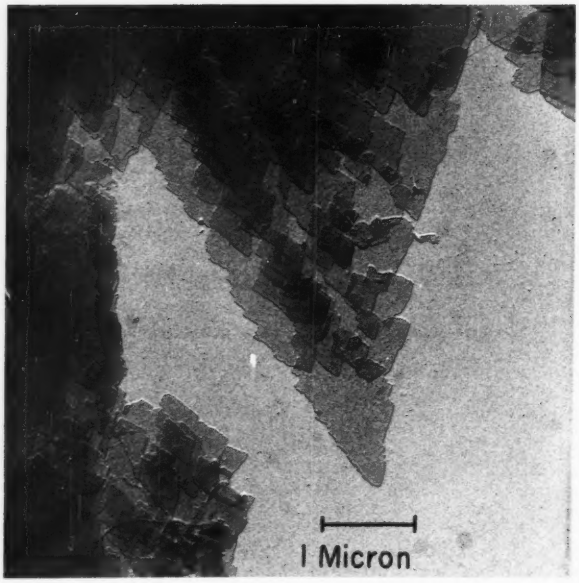

FIGURE 2. *Electron micrograph of a portion of a dendrite similar to those shown in figure 1 (c).*

Weights were taken to the nearest 0.05 mg on a Mettler single-pan balance. The temperature, barometric pressure, and relative humidity were measured at each weighing and the density of the air was calculated, so that the observed weights could be corrected for the net buoyant force of the atmosphere.

The pycnometers were filled at 30.15 °C in a water bath which was regulated within ±0.01 °C. The liquid was first adjusted above the line on the capillary tube; then small, rolled strips of lens tissue were dipped in it until the level was lowered almost to the line. The liquid was then allowed to evaporate until the meniscus just touched the line when observed through a jeweler's eyepiece.

After weighing empty and filled with boiled, distilled water, the pycnometers were weighed filled with distilled *p*-xylene which had been taken from the same flask as that used for preparing the crystals and had been carried through exactly the same heat treatment prior to having been put in the pycnometers. The average of six determinations gave a density of 0.852241 g/cm^3 for the *p*-xylene at 30.15 °C. The standard deviation of an individual result was 0.000003 g/cm^3.

In the final step in the procedure, after the pycnometer had been weighed filled with the mixture of *p*-xylene and polyethylene crystals, it was necessary to evaporate the liquid and weigh the pycnometer and dried crystals alone. This was done in a vacuum. However, if the pycnometer was placed immediately in the vacuum chamber, vapor bubbles could form and cause some of the liquid and crystals to splash

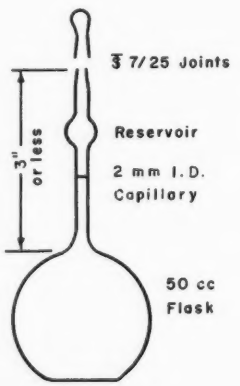

FIGURE 3. *Pycnometer, Pyrex glass.*

out. To avoid this the pycnometer was heated between 35 and 40 °C for several days to evaporate some of the liquid and create a space below the capillary. The reservoir above the capillary prevented overflowing during the heating. After heating, the pycnometer was placed in a desiccator connected to a vacuum pump and the valve opened very gradually so that an hour or more was required to produce the final vacuum. Pumping at room temperature was continued for a day after the crystals appeared dry. The pycnometer was then placed in a vacuum oven at 100 °C for several days. No significant change in weight was observed after the first day in the vacuum oven.

After this treatment, it was assumed that there was not enough xylene left in the crystals to have an appreciable effect on their density. Although we know of no data on the retention of xylene when crystals of polyethylene are dried under our conditions, experiments with such crystals grown in tetrachloroethylene have shown that approximately 0.1 percent by weight of that solvent remained in the crystals when they were heated to 60 °C in a vacuum [5]. If this much xylene remained in our crystals, it would reduce the density by only 0.0002 g/cm³, which is well within the experimental error from other sources. Moreover, in order for the density of the crystals to be lowered from the crystallographic value of 1.00 g/cm³ to the observed value of 0.98 g/cm³, the crystals would have had to retain approximately 12 percent of xylene. This is at best extremely unlikely. These calculations assume additivity of volumes. If the volume of the crystals and xylene were slightly less than the sum of the separate volumes, the effect on the density would be even smaller.

A separate test showed that no observable amount of polymer remained dissolved in the supernatant xylene, so it was not necessary to make a correction for this.

3. Calculations

If we let P = wt of empty pycnometer, W = wt of pycnometer filled with water, X = wt of pycnometer filled with xylene, T = wt of pycnometer filled with mixture of xylene and crystals, and D = wt of pycnometer and dried crystals, the density of the crystals, ρ_c, can be expressed in terms of the density of water, ρ_w, by:

$$\rho_c = \frac{\rho_w (X-P)(D-P)}{(W-P)(X-P-T+D)}. \qquad (1)$$

The uncertainty in a density determination may be estimated from the uncertainties in the weights by taking the total differential of ρ_c in eq (1). We assume that the uncertainty in the "dry" weights P and D is ± 0.0002 g. In the case of W, X, and T an error of ± 0.01 cm in filling the pycnometer to the line would produce an additional uncertainty of ± 0.0003 g, so the total uncertainty for these weights is taken as ± 0.0005 g. Using typical values of the weights themselves with these estimates gives an uncertainty in the density of ± 0.0040 g/cm³, which is not far from the standard deviations actually observed.

The uncertainty in the density varies approximately inversely with the amount of crystals used. The uncertainty is caused chiefly by errors in X and T. A difference between the density of the xylene used in taking weight X and that used for T could produce a difference several orders of magnitude greater in the calculated density of the crystals for the amount of crystals used here (0.2 to 0.4 g). The need for fairly large amounts of crystals was the principal reason for using solutions of the relatively high concentration of 0.75 percent rather than a lower concentration, which would have been desirable because of the lower complexity of the crystals formed.

The weights used in eq (1) are the calculated values in vacuum, i.e., the observed weights plus the net buoyant force of the air. In finding the buoyant force the volumes of the materials being weighed are computed from the assumed values of their weights (and densities) and used to carry through the calculations. These new values of weight (and density) are now used and the calculations repeated. This continues until the assumed and calculated values are equal. Fortunately, we are dealing with a small correction to the weight and the process converges rapidly.

With no liquid in the pycnometer, it was simply weighed daily for a week or so, the weight in vacuum calculated each time, and the average of these values used. The standard deviation of an individual weight was about 0.15 mg. When this method was applied to the liquid-filled pycnometer, it was found that the weight decreased at a fairly constant rate—a typical value was 0.1 mg per day. Therefore, the weights in vacuum were plotted against the time and a least squares line was fitted to these points. Figure 4 shows typical plots for three of the pycnometers filled with water. The least squares line was extrapolated to zero time to find the weight used in the calculations. The standard error of this estimate was close to 0.1 mg. It was found that a reading taken a few hours after removing the pycnometer from the constant temperature bath often differed slightly from the value obtained by extrapolation.

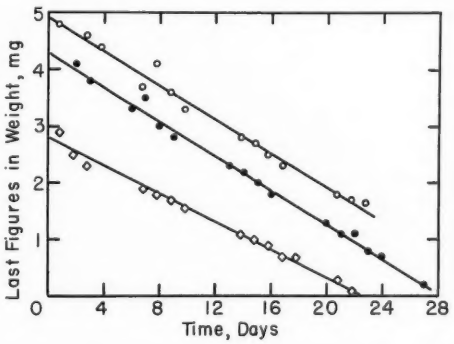

FIGURE 4. *Weight loss of pycnometers filled with water.*
○ #15 ◇ #13 ● #16

4. Results and Discussion

The results of eight determinations of the crystal density are given in table 1. The first series of two was not done in the manner outlined. The crystallization was carried out for 48 hr at 70 °C rather than 1 week. Ordinary xylene (a mixture of isomers) was distilled and used instead of *p*-xylene. Corrections for the buoyant force of the air were not made, nor was any allowance made for evaporation of liquid from the pycnometer. Attempts to repeat these first two determinations gradually led to the realization that xylene from different bottles varied in density, that the observed weights could change with atmospheric conditions, and that liquid slowly evaporated from the pycnometers no matter how carefully the joints were fitted. Hence, it is felt that the close agreement is not a reliable indication of the accuracy of these two determinations, but may be partly due to the fact that they were run at the same time and partly fortuitous.

The second and third series of measurements were carried out by the method outlined using distilled *p*-xylene, calculating the weights in vacuum, and extrapolating to zero time to determine the weight of the liquid-filled pycnometer. In the second series the needle used to fill the pycnometers did not reach the bottom, so the mixture of xylene and crystals was exposed to a small air gap at the start of the filling process. For the third series a longer needle was used and a little xylene placed in the bottom before adding the mixture, so that there was no exposure to air. The three determinations in the second series were run fairly close to the same time. In the third series #13 was run first using a mixture that had been stored at room temperature for several months, while #14 and #15 were run together using a mixture only a week old.

TABLE 1. *Density of polyethylene single crystals grown from solution*

Pycnometer		Density	Avg. density for series	Std. dev. of an individual value
		g/cm³	*g/cm³*	*g/cm³*
First series	#1	0.9637	0.9645	0.0015
	#2	.9654		
Second series	#14	.9745		
	#15	.9815	.9769	.0040
	#16	.9746		
Third series	#13	.9885		
	#14	.9798	.9827	.0050
	#15	.9798		

A Student's "*t*" test at the 95 percent confidence level shows that the averages for the second and third series are significantly different. A similar test at the 95 percent confidence level indicates that the average for the third series is significantly lower than the crystallographic density, taken as 0.997 g/cm³. However, it is possible that the density of the crystals increases upon standing at room temperature and the higher value for pycnometer #13 is due to this cause. If pycnometer #13 is ruled out and the other two values in the third series are combined with the second series, the five readings give an average density of 0.9780 g/cm³ with a standard deviation of 0.0033 g/cm³ for an individual reading. Whichever interpretation of the data is made, our result, though slightly higher than the previously quoted values around 0.97 g/cm³, is significantly less than the crystallographic density.

While it is not our purpose to dwell on the cause of this low density, several possible explanations may be mentioned. The first is that there is an amorphous phase arising perhaps from nonadjacent reentry. This model is difficult to reconcile with the regular crystallographic surfaces usually seen on polyethylene crystals and with the well-known behavior of these crystals upon fracture. Both these pieces of evidence indicate adjacent reentry.

A second possibility is adjacent reentry with a fold length which is not well defined, i.e., an irregular, short-range variation in the fold length of one or two unit cell *c*-dimensions. This is also difficult to reconcile with the regular surfaces of polyethylene crystals. However, it should be pointed out that the experiments which indicate regular surfaces are usually done on crystals grown from very dilute solution and such crystals may be more perfect than the rather complex ones used in our study. If our crystals had irregular surfaces, with an irregularity of sufficiently short period, then the inability of the solvent to pack regularly on the surface would give spuriously low density results.

A third possible explanation is based on the effect of chain ends. If chain ends are included in the crystals and, as is very likely, if ends of adjacent molecules do not pack in close juxtaposition, an end could cause a large vacancy extending on the average halfway through the thickness of the crystal. This would lead to a density which is dependent on the number-average molecular weight. For our polymer such an effect might cause a density deficiency of about 2 percent, just as was observed.

We are deeply indebted to F. Khoury and J. D. Barnes for the optical and electron micrographic observations.

5. References

[1] E. W. Fischer and R. Lorenz, Kolloid-Z. & Z. Polymere **189,** 97 (1963).
[2] J. B. Jackson, P. J. Flory, and R. Chiang, Trans. Faraday Soc. **59,** 1906 (1963)
[3] T. Kawai and A. Keller, Phil. Mag. **8,** 1203 (1963)
[4] T. Kawai and A. Keller, Phil. Mag. **8,** 1973 (1963)
[5] K. M. Sinnott, J. Polymer Sci., in press.

(Paper 70A3–397)

JOURNAL OF RESEARCH of the National Bureau of Standards—A. Physics and Chemistry
Vol. 70A, No. 3, May–June 1966

Mechanical Relaxation in Polyethylene Crystallized With Various Degrees of Lamellar Orientation

John M. Crissman* **and Elio Passaglia**

Institute for Materials Research, National Bureau of Standards, Washington, D.C.

(February 19, 1966)

The mechanical relaxation behavior of a set of well-characterized samples of polyethylene crystallized with different degrees of lamellar orientation is reported. The various samples ranged in morphology from unoriented isotropic samples to ones which showed a high degree of orientation of the *b*-axis along the sample growth direction. The mechanical measurements were made using a torsion pendulum apparatus of standard design, the direction of shear being normal to the *b*-axis for the oriented samples. The temperature range covered was from 100 to 400 °K. No definite effects attributable to orientation were observed for either the γ or β relaxation process, whereas for the α relaxation results for G'' indicate that a slight decrease in peak height resulted from the presence of lamellar orientation, particularly on the high temperature side of this peak. Data for the real and imaginary parts of the complex shear compliance are also discussed.

Key Words: Polyethylene, mechanical relaxation, lamellar orientation, torsion pendulum, shear modulus, shear compliance, orientation effects.

1. Introduction

Density and morphological factors such as lamellar thickness and spherulite size are known to affect the relaxation behavior of crystalline polymers. This dependence on morphology is often very complicated, affecting the loss measures tan δ, G'', and J'' in different ways [1][1] and making it difficult to determine the molecular mechanisms responsible for the various relaxation processes observed.

One of the morphological variables that has been little studied is orientation, despite the fact that in simpler solids, [2, 3, 4] for certain crystal symmetries, and for certain molecular mechanisms, the direction of the applied stress with respect to the crystal axis is known to affect the relaxation behavior. In polyethylene, Takayanagi [5] has reported striking differences between unoriented samples and samples crystallized with preferred orientation of the *b*-axis. The experiments were in tension, the direction of stress being along the *b*-axis. However, the two samples were of somewhat different compositions of polyethylene, and it is not clear to what extent the observed differences were due primarily to orientation.

In addition, Eby and Colson [11] have shown for samples of polyethylene prepared with an oriented surface layer and for the same samples with the oriented layer removed that the mechanical relaxation behavior in shear is measurably different.

It is the purpose of the present paper to report the mechanical relaxation behavior (in shear) of a set of well-characterized samples of polyethylene having different degrees of lamellar orientation, the direction of shear being normal to the *b*-axis for the oriented samples. As will be seen, no definite effects attributable to orientation were found for either the γ or β relaxation process. However, for the α relaxation the experimental results for G'' indicate that a slight decrease in peak height resulted from the presence of lamellar orientation, particularly on the high temperature side of this peak.

2. Experimental Procedure

2.1. Sample Preparation

The samples were prepared from Marlex 6050[2] polyethylene supplied through the courtesy of R. J. Martinovich of the Phillips Petroleum Company. This polymer contains a small amount of thermal stabilizer and has a weight average molecular weight of approximately 90,000.

A quenched sample and two isothermally crystallized samples were obtained using a technique employed by Passaglia and Martin [1] for samples of polypropylene. The polymer was initially prepared as a flat strip by compression molding. The flat strip was subsequently placed between two strips of aluminum cut to the desired dimensions and the sandwich then wrapped tightly in aluminum foil. The wrapped sandwich was mounted between two bronze plates held together by slight spring tension. The entire

*This research was carried out while the author was pursuing a Postdoctoral Resident Research Associateship in association with N.A.S., N.R.C.

[1] Figures in brackets indicate the literature references at the end of this paper.

[2] Certain commercial materials and equipment are identified in this paper in order to specify the experimental procedure adequately. In no case does such identification imply recommendation or endorsement by the National Bureau of Standards.

assembly was heated in an oven to 165 °C for about 30 min. One sample was quenched in dry-ice and acetone. The two isothermally crystallized samples were prepared in a crystallization bath, one being held at 127.5 °C for three days followed by rapid cooling to room temperature, and the second being held at 129 °C for 12 days, 128 °C for 1 day, 127 °C for 1 day, and then followed by rapid cooling to room temperature.

The oriented samples were prepared according to a method outlined by Seto and Fujiwara [6] and a diagram of the apparatus used is shown in figure 1. The apparatus consisted of a cylindrical copper block separated by a thin layer of transite (~ 1 mm) from a similar copper block which was water cooled. A hole was drilled down the axis of the assembly. The upper block was maintained at approximately 200 °C while the lower block was at room temperature. The polymer sample, contained in an evacuated glass tube of about 2 mm I.D., was lowered slowly through the hole. Crystallization was restricted to a very narrow region in the vicinity of the insulating layer, and by controlling the rate at which the sample was lowered, samples with varying degrees of lamellar orientation were obtained. For this investigation lowering rates were varied from 19.0 mm/hr, at which rate a sample with essentially no orientation was produced, to 0.28 mm/hr for a sample with a relatively high degree of lamellar orientation.

However, inasmuch as the drop rate also influenced the crystallization temperature—a rapid drop rate corresponding to a low crystallization temperature—a variation in the crystalline lamellar thickness also resulted. That is, the lamellar thickness, or correspondingly the density [7], increased with an increase in the degree of orientation.

Samples grown in this manner show orientation of the *b*-crystallographic axis along the sample growth direction as indicated by the wide angle x-ray photographs presented in figure 2 for four of the samples studied. For samples 3 and 6, orientation is indicated by arcs representing the (110), and (200) reflections for sample 3, and (110), (200), and (020) reflections for sample 6, whereas for the unoriented quenched or fast cooled samples (1 and 2) (the fast cooled sample was produced in the apparatus just described) uniformly continuous rings are observed corresponding to these reflections.

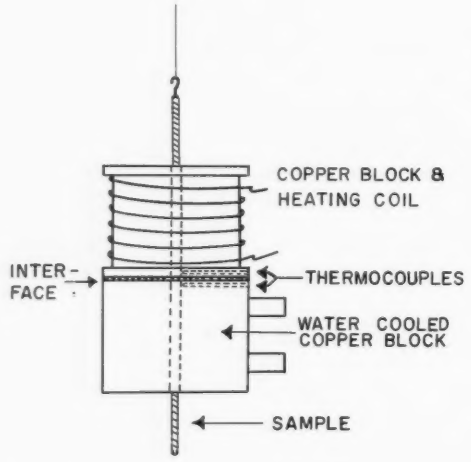

FIGURE 1. *Apparatus for growing oriented polyethylene samples.*

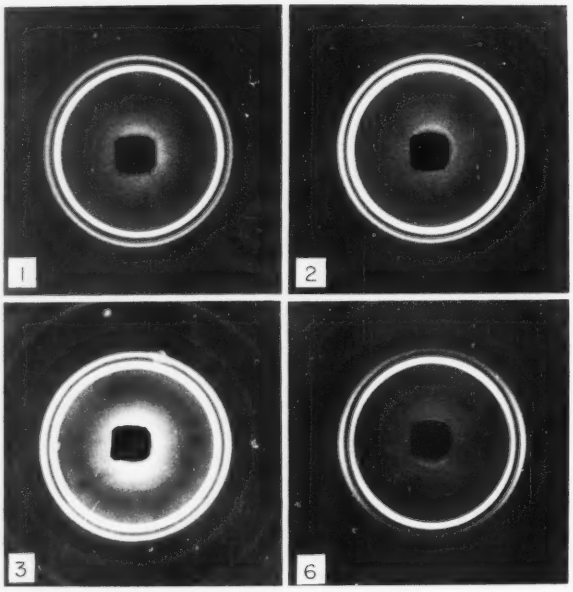

FIGURE 2. *Wide angle x-ray photographs of polyethylene samples: Sample 1, unoriented quenched; Sample 2, unoriented, grown in apparatus described in figure 1; Sample 3, slightly oriented; Sample 6, highly oriented.*

A further indication of the orientation obtained is provided by figure 3 which shows photomicrographs of sections cut longitudinally from the same four samples referred to in figure 2. Here ringed spherulites typical of polyethylene are observed for the unoriented samples. However, for the highly oriented sample 6, the dark bands caused by the twisting of the crystalline lamellae no longer form rings but are now nearly straight lines indicating that a large fraction of the lamellae run parallel to the sample growth direction.

A summary of the characteristics for each sample studied is given in table 1. The densities were measured by the displacement technique using distilled water. The low angle x-ray spacings were determined photographically using a Rigaku-Denki low angle x-ray camera. The column at the far right indicates a rough qualitative estimate of the degree of lamellar orientation for each sample.

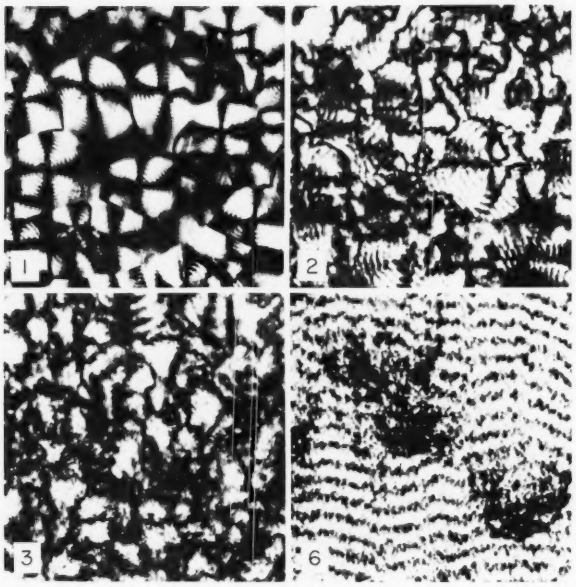

FIGURE 3. *Photomicrographs of polyethylene samples: Sample 1, unoriented quenched; Sample 2, unoriented, grown in the apparatus described in figure 1; Sample 3, slightly oriented; Sample 6, highly oriented.*

TABLE 1. *Summary of sample characteristics*

Sample	Density	Approximate Low angle spacings		Degree of orientation
	g/cm³	l_1(A)	l_2 (A)	
1 (Quenched)	0.9516 (24.0 °C)	232	Not measurable	None.
2	.9623 (26.6 °C)	256	119	None.
3	.9704 (26.0 °C)	316	156	Poor.
4	.9710 (25.8 °C)	322	156	Medium.
5	.9730 (24.8 °C)	377	183	Good.
6	.9714 (26.6 °C)	385	164	Good.
7 (Isothermally crystallized)	.9664 (26.5 °C)	275	135	None.
8 (Isothermally crystallized)	.9836 (25.5 °C)	Not measurable	204	None.

It will be noticed, as previously mentioned, that orientation, lamellar thickness, and density all vary in the same direction from sample to sample. That is, due to the manner of sample preparation, an increase in orientation is accompanied by an increase in lamellar thickness and density. This has the unfortunate consequence of making it difficult to correlate an observed change in mechanical properties with a morphological change.

2.2. Apparatus

The mechanical measurements were obtained using a torsion pendulum apparatus which has been described in some detail previously [8].

The samples were made to the proper dimensions so as to provide an operating frequency of about 1 Hz. In the case of the quenched and isothermally crystallized samples, which were flat strips, the thickness dimension varied from position to position on each sample by up to 5 percent, while variations in the other dimensions were small enough to be considered negligible. Therefore, an average sample thickness determined from measurements taken at 10 different positions on each sample was used in calculating the real part of the shear modulus, G'. For each cylindrical rod sample, the diameter of which varied over its length by up to 3 percent, six measurements were made. From these an average diameter was determined for computation purposes.

2.3. Effects of Thermal Expansion

As is customary in studies of mechanical relaxation in polymers, we have neglected dimensional changes with temperature in calculating the moduli, using the dimensions measured at room temperature for this purpose. Generally this is justifiable inasmuch as changes in modulus resulting from thermal expansion are small compared with observed changes in the modulus. It is also justified when relative difference among samples is of interest and the samples are all isotropic. When samples of different orientations are compared, however, the known anisotropy [9] of the thermal expansion of polyethylene must be considered.

The moduli are sensitive to the transverse dimensions of the specimen, being inversely proportional to the cube of the thickness for a flat specimen, and to the fourth power of the radius for a cylindrical one. Now, it is known [9] that the a-axis of polyethylene has by far the largest expansivity, and our oriented samples are such that this dimension is preferentially normal to the growth direction, whereas in the unoriented sample it has, of course, no preferred direction. This will cause differences in the thermal expansion of the dimension normal to the growth direction, which in turn will cause relative differences in the moduli for the two types of samples at any temperature but room temperature. Without actual measurements on our samples it is impossible to make a quantitative correction for this, but using the data of Swan [9] it can be estimated that the isotropic sample moduli should be lowered by several percent relative to the oriented sample moduli at liquid air temperature, and raised by somewhat less at the highest temperatures achieved. The effect of this difference on the observed differences in the curves will be commented on below.

3. Results

The experimental data for the imaginary and real parts of the complex shear modulus as functions of temperature are presented in figures 4 and 5 respectively. For clarity the data for samples 4 and 5 have not been included, but the results for them will be commented on when necessary.

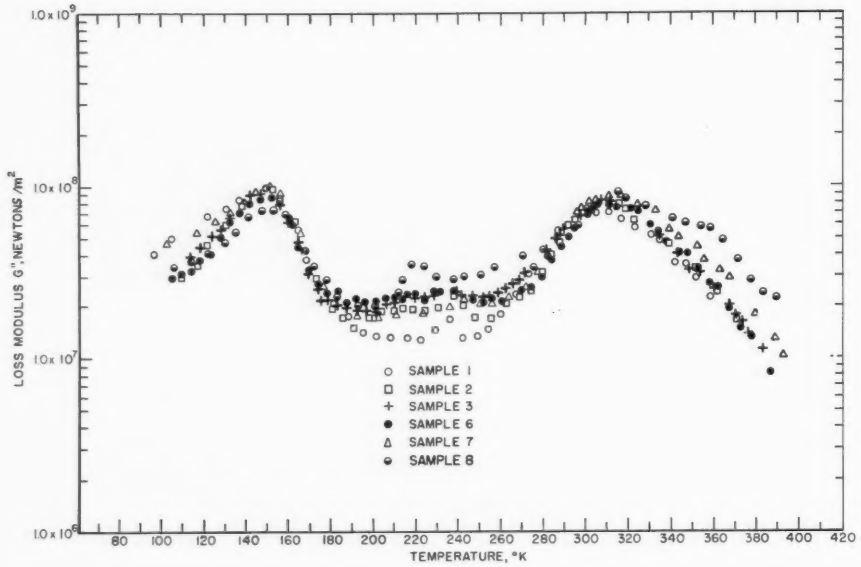

FIGURE 4. *Loss modulus,* G″, *versus temperature for unoriented and* b*-axis oriented polyethylene samples.*

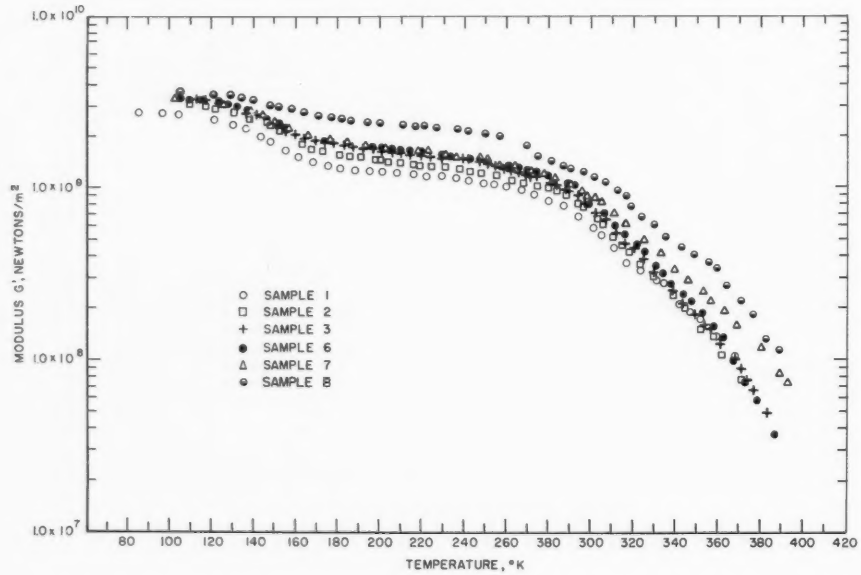

FIGURE 5. *Storage modulus,* G′, *versus temperature for unoriented and* b*-axis oriented polyethylene samples.*

In order to facilitate a more direct comparison of our results with other data reported in the literature the loss modulus G'' will be used for discussion purposes rather than the logarithmic decrement which is customarily reported. From figure 4, which gives the results for G'', the three regions of mechanical relaxation characteristic of polyethylene are observed. We shall here follow the notation generally used and refer to the high temperature relaxation (~313 °K) as the α process, the low temperature

TABLE 2. *Experimental results for the observed α- and γ-relaxations*

	γ Relaxation peak				α Relaxation peak			
Sample	T_{max}	ν_0	$G'(T_{max})$	$G''(T_{max})$	T_{max}	ν_0	$G'(T_{max})$	$G''(T_{max})$
	°K	Hz	Newtons/m²	Newtons/m²	°K	Hz	Newtons/m²	Newtons/m²
1	152	0.840	1.75×10^9	1.0×10^8	303	0.476	5.60×10^8	7.5×10^7
2	152	1.29	2.17×10^9	9.8×10^7	310	.704	5.50×10^8	7.8×10^7
3	146	.26	2.44×10^9	9.1×10^7	311	.597	5.60×10^8	8.1×10^7
4	146	1.26	2.40×10^9	9.1×10^7	311	.599	5.40×10^8	8.0×10^7
5	146	1.40	2.25×10^9	8.0×10^7	311	.735	6.1×10^8	7.9×10^7
6	151	1.37	2.40×10^9	8.8×10^7	313	.685	5.80×10^8	7.9×10^7
7	151	1.46	2.47×10^9	1.0×10^8	316.5	.727	6.16×10^8	8.9×10^7
8	152	2.53	3.04×10^9	7.4×10^7	315	1.34	8.87×10^8	9.29×10^7

relaxation (~150 °K) as the γ process, and the less well defined relaxation in the region from 200 to 250 °K as the β process.

For convenience a resumé of the experimentally determined parameters for the α and γ relaxation peaks is given in table 2 for the samples investigated. Included in the table are the temperature of the peak maximum, the experimental frequency at that temperature, and the values of G' and G'' at the peak maximum. Because of the rather poor resolution of the β relaxation process and also as a result of some overlap of both the α and γ relaxations in this temperature region, the determination of a peak maximum is too uncertain in most cases and thus no values have been included for this relaxation process.

It is apparent from figure 4 that the behavior in all three regions is dependent upon the morphological characteristics of the specimens. These differences are particularly evident in the α and β relaxations, and less so in the γ. Indeed, when account is taken of the differences in thermal expansion as mentioned above, only slight differences remain at the γ peak, and these are such that the higher density samples have lower relaxations. For the quenched and isothermally crystallized specimens a tail appears on the low temperature side of the γ loss peak suggesting that for these samples relaxation mechanisms exist which are not observed in the others.

In the β region, results for the quenched and isothermally crystallized samples (1, 7, and 8) indicate that the magnitude of G'' increases as the density, and correspondingly the lamellar thickness, increases. For the two oriented samples (3 and 6), the densities of which are intermediate to those for samples 7 and 8, the magnitude of G'' falls within the values found for samples 7 and 8. Therefore, it is concluded that the observed differences in these samples are not due to orientation, but to density and/or lamellar thickness differences.

The results for G'' above room temperature reveal that the α relaxation is comprised of at least two peaks, one peak (α) having a maximum centered near 315 °K, and a second weaker peak, appearing as a shoulder, at higher temperatures in the vicinity of 360 °K. This secondary loss peak will be denoted by α′. For the unoriented samples both the α and α′ relaxations increase with increasing density, but the α′ process is not observed in the quenched sample. The behavior of the oriented samples, however, deviates to a small extent from this trend since in the region of maximum loss, for both the α and α′ peaks, values for G'' are somewhat smaller than would be expected from density considerations alone, based on the results for the unoriented specimens. This will be demonstrated more explicitly later for the main α peak.

The data indicate no significant dependence of the temperature of the maximum on morphology in the γ region, whereas the α peak is shifted slightly to higher temperatures as the density increases (see table 2). This may be due to the dependence of the temperature of the α maximum on lamellar thickness [10].

In figure 5 the data representing the real part, G', of the modulus are given. These data require little comment except that over the entire temperature range covered, G' for the unoriented samples increases with increasing density; and, within the experimental accuracy, the data below room temperature for the oriented samples show no significant deviations from this behavior. However, above room temperature through the region of the α relaxation G' appears to drop off more steeply for the oriented samples than for the unoriented ones.

4. Discussion

It is impossible from the data in figures 4 and 5 to ascribe unambiguously the observed differences in the behavior of the samples to any single morphological parameter. However, the consideration of other published work does permit a fairly definite statement about the effect of orientation.

Illers [10] has carried out experiments employing torsional shear stresses (~ 1 Hz) on samples of unoriented polyethylene crystallized isothermally from the melt. His results showed that both the α and γ relaxations involve at least two processes. That is, weaker secondary loss peaks were observed as shoulders, one being on the low temperature side of the γ peak, and a second on the high temperature side of the α peak. It was found that as the sample density, or lamellar thickness, increases, the magnitude of both components of the γ peak decreases, whereas the β peak as well as both the α and α′ relaxations show increases. At the same time values for the modulus, G', were found to increase as the density increased.

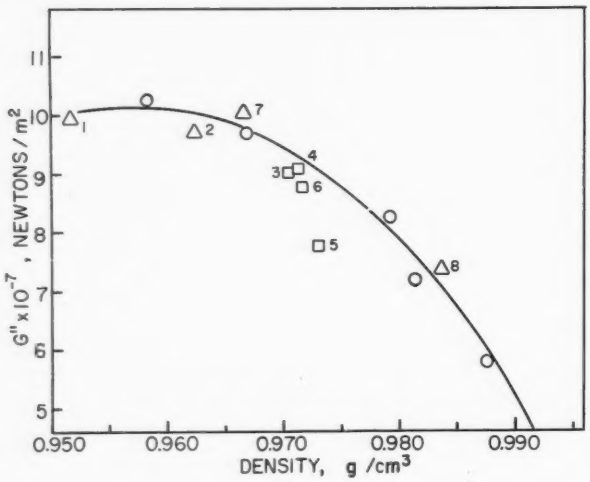

FIGURE 6. *Loss modulus, G", at the peak maximum versus density for the γ relaxation in polyethylene: Δ-unoriented samples, □-oriented samples, ○-data of Illers.*
The solid line represents a least squares fit to all the data points for unoriented samples.

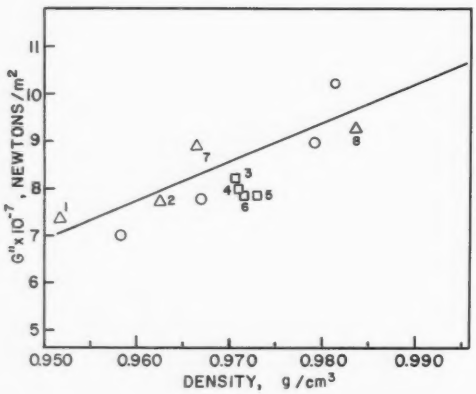

FIGURE 7. *Loss modulus, G", at the peak maximum versus density for the α relaxation in polyethylene: Δ-unoriented samples, □-oriented samples, ○-data of Illers.*
The solid line represents a least squares fit to all the data points for unoriented samples.

In addition, investigations by Eby and Colson [11] and by Flocke [12], using similar techniques, indicate analogous results for samples of polyethylene quenched from the melt and slowly cooled from the melt. However, in the latter two investigations no distinct secondary maxima, or shoulders, associated with the γ process were observed, although the data of Eby and Colson indicate a definite tail on the low temperature side of this peak, the tail being slightly higher for the quenched sample.

Although quantitative correlation is difficult, our own results show the same trends as observed by these workers. With regard to the γ and α relaxations, it is instructive to plot the values of the loss modulus, *G"*, at the peak maximum as a function of sample density, and these plots are given in figures 6 and 7 respectively. Included in the figures are the data of Illers [10], as well as our own.

The solid lines represent a least squares fit to the data points for the unoriented samples including the data points of Illers.

For the γ relaxation it is seen from figure 6 that our own results for the unoriented samples are in good agreement with the data of Illers. Moreover, except for sample 5, the data points for the oriented samples show no significant deviations from this trend. The point for sample 5, however, does depart somewhat from the trend observed for the others. Examination of photomicrographs along with low angle x-ray photographs indicate that sample 6 has a higher degree of lamellar orientation than does sample 5, although 5 has the greater density. Consequently, it is not certain that the lower peak height observed for this sample is a result of orientation or represents an inconsistency in the data. We would conclude from these data that the magnitude of the γ relaxation is not dependent upon orientation, but obviously depends upon density and/or lamella thickness.

These conclusions may be contrasted with the measurements of Takayanagi [5] who, as mentioned in the introduction, found distinct differences in the region of the γ relaxation, between oriented and isotropic samples in tension. However, the oriented specimen was of a different type of polyethylene from the isotropic specimen, and it is not clear that the observed differences were not due to polymer type.

A similar plot is shown in figure 7 for the α relaxation. Again, our own results for the unoriented specimens, 1, 2, 7, and 8 show the same trend as do those of Illers, although here the agreement is not quite as good as in the case of the γ process. However, the data points for the oriented samples 4, 5, and 6, which are all well oriented, fall consistently below the line fitted to the points for the unoriented specimens.

It might be mentioned that if our own data alone are considered an alternative interpretation is possible. That is, a line fitted to the points for samples 1 through 6 will fall well below the points for the isothermally crystallized samples 7 and 8. Since these two samples were prepared somewhat differently one might conclude that the observed effect was a result of the method of crystallization rather than orientation. However we see no reason to exclude Illers' data from consideration, especially in view of the fact that our own results for unoriented samples show the same trends as do his. Therefore, it is concluded that for this process, in addition to density and/or lamellar thickness effects, orientation does have a small effect, and in such a manner that the loss modulus, *G"*, decreases as the degree of lamellar orientation increases, for the type of orientation our samples have.

Concerning the two weaker secondary relaxations also observed, it can be further stated that it appears reasonable to associate the tail, observed both from

the present work and from that of Eby and Colson [11], with the loss mechanism found by Illers on the low temperature side of the γ relaxation peak. However, due to the as yet obscure nature of this process, no statement can be made with respect to possible orientational effects. On the other hand, the α' shoulder does appear to be influenced by orientation since, as mentioned earlier, the loss modulus data for the oriented samples 3 and 6 in the region of this shoulder fall below that for sample 7, a sample of lower density than either 3 or 6 (see fig. 4).

The orientation in these samples is such that the *b*-axis of the unit cell is preferentially along the rod axis, the *a*- and *c*-axes being randomly oriented normal to this direction. Since the deformation is torsional and the oriented samples are cylindrical, the strain is such that the *a*-*b* and *b*-*c* faces of the crystal are preferentially sheared in these samples. Inasmuch as the oriented specimens show a lower G'' than the unoriented specimens in both the α and α' regions, it may be tentatively concluded that the relaxation is preferentially activated by shearing the (010), (010), and (100), or (010) and (001) faces of the crystal. When our results are compared with those of Eby and Colson [11], it appears most likely that the relaxation is preferentially activated by shearing of the (010) and (100), or (010) and (001) faces of the crystal, but the tenuous nature of the conclusion is apparent.

Moreover, it may very well be that the relaxation is associated with some aspect of the lamellar "superstructure" rather than processes within the primary crystals. In this regard, the results could just as well be rationalized by saying that the α and α' relaxations are preferentially activated by shear such that fold planes try to move past one another. This would imply that the process is associated with the fold planes themselves or perhaps associated with movement of the chains because of their coupling to the fold planes. Beyond this one cannot say on the basis of these results.

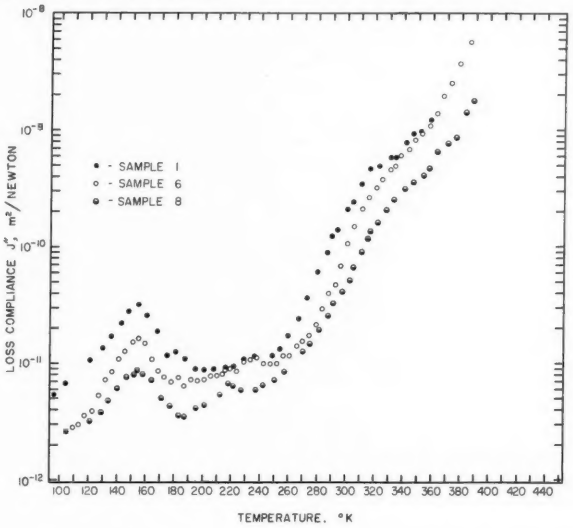

FIGURE 8. *Loss compliance, J'', versus temperature for polyethylene: Sample 1, quenched, unoriented; Sample 6, highly oriented; Sample 8, isothermally crystallized, unoriented.*

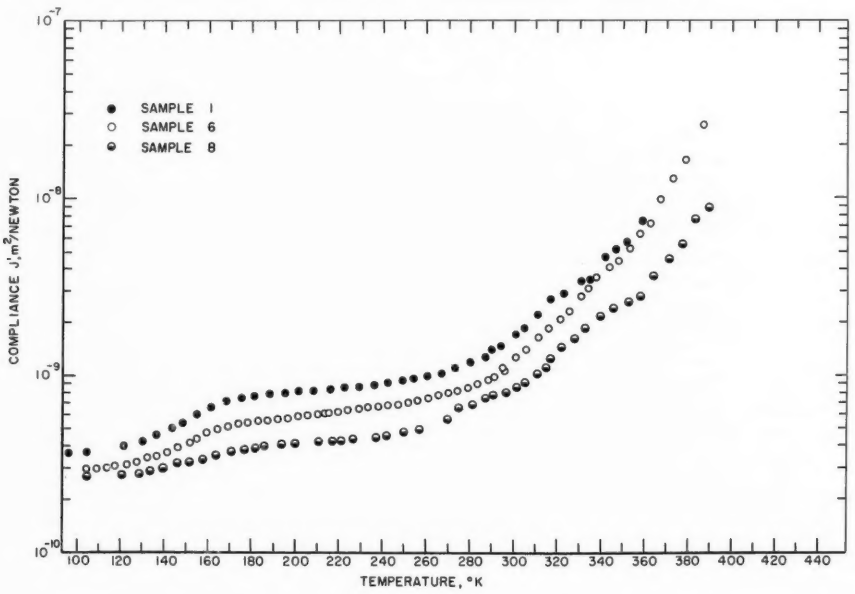

FIGURE 9. *Storage compliance, J', versus temperature for polyethylene: Sample 1, quenched, unoriented; Sample 6, highly oriented; Sample 8, isothermally crystallized, unoriented.*

5. Other Viscoelastic Functions

It can be seen from figure 4 that G'' is not strongly dependent upon morphological factors, and that except in the β and α' regions all the samples are nearly the same. It has been pointed out [1] however that the relationship of extent of relaxation to density and other morphological factors depends upon whether the various samples are compared at constant macroscopic stress or macroscopic strain. This comes about because crystalline polymers are mechanically composite systems consisting of a reasonably well-ordered crystalline phase and less well-defined interlamellar regions which may partake of some of the characteristics of an amorphous phase. In the case of polypropylene [1], for instance, one can come to opposite conclusions about the site, if not the nature, of the relaxation process depending upon whether one compares samples of different morphologies at constant strain by considering the behavior of G'', or at constant stress by considering J'', the shear loss compliance.

We have, therefore, shown in figures 8 and 9 J'' and J' for samples 1, 6, and 8. All the other samples fall within the two extremes represented by samples 1 and 8. It is to be noted that whereas on the G'' plot (fig. 4) the curves were nearly coinsident in the α and γ regions but separated in the β region, the opposite is now true. The curves are more nearly coincident in the β region but separated in the α and γ regions. Moreover, whereas on the G'' plot the curve for sample 8 was higher in the α region but lower in the γ than for sample 1, it is now lower throughout the whole temperature range.

Finally, it should be mentioned that, although not shown, an effect due to orientation is also reflected in J'' if the data for all the samples are considered. Unfortunately however, J'' does not show a definite peak in the region of the α process as in the case of G'', and the relaxation appears only as a small shoulder on a rapidly increasing background. Consequently, no conclusions can be drawn from the J'' data as to how the relaxation peak varies with variations in the degree of lamella orientation.

It is clear that if one were to consider this behavior on a simple two-phase model, one could again come to quite different conclusions regarding the site of the relaxation process. In actual fact Illers [10] has shown that no "amorphous phase" is necessary for the presence of α and γ relaxations and any explanation of the behavior of the curves in figures 4 and 8 must await the solution of the complex mechanical problem involved in the deformation of a crystalline polymer.

6. References

[1] Passaglia, E., and G. M. Martin, J. Res. NBS **68A**, No. 5, 519 (1964).
[2] King, J. C., Bell System Tech. J. **38**, 573 (1959).
[3] King, J. C., Phys. Rev. **109**, No. 5, 1552 (1958).
[4] Wachtman, J. B., Jr., Phys. Rev. **131**, 517 (1963).
[5] Takayanagi, M., Mem. Fac. Eng., Kyushu Univ. **23**, 41 (1963).
[6] Fujiwara, Y., and T. Seto, Annual Meeting of the Society of Polymer Science, Japan, May 27, 1962.
[7] Brown, R. G., and R. K. Eby, J. Appl. Phys. **35**, 1156 (1964).
[8] Passaglia, E., SPE Transactions **4**, No. 3, 1 (1964).
[9] Swan, P. R., J. Poly. Sci. **56**, 403 (1962).
[10] Illers, K. H., Rheologica Acta, Band 3, Heft 4, Seite 202–212 (1964).
[11] Eby, R. K., and J. P. Colson, Paper presented at the 67th Annual Meeting of the Acoustical Society of America, June 1964, Abstracted in the J. Acoust. Soc. Am. **36**, 1041 (1964).
[12] Flocke, A. H., Kolloid Zeitschrift and Zeit. Fur Polymere, Band 180, Heft 2, Seite 118–126 (1961).

(Paper 70A3–398)

JOURNAL OF RESEARCH of the National Bureau of Standards—A. Physics and Chemistry
Vol. 70A, No. 3, May-June 1966

Pentafluorophenyl Alkyl and Vinyl Ethers[1]

Walter J. Pummer and Leo A. Wall

Institute for Materials Research, National Bureau of Standards, Washington, D.C.

(February 16, 1966)

The synthesis of various derivatives of pentafluorophenetole of the type $C_6F_5OCH_2CH_2R$ is described. The R group was chlorine, bromine, hydroxyl, pentafluorophenoxy, acetoxy, and trifluoroacetoxy. 2-Pentafluorophenoxy-1,1,1-trifluoroethane and 1,1-bis(pentafluorophenoxy)ethane were similarly synthesized. A study was made of the behavior of these ethers toward pyrolysis, acids, and bases. In general, those ethers containing β-hydrogen atoms give pentafluorophenol on pyrolysis. Some compounds, such as 2-pentafluorophenoxyethyl bromide, give rearranged products as well. Under basic conditions, cleavage to pentafluorophenol was observed with aqueous potassium hydroxide, whereas the use of solid potassium hydroxide pellets gives dehydrohalogenated products. Concentrated sulfuric acid causes cleavage of most of the ethers employed. 2-Pentafluorophenoxy-1,1,1-trifluoroethane resists attack both by acids and bases.

The synthesis and polymerization of two new vinyl monomers, pentafluorophenyl vinyl ether and 1,2-difluorovinyl pentafluorophenyl ether, are also presented.

Key Words: Ethers, pentafluorophenyl, pentafluorophenoxy, alkyl, vinyl, difluorovinyl, polymerization, and pyrolysis.

1. Introduction

In a previous report [1],[2] we have described the synthesis and polymerization of phenyl trifluorovinyl ether and pentafluorophenyl trifluorovinyl ether. Although these low molecular weight polymers were not exceptionally stable thermally, the complex mechanism by which these polymers decompose was of interest. To aid in the elucidation of this decomposition, two new monomers were synthesized—(1) pentafluorophenyl vinyl ether and (2) 1,2-difluorovinyl pentafluorophenyl ether. The pyrolysis of these polymers, along with that of model compounds, would yield information regarding the relative ease with which hydrogen fluoride or pentafluorophenol (probable breakdown products) are removed from various positions in the polymer chain as the possible first step leading to degradation.

2. Pentafluorophenyl Alkyl Ethers

The pentafluorophenyl alkyl ethers were synthesized as precursors to pentafluorophenyl vinyl ether. In the past, various derivatives of fluorinated anisoles [2–4] and phenetoles [3, 5] have been prepared by the nucleophilic alkoxide attack on hexafluorobenzene. Similarly, we have synthesized 2-pentafluorophenoxy-1,1,1-trifluoroethane from hexafluorobenzene and sodium trifluoroethoxide using tetrahydrofuran as the solvent. In an attempt to prepare 2-pentafluorophenoxyethyl bromide by this procedure, difficulties were encountered in making the salt of 2-bromoethanol. Apparently, the salt readily decomposes to sodium bromide and ethylene oxide. However, 2-pentafluorophenoxyethyl bromide was conveniently synthesized by the reverse reaction, i.e., from potassium pentafluorophenoxide and 1,2-dibromoethane. This reaction was found to proceed more rapidly in *N,N*-dimethylformamide than in tetrahydrofuran. In this reaction, even though a large excess of dibromoethane was employed, a fair amount of 1,2-bis(pentafluorophenoxy)ethane was always isolated. By a similar reaction, attempts to prepare the isomeric 1-bromo-1-pentafluorophenoxyethane failed to yield any of this compound, only the 1,1-bis(pentafluorophenoxy)ethane being isolated. Apparently, when one pentafluorophenoxy group is attached to the carbon atom bearing the bromine atom, the remaining bromine atom is easily displaced by pentafluorophenoxide ion under the basic reaction-conditions. The fact that some free pentafluorophenol was obtained would seem to indicate that some of the pentafluorophenoxide was depleted, due to some dehydrohalogenation reaction.

In a like manner, 2-pentafluorophenoxyethyl chloride was prepared from 1,2-dichloroethane and potassium pentafluorophenoxide. Only the monochloro derivative was obtained in this reaction.

2-Pentafluorophenoxyethanol was also synthesized by this method from 2-bromoethanol and potassium pentafluorophenoxide, except that, in this case, tetrahydrofuran served satisfactorily as the reaction medium. This compound, 2-pentafluorophenoxyethanol, was recently [7] prepared from hexafluorobenzene and ethylene glycol in the presence of sodium hydroxide.

[1] Based on research supported by the Bureau of Naval Weapons, Department of the Navy. Presented before the Division of Fluorine Chemistry at the 148th ACS Meeting, Chicago, Ill., August 1964.

[2] Figures in brackets indicate the literature references at the end of this paper.

Both the acetate and trifluoroacetate of 2-pentafluorophenoxyethanol were prepared in high yield by refluxing the alcohol and the appropriate anhydride for 1 hr.

Since pentafluorophenoxide is considered a weak nucleophile [4, 6], the choice of either tetrahydrofuran or *N,N*-dimethylformamide as the solvent for these reactions appears to depend on the relative activity of the halide to be replaced. For example, at 90 °C in *N,N*-dimethylformamide, the reaction between pentafluorophenoxide and 1,2-dibromoethane is essentially complete in a few hours, whereas the yield of product on refluxing in tetrahydrofuran for 18 hr was only 10 percent.

3. Pentafluorophenyl Vinyl Ether

Phenyl vinyl ether [8–10] and pentachlorophenyl vinyl ether [11–13] have been prepared previously, usually by the base-catalyzed addition of phenol or pentachlorophenol to acetylene. We have now extended this reaction to pentafluorophenol. Pentafluorophenyl vinyl ether can be prepared in 50 percent yield by this method. The reaction temperature was 200 °C, and a fair excess of acetylene was used to control the by-products, mainly 1,1-bis(pentafluorophenoxy)ethane. Previously, methanol [11] and water [12] were the preferred solvents. To prevent possible exchange reactions between potassium pentafluorophenoxide and protonic solvents at high temperature, we have used *N,N*-dimethylacetamide for this reaction with equal success.

Although the above method for the synthesis of pentafluorophenyl vinyl ether was satisfactory, we have also investigated alternative methods of preparation. These methods included dehydrohalogenation or cleavage of various substituted alkyl ethers by pyrolytic means or basic reagents, or both. These reactions also gave valuable information regarding the relative stability of the fluoroaryl ethers under these conditions. Furthermore, these compounds may serve as model compounds in studying the decomposition products obtained from the pyrolysis of the polymeric fluoroaryl vinyl ethers.

4. Pyrolysis

The pyrolysis of a number of these fluoroaryl ethers having various substituents on the alkyl side-chain was performed in a flow system using glass helices, charcoal pellets, or 20 percent potassium hydroxide–charcoal pellets as the column packing. Temperatures ranged from 400 to 600 °C. Usually, atmospheric pressure was maintained, but in a few cases, the pyrolysis was done under reduced pressure. The conditions and the results of the pyrolyses of these pentafluorophenyl ethers are listed in table 1. For the most part, the pyrolyses appear to follow the paths as outlined in eqs 1 and 2.

$$C_6F_5{-}O{-}CH_2{-}CH_2R \longrightarrow \begin{cases} C_6F_5OH + CH_2{=}CHR & (1) \\ C_6F_5OCH{=}CH_2 + HR. & (2) \end{cases}$$

In general, more pentafluorophenol than pentafluorophenyl vinyl ether was found in the pyrolyzates. The proportion of each compound appears to depend on the nature of the *R* group, as well as on the temperature employed in the pyrolysis. At no time have these pyrolyses shown any definite trend in any one direction, i.e., in preferred scission to pentafluorophenol (except where no β-hydrogen atoms are present) or pentafluorophenyl vinyl ether. The distribution of products seems to indicate that random scissions occur according to eqs 1 and 2. The pyrolysis products were further complicated by competing secondary reactions, which appeared to yield products which were simple addition products of the olefin formed from the initial pyrolysis, as shown in eqs 3 and 4 (or various combinations thereof),

$$\left.\begin{array}{l} CH_2{=}CHR + C_6F_5OH \\ C_6F_5OCH{=}CH_2 + HR \end{array}\right\} \longrightarrow C_6F_5O\underset{\displaystyle R}{\underset{|}{C}}H{-}CH_3, \quad \begin{matrix} (3) \\ (4) \end{matrix}$$

This was especially evident in the case of the bromine derivative (table 1, R = Br). The large proportion of 1-bromo-1-pentafluorophenoxyethane formed in this pyrolysis would seem to indicate that both types of reaction (eqs 3 and 4) had occurred.

TABLE 1. *Pyrolysis of* $C_6F_5OCH_2CH_2R$

R	Wt	Packing[a]	Temp	Press	Wt recovered	Products (VPC)
	g		*C°*	*mm*	*g*	
Br	3	A	500	760	2.5	37% $C_6F_5OCHBrCH_3$; 19% C_6F_5OH; 15% $C_6F_5OCH{=}CH_2$; 4% $C_6F_5OCH_2CH_2Br$; 2% $(C_6F_5O)_2CHCH_3$.
Cl	1	A	520	760	0.75	70% $C_6F_5OCH_2CH_2Cl$; 5% C_6F_5OH; 5% $C_6F_5OCH{=}CH_2$; 1% $C_6F_5OCClHCH_3$.
OAc	1.3	A	560	760	.9	35% C_6F_5OH; 20% $C_6F_5OCH{=}CH_2$; 15% CH_3CO_2H; 20% 7-products.
OAc	1.3	A	600	0.8	1.0	75% $C_6F_5OCH_2CH_2OAc$; 10% C_6F_5OH; 3% $C_6F_5OCH{=}CH_2$; 2% CH_3CO_2H.
CF_3CO_2	2	A	540	25	1.6	70% $C_6F_5OCH_2CH_2OAcF_3$; 25% C_6F_5OH. CF_3CO_2H, $C_6F_5OCH{=}CH_2$.
OC_6F_5	3	A	480	760	2.6	70% $C_6F_5OCH_2CH_2OC_6F_5$; 14% C_6F_5OH.
OH	5	B	420	760	2.0	99% C_6F_5OH.
OH	3	B	300	760	1.2	99% C_6F_5OH.
OH	2	$KHSO_4$	220	50	1.7	No reaction.

[a]Key: A, glass helices; B, Al_2O_3 pellets.

At 500 °C, the chlorine analog (table 1, R = Cl) is more stable than the bromine derivative, as a result, conversion was much lower. However, pentafluorophenol and pentafluorophenyl vinyl ether were formed in approximately equal quantities, along with a trace of 1-chloro-1-pentafluorophenoxyethane.

From the pyrolysis of the acetate (table 1, R = OAc), pentafluorophenol was usually the main product, with lesser quantities of the pentafluorophenyl vinyl ether and acetic acid, along with traces of five other products (unidentified). When the acetate was pyrolyzed under reduced pressure at different temperatures, no significant change in product distribution was observed, except that conversions were lower. At the same pressure (0.8 mm), a rise in the temperature from 550 to 600 °C simply increased the yield of pentafluorophenol, so higher temperatures were not further investigated. At a higher pressure (25 mm) and 540 °C, the pyrolysis of the acetate gave essentially the same products as observed at atmospheric pressure and 560 °C. The above acetate pyrolyses agree to some extent with those reported for 2-phenoxyethyl acetate [10]. In our case, the yield of pentafluorophenyl vinyl ether is higher and probably reflects the increased stability of the vinyl ether due to the ring fluorine atoms. As expected, no products were obtained which could be attributed to the Claisen [14] rearrangement. Although Ritchie [9] has reported benzaldehyde as one of the breakdown products of 2-phenoxyethyl acetate, we have been unable to isolate any pentafluorobenzaldehyde from the pyrolysis of 2-pentafluorophenoxyethyl acetate.

The pyrolysis of 2-pentafluorophenoxyethyl trifluoroacetate was expected to cause preferential cleavage at the alkyl-trifluoroacetate bond, to yield pentafluorophenyl vinyl ether in greater quantity. Actually, the additional fluorine atoms stabilized the compound, in as much as only 30 percent conversion to products was obtained at 540 °C/25 mm pressure. Pentafluorophenol, pentafluorophenyl vinyl ether, and trifluoroacetic acid were formed in almost equal amounts. Since no selective cleavage was encountered, further pyrolyses of the acetates were not pursued.

The pyrolysis of 2-pentafluorophenoxyethanol (table 1, R = OH) over alumina at 300 or 420 °C resulted in the formation of pentafluorophenol and acetaldehyde. No dehydration to pentafluorophenyl vinyl ether was observed. Similar results have been reported [10] for 2-phenoxyethanol.

Potassium acid sulfate at 220 °C failed to dehydrate the alcohol, and no product other than 2-pentafluorophenoxyethanol was recovered.

In an attempt to explain some of the foregoing results, especially the formation of rearranged products, some additional pyrolyses were performed on compounds containing the pentafluorophenoxy group (table 2A). For comparison, some hydrocarbon samples (table 2B) were also included. It was first believed that some of the products were breakdown products of pentafluorophenyl vinyl ether. However, this compound (table 2A, R = $CH{=}{=}CH_2$) does not show any appreciable decomposition until it is heated to 600 °C. Similarly, it was thought that 1,1-bis(pentafluorophenoxy)ethane (table 2A, R = $-\overset{OC_6F_5}{\underset{|}{C}}HCH_3$), formed from the pyrolysis of 2-pentafluorophenoxyethyl bromide (table 1, R = Br), was produced by the addition of pentafluorophenol to pentafluorophenyl vinyl ether (eq 4, R = C_6F_5O-). However, the pyrolysis of a 50 percent mixture of the two (table 2A, R = $CH{=}{=}CH_2$ and H) gave only starting materials. This mode of addition is not entirely without merit, since it was subsequently shown that 1,1-bis(penta-

TABLE 2. *Comparison of the pyrolyses of* C_6F_5OR *and* C_6H_5OR

R	Wt	Packing[b]	Temp	Wt recovered	Products
			A. Pyrolysis of C_6F_5OR[a]		
	g		*°C*	*g*	
$CH{=}{=}CH_2$	2	A	500	1.7	90% $C_6F_5OCH{=}{=}CH_2$; 5% C_6F_5OH
$CH{=}{=}CH_2$	2	A	600	1.6	60% $C_6F_5OCH{=}{=}CH_2$; 25% C_6F_5OH
CH_3	2	A	525	1.6	95% $C_6F_5OCH_3$; 2% C_6F_5OH
CH_2CH_3	2	A	525	1.4	60% $C_6F_5OCH_2CH_3$; 25% C_6F_5OH; 10% others
$CH{=}{=}CH_2$	0.8	A	525	1.6	50% $C_6F_5OCH{=}{=}CH_2$; 50% C_6F_5OH
H	1.0				
$\overset{OC_6F_5}{\underset{|}{C}}HCH_3$	2.5	A	520	2.0	49% C_6F_5OH; 49% $C_6F_5OCH{=}{=}CH_2$; 2% $(C_6F_5O)_2CH{-}CH_3$
CH_2CF_3	2	A	500	1.8	80% $C_6F_5OCH_2CF_3$; 5% $C_6F_5OCH{=}{=}CF_2$; 5% 7-products
CH_2CF_3	3	B	460	2.5	100% $C_6F_5OCH_2CF_3$
			B. Pyrolysis of C_6H_5OR[a]		
CH_2CH_3	2	A	525	1.5	98% $C_6H_5OCH_2CH_3$
$CH{=}{=}CH_2$	2	A	520	1.6	60% $C_6H_5OCH{=}{=}CH_2$; 25% C_6H_5OH
CH_2CH_2Br	25	A	400	20	98% $C_6H_5OCHBr{-}CH_3$

[a] All at atmospheric pressure.
[b] Key: A, glass helices; B, charcoal pellets.

fluorophenoxy)ethane (table 2A, $R = -\overset{OC_6F_5}{\underset{|}{C}}HCH_3$) decomposes almost quantitatively to pentafluorophenol and pentafluorophenyl vinyl ether. The high yield of olefin formed in this pyrolysis was similar to that obtained by Reppe [11] for 1,1-diethoxyethane.

The other rearranged product obtained from the pyrolysis of 2-pentafluorophenoxyethyl bromide (table 1, R = Br) was 1-bromo-1-pentafluorophenoxyethane. Simply, this compound may have been formed as visualized in eqs 3 and 4. As yet, this has not been proved experimentally. The instability of α-halo ethers is well known. Surprisingly, the pyrolysis of 2-phenoxyethyl bromide (table 2B, R $= CH_2CH_2Br$) gave only the 1-bromo-1-phenoxyethane as the main product, similar to the behavior in the fluorocarbon series. The two isomeric bromides (hydrocarbon) differ greatly in chemical properties and can readily be distinguished by their behavior with water at room temperature. 1-Bromo-1-phenoxyethane decomposes spontaneously into a red resinous product, with the liberation of hydrogen bromide, by the addition of a trace of water. On the other hand, the 2-bromo derivative has little tendency toward this type of reaction. In the fluorocarbon series, 1-bromo-1-pentafluorophenoxyethane does not exhibit this readiness to react with water, unlike the hydrocarbon analog. However, on storage at 25 °C in the dark for several weeks, the 1-bromo-1-pentafluorophenoxyethane decomposes to a blackish mass. Unfortunately, 1-bromo-1-pentafluorophenoxyethane was not obtained in the pure state, so that its thermal stability has not been recorded.

5. Discussion

From the results of the pyrolysis of the fluoroaryl ethers listed in table 1, some generalizations are apparent. In these cases, where the reaction path could have proceeded in two directions, i.e., according to eqs 1 and 2, pentafluorophenol was usually obtained in greater quantity. The conversion into products at the temperatures employed also serves as a measure of the thermal stability of the alkyl fluoroaryl ethers. The results in tables 1 and 2 indicate that the pentafluorophenoxy group is a more effective leaving group when in competition with the other functional groups (R) shown. This effect appears to be associated with the number and activity of the β-hydrogen atoms in the molecule. In the pyrolysis of 2-pentafluorophenoxy-1,1,1-trifluoroethane (table 2A, $R = CH_2CF_3$) (a compound containing only α-hydrogen atoms with no hydrogen atoms β to the oxygen atom), no cleavage to pentafluorophenol was observed, but only dehydrofluorination to the olefin. Similarly, where the β-hydrogen atoms are attached to a double bond, as in pentafluorophenyl vinyl ether (table 2A, $R = CH=CH_2$), pentafluorophenol is formed at higher temperatures. However, pentafluorophenetole (table 2, $R = CH_2CH_3$) containing three β-hydrogen atoms, yields pentafluorophenol at lower temperatures. Pentafluoroanisole also yields a trace of pentafluorophenol, even though no β-hydrogen atoms are available (probably a bimolecular reaction, similar to that of anisole [15]).

In the case of the isomeric bis(pentafluorophenoxy) ethanes (1,2 table 1, $R = OC_6F_5$ and 1,1 table 2A, $R = -\overset{OC_6F_5}{\underset{|}{C}}HCH_3$), the position of the R group has a decided effect on the course of pyrolysis. Each pentafluorophenoxy group in the 1-position has three available β-hydrogen atoms for reaction, whereas, in the 1,2-derivative, each pentafluorophenoxy group has only two. On this basis, the 1,1-derivative would be the less stable. Also, the 1,1-derivative is an acetal containing two bulky groups, a situation which is in itself conducive to thermal decomposition at lower temperatures.

A considerable amount of data is available in the literature concerning the pyrolysis of ethers [9, 10, 15, 16], as well as of other types of compounds, such as esters, halides, and amides. The decomposition is for the most part considered to be unimolecular, and a cyclic mechanism was proposed [16]. Later work by Bailey [17, 18] and others [19] has shown the cyclic process to be the preferred route. Bailey [18] views the pyrolysis of vinyl ethers to occur as follows:

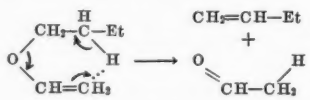

(5)

Certainly, a similar mechanism may be written for the fluoroaryl ethers,

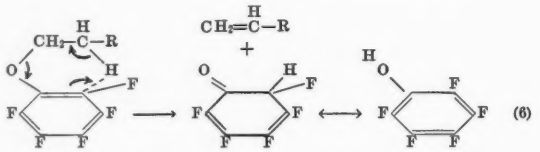

(6)

An alternative mechanism may be written for the fluoroaromatic ethers, as follows:

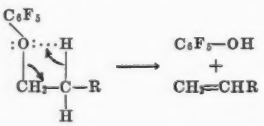

(7)

This is similar to the mechanism for the decomposition of alkyl halides proposed by Maccoll [20]. In this case, the pentafluorophenyl group is not involved in the transfer of electrons, thereby preserving aromaticity; but a four-membered ring supersedes the more-favored six-membered ring. At present, since both mechanisms involve β-hydrogen atoms, the products may

be explained by either. The fact that no fluorophenols containing ring-hydrogen atoms were produced would indicate that hydrogen rather than fluorine migration occurs in eq 6, which is expected. The pyrolysis of a more varied group of ethers would be required in order to permit us to ascertain fully which mechanism in predominant.

The mechanism for the pyrolysis of the aryl perfluoroalkyl ethers is different from that reported here for the alkyl fluoroaryl ethers. Sheppard [21] has pyrolyzed a number of ethers (such as phenyl pentafluoroethyl ether), and has found that one of the primary pyrolytic products is biphenyl (not phenol). In these cases, cleavage occurs at the phenyl–oxygen link, not the alkyl–oxygen bond. The fact that fluorobenzene was also reported as one of the products at higher temperatures (625 °C) would indicate that the mechanism(s) for the decomposition of the aryl perfluoroalkyl ethers are more complex than those of the decomposition of the alkyl fluoroaryl ether type.

6. Basic Reagents

The reactions of some alkyl fluoroaryl ethers with potassium hydroxide are listed in table 3. These ethers could have reacted in any of several ways—(a) dehydrohalogenation to an olefin, (b) cleavage at the ether oxygen atom to a phenol, (c) attack on the ring fluorine atoms, or (d) various combinations of these. Information regarding the stability of these alkyl fluoroaryl ethers towards basic reagents may aid in elucidating the cleavage reaction found when pentafluoroanisole is treated with ammonia [4] or when the fluoro-dihydroxy compounds are obtained from the reaction of hexafluorobenzene with alcoholic potassium hydroxide [3]. From the limited number of reactions attempted, only the pentafluorophenoxyethyl bromide shows any reactivity below 200 °C.

TABLE 3. *Reaction of* C_6F_5OR *with some bases*

R	Wt	Base	Temp	Wt recovered	Products
	g	g	°C	g	
CH_2CH_2Br	8.5	KOH (5) paraffin oil (5)	180	3.5	86% $C_6F_5OCH_2CH_2Br$, 14% C_6F_5OH.
CH_2CH_2Br	3	KOH (5) K_2CO_3 (10)	200	1.2	50% $C_6F_5OCH_2CH_2Br$, 50% $C_6F_5OCH{=}CH_2$.
CH_2CH_2Br	5	KOH (5) H_2O (20)	100	4.0	62% $C_6F_5OCH_2CH_2Br$, 37% C_6F_5OH.
CH_2CH_2Br	5	Collidine	160	3.0	83% $C_6F_5OCH_2CH_2Br$, 16% $C_6F_5OCH{=}CH_2$.
OC_6F_5 | $-CHCH_3$	0.4	KOH (1) H_2O (5)	100	0.3	No reaction.
CH_2CF_3	8.5	KOH (5) K_2CO_3 (10)	200	8.0	No reaction.
CH_2CF_3	1.4	MgO (5)	150	1.3	No reaction.
CH_2CF_3	20	20% KOH/charcoal	480	16	80% $C_6F_5OCH_2CF_3$, 15% $C_6F_5OCH{=}CF_2$.
CH_2CF_3	2	20% KOH/charcoal	550	.....	Decomposed.
CF_2CF_2H	2	20% KOH/charcoal	550	.....	Decomposed.

In this case, cleavage to pentafluorophenol is the main route, when potassium hydroxide and water (or paraffin oil) are used. Dehydrohalogenation was the preferred course with solid potassium hydroxide pellets, yielding pentafluorophenyl vinyl ether. Similar results were obtained by Corley [22] with the latter reagent and with 2-chloro-1,1,2-trifluoroethyl phenyl ether. Here again, as proposed earlier [4], it appears that aqueous, basic systems preferentially lead to aryl ether cleavage. All of the ethers, the synthesis of which is described in this article, along with those prepared previously [4], were prepared in basic, nonaqueous solvents, and yet, little cleavage of the ether was observed.

2-Pentafluorophenoxy-1,1,1-trifluoroethane (table 3, $R = CH_2CF_3$) failed to react either with solid potassium hydroxide or magnesium oxide at 200 °C. Some olefin was formed by the use of 20 percent potassium hydroxide mounted on charcoal pellets at 480 °C. Higher temperatures decomposed the compound; this decomposition was also observed for 2-pentafluorophenoxy-1,1,2,2-tetrafluoroethane (table 3, $R = CF_2—CF_2H$).

The stability of 1,1-bis(pentafluorophenoxy)ethane toward aqueous potassium hydroxide was unexpected in view of the acidic hydrogen atom present because of the effect of the pentafluorophenoxy groups attached to the same carbon atom. This behavior toward aqueous bases is more analogous to that of such compounds as difluoromethyl ethyl ether [23] or difluoromethyl phenyl ether [24], rather than to that of an acetal.

7. Reactions in Acid

From the preceding sections, data were obtained regarding the stability of these fluoroaryl ethers under pyrolysis conditions or toward basic reagents. It was desired, therefore, to obtain data concerning their reactivity with sulfuric acid. Pentafluoroanisole [3] was shown to be cleaved with hydriodic acid to pentafluorophenol. Later, hydrobromic or aluminum chloride [25] was also found effective for this reaction. Recently, Tatlow and coworkers [26] have shown that 4-(trifluoromethyl)-2,3,5,6-tetrafluorophenetole cannot be cleaved preferentially without reaction at another part of the molecule [primarily due to the *p*-(trifluoromethyl) group]. Most of the ethers listed in table 4 are cleaved to pentafluorophenol under the reaction conditions. Only 2-pentafluorophenoxy-1,1,1-trifluoroethane (table 4, $R = CH_2CF_3$) failed to yield any product. The stability of this compound is probably associated with the decrease in basicity of the oxygen linkage due to the added trifluoromethyl group. Cleavage of ethers by acids is usually preceded by oxonium salt formation. The fact that 1,1-bis(pentafluorophenoxy)ethane (table 4, $R = —\overset{OC_6F_5}{\underset{}{\overset{|}{C}}}HCH_3$) decomposes under these conditions is not surprising, since the trifluoromethyl group is a more effective electronegative group than the pentafluorophenoxy group. As such, the lessening in oxygen basicity is not sufficient to prevent oxonium salt formation and eventual cleavage.

TABLE 4. *Reaction of* C_6F_5OR *with sulfuric acid at 125 °C*

R	Wt	H_2SO_4	Wt recovered	Products
	g	*ml*	*g*	
CH_2CH_2Br	1	7	0.5	99% C_6F_5OH.
CH_2CF_3	3	7	2.7	No reaction.
$CH_2—CH_3$	5	10	3.2	60% C_6F_5OH. 40% $C_6F_5OCH_2CH_3$.
CH_2CH_2OH	1.5	7	1	50% C_6F_5OH. 50% $C_6F_5OCH_2CH_2OH$.
OC_6F_5 | $—CHCH_3$	0.3	1	.....	Decomposed, some C_6F_5OH.

8. Polymerizations

In an earlier report [1], the polymerization of phenyl and pentafluorophenyl 1,1,2-trifluorovinyl ethers was described. Usually, cationic or peroxide-initiated catalysis of the monomers gave little or no polymer. However, by the use of high pressure and γ-irradiation [27], these monomers were converted into low molecular weight polymers ($DP_n \sim 4000$).

In line with the above results, 1,2-difluorovinyl pentafluorophenyl ether failed to yield any polymer with azobis(isobutyronitrile) (ABIN). Thermally (at 110 °C), it appears that only the dimer was formed. As yet, no high-pressure techniques have been employed in the polymerization of this monomer.

Pentafluorophenyl vinyl ether appears to be a more reactive monomer. A white, solid polymer can be obtained from pentafluorophenyl vinyl ether in pentane solution by the use of boron trifluoride gas at −78 °C. After 24 hr under these conditions, the conversion into polymer was 17 percent and the molecular weight (vapor pressure osmometer) was 10,000 (mp 75–88 °C). Higher conversion (30%) and polymers having increased molecular weights (17,000) were obtained by longer storage times (7 days) at −78 °C and by periodic addition of the catalyst, boron trifluoride–water. Some observations made during this latter process appear to indicate that the proportion of the co-catalyst (water) has more effect on the conversion into polymers than either an excess of boron trifluoride or longer reaction times. After 3 days, the amount of polymer formed is approximately the same as after the 24-hr period, but polymer formation again appears to increase when additional water or moisture is introduced. The polymer obtained in this fashion (17,000 mol wt) was a hard, white solid. It is soluble in benzene, hexafluorobenzene, and acetone. The polymer is insoluble in methanol and in water. Also, the melting point, 55 to 60 °C, is lower than that of the polymer of 10,000 mol wt.

Aluminum chloride and pentafluorophenyl vinyl ether in bulk at 35 °C gave only blackish tars. However, a low molecular weight polymer was obtained when the polymerization was performed in benzene solution at 80 °C. Methanol was used to precipitate the polymer. The molecular weight was 2300 as determined with a vapor-pressure osmometer (benzene as solvent). The polymer thus obtained was a yellow glass which melted over the range 120 to 180 °C. The low molecular weight of the polymer is in accord with recent observations [28] concerning the polymerization of various mono- and di-halogenated phenyl vinyl ethers.

Cationic reagents, such as concentrated hydrobromic acid, have no effect on pentafluorophenyl vinyl ether. This is in contrast to the behavior of phenyl vinyl ether, which yields resinous materials after a slight induction period. Similar material was obtained by the addition of water to 1-bromo-1-phenoxyethane.

Again, by the use of high pressure (9500 atm) and γ-irradiation (0.009 Mr/hr) at 105 °C for 68 hr, a poly (pentafluorophenyl vinyl ether) having a molecular weight of 30,000 (vapor-pressure osmometry) was obtained in low yield. The polymer was a fluffy, pink solid, softening at 95 °C and melting below 150 °C.

Pyrolysis of the poly(pentafluorophenyl vinyl ether), 17,000 mol wt, at 300 °C for 1 hr resulted in a 43.2 percent weight loss, and yielded mainly pentafluorophenol and a dark-brown glassy residue. The low order of thermal stability of this polymer was in accord with the results obtained from the pyrolysis of the smaller molecule.

$$\sim\!\!\sim CH(O{-}C_6F_5){-}CH_2\sim\!\!\sim \xrightarrow[\Delta]{} \sim\!\!\sim CH{=}CH_2\sim\!\!\sim + C_6F_4OH \quad (8)$$

The thermal stability of the poly(phenyl trifluorovinyl ether), 4,000 mol wt [29], was shown to be greater than that of the poly(pentafluorophenyl vinyl ether) reported here. Since there are no hydrogen atoms on the polymer backbone in the former, phenol cannot be readily removed. However this polymer loses hydrogen fluoride quite readily, and this is followed by cross-linking and carbonization. Presumably, the removal of hydrogen fluoride is an intermolecular process. From the preceding evidence, it is, therefore, reasonable to assume that the poly(pentafluorophenyl 1,1,2-trifluorovinyl ether) prepared previously [1] should have good thermal stability, since there is no ready route to decomposition as experienced above, especially in the absence of hydrogen atoms. The difficulty still remains in producing polymers of high molecular weight.

9. Experimental Procedure

Infrared spectra were obtained with a Perkin-Elmer "Infracord," Model 137B spectrophotometer,[3] using a 0.025-mm sodium chloride cell for liquid samples, or pellets containing 1-2 mg of the solid sample in 300 mg of potassium bromide. Molecular-weight

[3] Certain commercial materials and equipment are identified in this paper in order to adequately specify the experimental procedure. In no case does such identification imply recommendation or endorsement by the National Bureau of Standards, nor does it imply that the material or equipment identified is necessarily the best available for the purpose.

determinations were made by vapor-pressure osmometry, using a 1-percent solution of the polymer in benzene.

9.1. 2-Pentafluorophenoxyethyl Bromide

a. In N,N-Dimethylformamide

A solution of 50 g (0.23 mole) of potassium pentafluorophenoxide in 100 ml of *N,N*-dimethylformamide was added to a solution of 50 g (0.27 mole) of 1,2-dibromoethane in 100 ml of *N,N*-dimethylformamide maintained at 90 °C. After a slight induction period, potassium bromide began to be precipitated and this increased with time. When the addition was complete (0.5 hr), the contents were refluxed for 2 hr, cooled, and poured into 500 ml of water. The bottom layer was separated and dried ($CaSO_4$). Distillation of the products afforded 30 g (46%) of 2-pentafluorophenoxyethyl bromide, (bp 112 °C/10 mm, $n_D^{20} = 1.4647$) and 9.82 g (11%) of 1,2-bis(pentafluorophenoxy)ethane (bp 108–110 °C/0.8 mm, mp 31–32 °C).

Analysis: Calculated for $C_8H_4BrF_5O$: C, 33.0; H, 1.4; F, 32.7; Br, 27.5. Found: C, 33.6; H, 1.3; F, 31.0; Br, 24.5.

Analysis: Calculated for $C_{14}H_4F_{10}O_2$: C, 42.9; H, 1.0. Found: C, 42.8; H, 1.3.

b. In Tetrahydrofuran

A solution of 11 g (0.05 mole) of potassium pentafluorophenoxide and 19 g (0.1 mole) of 1,2-dibromoethane in 100 ml of tetrahydrofuran was refluxed for 18 hr. Very little potassium bromide was noticed. At the end of this time period, the mixture was cooled and poured into 200 ml of water. The bottom layer was separated, dried ($CaSO_4$), and distilled. After removal of 10 g of recovered 1,2-dibromoethane, 1.5 g (10.4%) of 2-pentafluorophenoxyethyl bromide was obtained. No 1,2-bis(pentafluorophenoxy)ethane was isolated from this reaction.

9.2. 2-Pentafluorophenoxyethyl Chloride

To 18 g (0.2 mole) of 1,2-dichloroethane in 25 ml of *N,N*-dimethylformamide at 80 °C was added 5 g (0.025 mole) of potassium pentafluorophenoxide in 25 ml of *N,N*-dimethylformamide. When the addition was complete (0.5 hr), the mixture was refluxed for 1 hr, cooled, and diluted with 150 ml of water. The usual isolation and distillation gave 3.1 g (56%) of 2-pentafluorophenoxyethyl chloride, bp 74–75 °C/2 mm; $n_D^{20} = 1.4442$.

Analysis: Calculated for $C_8H_4ClF_5O$: C, 39.0; H, 1.6; Cl, 14.3. Found: C, 40.1; H, 1.9; Cl, 12.9.

9.3. 1,1-Bis(pentafluorophenoxy)ethane

To 21.9 (0.11 mole) of 1,1-dibromoethane in 25 ml of *N,N*-dimethylformamide at 90 °C was added 5 g (0.025 mole) of potassium pentafluorophenoxide in 25 ml of *N,N*-dimethylformamide. After the addition (0.25 hr), the solution was refluxed for 4 hr, cooled, and diluted with 150 ml of water. The usual processing, followed by distillation, yielded 0.9 g (10%) of 1,1-bis(pentafluorophenoxy)ethane, bp 84 to 85 °C/0.6 mm, mp 25–27 °C.

Analysis: Calculated for $C_{14}H_4F_{10}O_2$: C, 42.7; H, 1.0. Found: C, 43.4; H, 1.5.

9.4. 2-Pentafluorophenoxy-1,1,1-trifluoroethane

To 100 g (1 mole) of 1,1,1-trifluoroethanol in 250 ml of tetrahydrofuran, 22.9 g (1 g-atom) of sodium was added in small pieces. When the evolution of hydrogen had ceased, the solution was added dropwise to a solution of 250 g (1.35 moles) of hexafluorobenzene in 125 ml of pyridine, maintained at 80 °C. When the addition was complete (2 hr), the mixture was refluxed for 2 hr. The mixture was cooled, and filtered from the sodium fluoride. The filtrate was poured into 500 ml of 10 percent hydrochloric acid. The bottom layer was separated and dried ($CaSO_4$). Distillation afforded: 82 g (33%) of recovered hexafluorobenzene; 159 g (66.2%, based on recovered C_6F_6) of 2-pentafluorophenoxy-1,1,1-trifluoroethane, bp 146.5–147 °C; $n_D^{23} = 1.3799$; and 34 g (10.9% based on recovered C_6F_6) of 1,4-bis(1,1,1-trifluoroethoxy)tetrafluorobenzene, bp 111 to 113 °C/10 mm, mp 67 to 69 °C.

Analysis: Calculated for $C_8H_2F_8O$: C, 36.3; H, 0.76; F, 57.2. Found: C, 36.4; H, 0.7; F, 56.2.

Analysis: Calculated for $C_{10}H_4F_{10}O_2$: C, 34.8; H, 1.2; F, 55.0. Found: C, 34.8; H, 1.2; F, 53.9.

9.5. Pentafluorophenetole

Pentafluorophenetole was prepared in much the same manner as reported previously [5], except that the following quantities were used: 150 ml of absolute ethanol, 150 ml of tetrahydrofuran, 22.9 (1 g-atom) of sodium metal, 250 g (1.35 moles) of hexafluorobenzene, and 125 ml of pyridine. Pentafluorophenetole was obtained in 74 percent yield (144 g), bp 152 to 153 °C, $n_D^{23} = 1.4120$.

9.6. 2-(Pentafluorophenoxy)ethanol

A solution of 25 g (0.2 mole) of 2-bromoethanol in 25 ml of tetrahydrofuran was added to a solution of 36 g (0.16 mole) of potassium pentafluorophenoxide in 100 ml of tetrahydrofuran at 64 °C. The mixture was refluxed for 3 hr and cooled. The usual processing afforded 16 g (53%, based on recovered C_6F_5OH, 6 g) of 2-(pentafluorophenoxy)ethanol, bp 82 to 83 °C/1.5 mm, $n_D^{23} = 1.4419$. (Reported [7] bp 110 °C/15 mm). In the infrared spectrum, the absorption band (OH frequency) is at 3490 cm^{-1}.

Analysis: Calculated for $C_8H_5F_5O_2$: C, 42.2; H, 2.2. Found: C, 41.6; H, 2.3.

9.7. 2-(Pentafluorophenoxy)ethyl Acetate

To 5 g (0.02 mole) of 2-(pentafluorophenoxy)ethanol and 5 g (0.05 mole) of acetic anhydride was added 0.1 g

of potassium acetate, and the solution was refluxed for 2 hr. The mixture was cooled, and poured into 50 ml of ice water. The solution was neutralized by the addition of saturated sodium hydrogen carbonate solution. The bottom layer was washed with 25 ml of water, separated, dried ($CaCl_2$), and distilled. 2-(Pentafluorophenoxy)ethyl acetate was obtained in 71 percent yield, bp 90–91 °C/1.5 mm, $n_D^{20} = 1.4352$. (In the infrared spectrum there was an absorption band, $>C=O$, at 1740 cm^{-1}.)

Analysis: Calculated for $C_{10}H_7F_5O_3$: C, 45.3; H, 2.6. Found: C, 44.6; H, 2.5.

9.8. 2-(Pentafluorophenoxy)ethyl Trifluoroacetate

This compound was prepared as described above. From 5 g (0.02 mole) of 2-(pentafluorophenoxy)ethanol, 5 g of trifluoroacetic anhydride, and 0.1 g of potassium carbonate, there was obtained 5 g (70%) of 2-(pentafluorophenoxy)ethyl trifluoroacetate, bp 88 to 89 °C/1.5 mm, $n_D^{20} = 1.4048$. (Infrared spectrum showed a band, $>C=O$, at 1780 cm^{-1}.)

Analysis: Calculated for $C_{10}H_4F_8O_3$: C, 37.8; H, 1.24. Found: C, 37.8; H, 1.20.

9.9. Pentafluorophenyl Vinyl Ether

Eighty-two grams (0.45 mole) of pentafluorophenol, 5 g of potassium hydroxide, and 150 ml of *N,N*-dimethylacetamide were placed in a 1400-ml bomb which was then sealed. The bomb was attached to a high-vacuum line by an outlet valve and tubing. After cooling (−190 °C) and evacuating the bomb, 13.62 g (0.61 mole) of acetylene gas was condensed in the bomb, which was then sealed and allowed to warm to 25 °C. The bomb was rocked and heated to 200 °C (at this temperature, the maximum pressure was 160 psi) for 1.5 hr or until no change in pressure was observed. The bomb was cooled and excess acetylene was allowed to escape. The contents was poured into 200 ml of water and extracted several times with 100-ml portions of dichloromethane. The organic layers were combined and dried ($CaSO_4$). After removal of the solvent by distillation, there was obtained 47.4 g (50%) of pentafluorophenyl vinyl ether, bp 141 to 142 °C, $n_D^{20} = 1.4252$. The infrared spectrum shows the olefin bond at 1640 cm^{-1}.

Analysis: Calculated for $C_8H_3F_5O$: C, 45.8; H, 1.44. Found: C, 46.3; H, 1.50. From the residue, 1,1-bis(pentafluorophenoxy)ethane (10%) was obtained; this had the characteristics described earlier. Small amounts of other products were also obtained, but these were not investigated.

9.10. Phenyl Vinyl Ether

This compound was prepared as described by Ritchie [9], from 2-(pentafluorophenoxy)ethyl bromide and potassium hydroxide.

9.11. 1,2-Difluorovinyl Pentafluorophenyl Ether

An 800-ml bomb containing 100 g (0.45 mole) of anhydrous potassium pentafluorophenoxide, 300 ml of dry benzene, and 100 ml of dry ($LiAlH_4$) tetrahydrofuran was attached to a high-vacuum line, cooled (−196 °C), and evacuated. In the bomb was condensed 110 g (1.34 moles) of 1,1,2-trifluoroethylene by means of the vacuum line. The sealed bomb was allowed to warm to 25 °C. It was then rocked and heated to 230 °C, at which temperature the pressure dropped from 1600 psi to 800 psi during 1 hr. The bomb was cooled and opened. The contents was poured into a flask and the liquids were flash-distilled. The residual solids were washed with benzene (100 ml), the benzene layer was combined with the flash distillate, and the liquid was distilled. After the solvents had been removed, there was obtained 36 g of a colorless liquid, bp 133 to 139 °C, which contained 90 percent of 1,2-difluorovinyl pentafluorophenyl ether. A pure sample of this ether was obtained by preparative, vapor-phase chromatography, using a 20 percent Viton A-Celite (see footnote 3) column at 150 °C. The pure vinyl ether (bp 132–132.5 °C, $n_D^{23} = 1.3940$, showing —CF═CFH at 1786 cm^{-1} in the infrared spectrum) was eluted first. The impurity appears to be mainly the saturated ether, pentafluorophenyl 1,1,2-trifluoroethyl ether, bp 155 to 158 °C (impure).

9.12. Pyrolysis Procedure

The pyrolysis apparatus consisted of a Pyrex tube, 45 cm long and 1 cm wide, having a female $^{14}/_{20}$ joint at the top and a male $^{14}/_{20}$ joint at the bottom. A pressure-equalizing, 25-ml, addition funnel was placed at the top of the tube. The top of the funnel was connected to the nitrogen gas-inlet system. To the bottom end of the pyrolysis tube was fitted a $^{14}/_{20}$ jointed connector which had take-offs to the first and second traps. The second trap was usually connected to a drying tube (atmospheric pressure experiments) or to a vacuum pump for experiments under reduced pressure. Both traps were cooled by solidified carbon dioxide acetone mixtures. The packing (5-in. cross section) was usually supported by a constriction in the glass tube. The tube was heated by a tube furnace to the desired temperature, and the compounds were added dropwise from the addition funnel. The nitrogen flow-rate was usually 3.5 cm^3/min. Other conditions are listed in tables 1 and 2. The first trap usually contained most of the pyrolyzate. Upon warming, a sample of the pyrolyzate was analyzed by vapor-phase chromatography, using columns of 20 percent silicone oil on Celite. Identification of the components of the pyrolyzate was made by comparison of the retention times with those of known samples. The relative percentage composition of the pyrolyzate was obtained from the peak height and width of the individual components.

9.13. Basic Reagents

The details are listed in table 3. The compound and the aqueous potassium hydroxide were mixed at 25 °C, heated at 100 °C for 1 hr, and cooled, and the aqueous solution was extracted with dichloromethane to remove the neutral compounds. Acidification of the basic layer with 10 percent hydrochloric acid gave pentafluorophenol. Where potassium hydroxide pellets were used, a bed of solid potassium carbonate was employed, to protect the glass surface during the reaction. The $KOH-K_2CO_3$ mixture was heated to 200 °C before the sample was added dropwise. The sample was then refluxed from the $KOH-K_2CO_3$ mixture for 30 min before allowing distillation to proceed. Cleavage products, usually pentafluorophenol, were obtained by acidification of the base after dilution with water. Pyrolyses over 25 percent KOH–charcoal pellets were accomplished in the same apparatus as described above. Products were identified by vapor-phase chromatography.

9.14. Acid Reactions

Concentrated sulfuric acid (98%) was the only acid employed in these reactions, listed in table 4. The acid and the compound were mixed at room temperature, and heated at 125 °C for 1 hr. Most of the compounds were immiscible with the reagent, and, occasionally, shaking and swirling were necessary. The products were isolated by cooling the reactants to 0 °C and adding crushed ice to the acid solution. The fluorocarbon layer could be separated from the aqueous layer. Again, identification of the products was made by vapor-phase chromatography.

9.15. Polymerization Reactions

a. Pentafluorophenyl Vinyl Ether

(1) *With α,α-Azobis(isobutyronitrile) (ABIN).* To 1 g of pentafluorophenyl vinyl ether in a Pyrex tube was added 0.01 g of ABIN. The tube was attached to a high-vacuum line and the contents degassed before the tube was sealed. It was then placed in a bath maintained at 60 °C. After 24 hr, only a slight yellow color had developed. The temperature was raised to 130 °C. After 7 days, the color was a darker yellow, but no polymerization had occurred. Recovered monomer (97%) was the main material. Only a trace of a brown solid was obtained; this was not investigated.

(2) *With Aluminum Chloride.* To 0.01 g of anhydrous aluminum chloride was added a solution of 1 g of pentafluorophenyl vinyl ether in 5 ml of anhydrous benzene. No reaction was observed at 25 °C. The solution was warmed to 50 °C, and an additional 0.01 g of aluminum chloride was added. An orange color now developed, and after refluxing the mixture for 2 hr, the color changed to deep purple. After cooling to 25 °C, 50 ml of methanol was added to the benzene solution, and the polymer was allowed to settle. The polymer was a yellow, glassy material, mp 120 to 180 °C, and its molecular weight was 2300 (VPO).

(3) *With Boron Trifluoride.* A solution of 3 g of pentafluorophenyl vinyl ether and 25 ml of pentane in a 50-ml flask was saturated with boron trifluoride gas. The flask was then sealed, and stored at −78 °C for 3 days; some white solid had then precipitated. Three drops of water were added to the mixture, and the mixture was sealed, and stored at −78 °C for 4 days. The tube was opened, and nitrogen was bubbled through the solution to remove the excess boron trifluoride as gas. The tan, solid polymer was removed by filtration, and dried under vacuum. The filtrate yielded 2 g of recovered monomer. The dried polymer weighed 0.9 g (30% conversion). The poly(pentafluorophenyl vinyl ether) was dissolved in 25 ml of benzene and filtered. The benzene solution was added to 20 ml of methanol, and the white precipitate allowed to settle. After filtration and vacuum drying, the white polymer weighed 0.31 g (mp 55 to 60 °C). It was soluble in benzene, hexafluorobenzene, and acetone. The molecular weight (VPO) was 17,000.

b. 1,2-Difluorovinyl Pentafluorophenyl Ether

Into each of two quartz tubes was placed 1 g of 1,2-difluorovinyl pentafluorophenyl ether, and each tube was sealed. One of the tubes also contained 0.01 g of ABIN. Both tubes were irradiated at 25 °C for 3.5 days with an ultraviolet lamp at a distance of 10 in. No reaction was visible. The tubes were then kept in a furnace at 110 °C for 4 days. At the end of this period, the contents of both tubes were black and viscous. Some solid was observed in both tubes. The tube containing ABIN had twice as much black liquid as the blank tube. The products of these reactions appear to be mainly dimers.

The authors are indebted to D. W. Brown of the Polymer Chemistry Section for the high-pressure polymerization of pentafluorophenyl vinyl ether, and to R. J. Hall of the Analysis and Purification Section for elementary analyses.

10. References

[1] W. J. Pummer and L. A. Wall, SPE Trans. **3,** 220 (1963).
[2] J. A. Godsell, M. Stacey, and J. C. Tatlow, Nature **178,** 199 (1956).
[3] W. J. Pummer and L. A. Wall, Science **127,** 643 (1958).
[4] L. A. Wall, W. J. Pummer, J. E. Fearn, and J. M. Antonucci, J. Res. NBS **67A** (Phys. and Chem.) No. 5, 481 (1963).
[5] J. M. Birchall and R. N. Haszeldine, J. Chem. Soc. (1959), 13.
[6] W. J. Pummer and L. A. Wall, J. Res. NBS **68A** (Phys. and Chem.) No. 3, 277 (1964).
[7] J. Burdon, V. A. Damodaran, and J. C. Tatlow, J. Chem. Soc. (1964), 763.
[8] W. Reppe, U.S. Patent 1,959,927.
[9] W. M. Lauer and M. A. Spielman, J. Am. Chem. Soc. **55,** 1572 (1933).
[10] H. V. R. Iengar and P. D. Ritchie, J. Chem. Soc. (1957), 2562.
[11] W. Reppe, Ann. **601,** 81 (1956).

[12] A. K. H. Filippova, E. S. Domnino, T. I. Ermolova, M. L. Navtanovich, and G. V. Dmitrieva, Izvest. Sibir. Otdel. Akad. Nauk SSSR **11,** 9 (1958).
[13] D. J. Foster and E. Tobler, Abstracts Papers Am. Chem. Soc. Meeting **138,** 53P (1960).
[14] L. Claisen, German Patent 268,099 (1913).
[15] C. D. Hurd, The Pyrolysis of Carbon Compounds, Am. Chem. Soc. Monograph **50,** 203 (1929).
[16] C. D. Hurd and F. H. Blunch, J. Am. Chem. Soc. **60,** 2419 (1938).
[17] W. J. Bailey and C. N. Bird, J. Org. Chem. **23,** 997 (1958).
[18] W. J. Bailey and J. DiPietro, Abstracts Papers Am. Chem. Soc. Meeting **138,** 41T (1958).
[19] C. H. DePuy and R. W. King, Chem. Rev. **60,** 431 (1960).
[20] A. Maccoll, Theoretical Organic Chemistry (Butterworths Scientific Publications, London, 1959) Kekulé Symposium, p. 240.
[21] W. A. Sheppard, J. Org. Chem. **29,** 11 (1964).
[22] R. S. Corley, J. Lal, and M. W. Kane, J. Am. Chem. Soc. **78,** 3489 (1956).
[23] A. L. Henne and M. A. Smook, J. Am. Chem. Soc. **72,** 4378 (1950).
[24] R. F. Clark and J. H. Simons, J. Am. Chem. Soc. **77,** 6618 (1955).
[25] E. J. Forbes, R. D. Richardson, M. Stacey, and J. C. Tatlow, J. Chem. Soc. (1959), 2019.
[26] D. J. Alsop, J. Burden, and J. C. Tatlow, J. Chem. Soc. (1962), 1801.
[27] D. W. Brown and L. A. Wall, SPE Trans. **3,** 300 (1963).
[28] A. V. Kalabina, S. Kh. Filippova, G. V. Dmitrieva, and L. Ya. Tsorick, Vysokomolekul. Soedin. **3,** 1020 (1961). Chem. Abstracts **56,** 1587b (1962).
[29] S. Straus and L. A. Wall, SPE Trans. **4,** 4 (1964).

(Paper 70A3–399)

JOURNAL OF RESEARCH of the National Bureau of Standards—A. Physics and Chemistry
Vol. 70A. No. 3, May-June 1966

Calibration of Germanium Resistors at Low Temperatures (2–20° Kelvin)

G. Cataland and H. H. Plumb

Institute for Basic Standards, National Bureau of Standards, Washington, D.C.

(February 11, 1966)

Two germanium resistors, C and D, have been referenced to values of temperature determined by the NBS acoustical thermometer. The resistance-temperature calibration data for these resistors have been fitted to a function of the form $\log_{10} R = \sum_{n=0}^{m} A_n(\log_{10} T)^n$ and the results are presented. The resistors C and D that are used as secondary standards maintain the scale, NBS Provisional Scale 2−20 (1965), to which public calibrations of germanium thermometers are referenced.

The calibration apparatus and measurement techniques that are employed in calibrating submitted resistors are described in detail. Additionally, data of three typical calibrations and their treatment by polynomial fitting are included to demonstrate the characteristics of some commercially available germanium resistors.

Key Words: Calibration, germanium resistors, low temperatures, secondary thermometers, thermometry.

1. Introduction

Recently at the National Bureau of Standards a provisional temperature scale in the region of 2 to 20 °K was established, based on temperature values derived with the Acoustical Thermometer [1, 2],[1] a primary thermometer. The temperature scale is presently maintained with six germanium resistance thermometers. Their calibration is in close agreement [2] with other secondary thermometers in regions where temperature calibrations overlap, i.e., 2 to 5 °K, the T_{58} He^4 Vapor Pressure Scale [3] and 12 to 20 °K, NBS (1955) Scale [4].[2]

In practice, temperature sensing devices should be independent of thermal history and have a measurable temperature coefficient which covers a prescribed temperature range as a smooth function of some parameter. Some materials, i.e., carbon, [5, 6, 7, 8], metals, [9, 10, 11], and piezoelectrics [12] meet these requirements but are limited in the cryogenic temperature range 2 to 20 °K because of insensitivity, instability, or nonreproducibility. Some of the pure metals become superconducting, i.e., indium [13] and lead at temperatures of 3.4 and 7.2 °K, respectively. Impurity doped germanium semiconductors [14, 15, 16, 17, 18, 19] exhibit a temperature-dependence of electrical resistance such that they are readily adaptable to the needs of precise low temperature thermometers. By controlling the impurity doping of germanium, thermometers can be produced to cover temperatures within various ranges of interest, i.e., 1 to 20 °K, 20 to 50 °K, etc. Within the useful range of these thermometers two conduction processes are involved [20]; at temperatures below 10 °K, impurity conduction is the dominant mechanism, while free hole conduction limits the resistivity at the higher temperatures. To cover the region 2 to 20 °K, a point-by-point calibration is necessary because of the complicated conduction processes; at the present time an accurate simple analytical representation of resistance versus temperature for germanium resistors does not exist.

We will discuss the NBS Provisional Scale 2–20 (1965) and a "Germanium Thermometer Calibrator" which is employed in calibrating germanium thermometers against it.

2. NBS Provisional Temperature Scale 2–20 (1965)

The temperature scale, against which calibrations are performed, is called NBS P 2–20 (1965) and is based upon values of absolute temperature that have been determined with the NBS Acoustical Thermometer. This instrument and its operation have recently been described [2] but a more detailed description (including tabular data that defines the isotherms) will appear in the near future.[3]

During the operation of the acoustical thermometer it was essential that secondary thermometers (in this

[1] Figures in brackets indicate the literature references at the end of this paper.

[2] The present NBS temperature scale in this region, 12 °K and above is maintained with platinum resistors, designated NBS (1955), and defined to be 0.01 deg lower than the scale given in reference [4].

[3] To be published in a future issue of Metrologia.

instance, germanium resistors that were in intimate thermal contact with the acoustical thermometer were used) be employed to indicate the constancy of maintaining an isotherm temperature,[4] as well as to retain a calibration of the acoustically determined isotherm temperature. This is accomplished by periodically monitoring the resistance values of the germanium resistors while the acoustical thermometer is in operation. Two particular germanium resistors, which we can label A and B, have always served this function and thus they have been calibrated by the acoustical thermometer. Additionally, two other germanium resistors have been mounted in the apparatus and have been used as additional monitoring resistors in the acoustical thermometer. We shall name two such resistors C and D. While C and D have been used for monitoring the acoustical thermometer for certain specific isotherms, they give reference to all of the isotherms through calibrations against resistors A and B.

Quite naturally the calibrations of C and D against A and B did not always take place at exactly the original acoustically-determined isotherm temperatures and thus a knowledge of $\frac{dR}{dT}$ (for resistors A and B) was required for properly assigning temperatures to C and D. Because the calibration temperatures of C and D were never more than 0.035 °K from the acoustically determined isotherms, the required interpolations and knowledge of $\frac{dR}{dT}$ (for A and B) did not critically affect the calibration of resistors C and D $\left(\frac{dR}{dT}\right.$ values could be established with sufficient accuracy for this interpolation from the calibrations of A and B$\left.\right)$. In fact the temperature of only six calibration points for resistor C differed more than 0.020 °K from the original acoustically defined isotherm-temperatures; for D, one was 0.016 °K and the remainder less than 0.012 °K. The resistors C and D were never in the acoustical thermometer together so their calibrations were performed independently with regard to time and environmental location within the acoustical thermometer apparatus.

At this point it is necessary to note that previous to their calibration some laboratory history of resistors C and D had been accumulated; this has been reported in an earlier article [21]. The resistors were repetitively, thermally cycled between room temperature and 4.2 °K, with systematic resistance-temperature calibrations performed at a temperature close to 4.2 °K. A "constant temperature" liquid helium bath contained the resistors during the 4.2 °K portion of the cycle and thus, by measurements of the liquid helium vapor pressure, a very reproducible temperature reference (to the T_{58} scale) was obtained. Resistor C had been thermally cycled 88 times and demonstrated a reproducibility of the 4.2 °K calibration within 0.0011 °K; resistor D underwent 86 cycles and demonstrated a constancy within 0.0005 °K. The estimated error from various measurements in the cycling process was equivalent to 0.0004 °K. Appropriate attention has always been applied to the measuring currents through the resistors to avoid undesired, appreciable Joule heating.

After being calibrated with reference to the acoustical thermometer, the resistors C and D were placed within the calibrator, which will be described in this article, and measurements of their resistances were conducted at temperatures which closely approximated the original isotherm temperatures. More specifically, the temperature of the apparatus was controlled until the resistance measurement of one resistor, for example, C, indicated that approximation to an original acoustical isotherm temperature had been achieved. Next, at this temperature a value was obtained for the resistance of D. Thus there was afforded a comparison of indicated temperatures between C and D within the calibrator since, to repeat, each resistor had been previously independently calibrated with reference to the acoustical thermometer. Temperature discrepancies between C and D (after appropriate small interpolations had been made), from comparison measurements within the calibrator, never exceeded 0.003 °K. Consequently our assignment of temperature values to future calibrations in the calibrator against C and D is slightly arbitrary. The maximum temperature discrepancy of 0.003 °K between resistors C and D, as obtained during the calibrator use, probably indicates that the combined errors of electrical measurements and temperature controlling correspond to about ± 0.002 °K.

Thus temperatures have been associated with resistors C and D for their use as secondary standards in the calibrator. This information is presented in columns 1 and 2 of tables 1 and 2. We were desirous of possessing more information about the resistors' calibrations and consequently have performed a computer analysis of the data. A polynomial of the form

$$\log_{10} R = \sum_{n=0}^{m} A_n (\log_{10} T)^n$$

was fitted to the R_{data} and T_{data} calibration data of each resistor by the method of least squares. A double precision computer program prepared by the Statistical Engineering Laboratory was used to overcome the roundoff error characteristic of fitting high order polynomials, and in this case the roundoff error was several orders of magnitude smaller than other experimental uncertainties. All data were given equal weight and m, the degree of the polynomial, was varied from 3 to 8. The eighth order polynomial produced a fit to the input data such that no datum point deviated from the polynomial by more than 0.0045 °K. The reduction in the sum of squares of deviations due to the addition of terms of higher order was statistically significant (0.05-probability level) in all cases up to and including the 8th degree. We have not extended the analysis since we feel that fit-

[4] An isotherm as determined by the acoustical thermometer consists of the speed of sound in helium gas as a function of the gas pressure.

ting the data within 0.004 °K is a reasonable limit. It is noteworthy to mention that as the lower temperature data points are excluded, comparable fitting is possible with fewer terms in the polynomial.

After obtaining values of the 9 coefficients we effected a computer generation of temperature, resistance, $\frac{dR}{dT}$, $\frac{d^2R}{dT^2}$, and $\frac{1}{R}\frac{dR}{dT}$ at intervals of 0.010 °K. Using the generated $\frac{dR}{dT}$, simple interpolations have been made to obtain values of generated resistance, R_{gen}, which correspond to the input temperatures, T_{data}. These resistances, R_{gen}, are listed in column 3 of tables 1 and 2. Column 4 shows the difference between the input and generated resistance; by again employing the generated $\frac{dR}{dT}$ of column 5 we obtain the temperature difference (ΔT of column 6) which corresponds to the resistance differences of column 4. It is readily apparent from column 6 of tables 1 and 2 that the temperature-resistance data for resistors C and D can be represented by an eighth order polynomial within 0.005 °K.

Additional information is obtained concerning the polynomial and therefore, the resistors also, since (for each resistor) the generated $\frac{d^2R}{dT^2}$ does not change its sign; the fitted polynomial function is monotonically smooth. Consequently one is reasonably confident that the fitted polynomials can be used for interpolating between original calibration points. Figures 1 and 2 depict the variation of R versus T, and $\frac{1}{R}\frac{dR}{dT}$ versus T, respectively, for both resistors, C and D.

TABLE 1. *Resistor C*

T_{data}[a]	R_{data}[a]	R_{gen}[b]	$\frac{R_{data}-R_{gen}}{\Delta R}$	dR/dT[c] (Ohms/0.001 °K)	ΔT[d] (0.001 °K)
°K	*Ohms*	*Ohms*	*Ohms*		
2.321	11.481.	11.481.4	−0.4	−13.5	0.0
2.805	7.058.7	7.056.7	2.0	−6.12	−.3
3.207	5.122.5	5.125.0	−2.5	−3.71	.7
4.206	2.800.9	2.798.9	2.0	−1.43	−1.4
5.020	1.916.0	1.917.8	−1.8	−0.817	2.2
6.060	1.272.9	1.271.8	1.1	−.471	−2.3
6.977	918.51	919.16	−0.65	−.312	2.1
8.066	645.32	645.29	.03	−.200	−1.5
8.989	489.99	489.93	.06	−.140	−0.4
9.889	382.65	382.53	.12	−.101	−1.2
10.901	296.86	296.82	.04	−.070	−0.6
12.018	230.85	230.97	−.12	−.049	2.4
12.962	190.74	190.82	−.08	−.037	2.2
14.036	157.05	157.01	.04	−.027	−1.5
14.993	134.26	134.24	.02	−.021	−1.0
16.050	114.77	144.76	.01	−.016	−0.6
16.970	101.36	101.32	.04	−.013	−3.1
18.004	89.051	89.100	−.049	−.011	4.5
18.940	79.997	80.006	−.009	−.0088	1.0
20.054	71.084				

[a] T_{data} and R_{data} refer to calibration quantities, temperature and resistance.
[b] R_{gen} is the resistance, at the temperature T_{data}, obtained by generating resistance as a function of temperature from the evaluated polynomial coefficients A_n.
[c] $\frac{dR}{dT}$ is generated from the evaluated coefficients A_n.
[d] ΔT is obtained by dividing $(R_{data}-R_{gen})$ by $\frac{dR}{dT}$.

TABLE 2. *Resistor D*

T_{data}[a]	R_{data}[a]	R_{gen}[b]	$\frac{R_{data}-R_{gen}}{\Delta R}$	dR/dT[c] (Ohms/0.001 °K)	ΔT[d] (0.001 °K)
°K	*Ohms*	*Ohms*	*Ohms*		
2.321	10.847.	10.848.	−1.0	−12.8	0.1
2.805	6.656.1	6.653.2	2.9	−5.8	−0.5
3.207	4.820.3	4.824.2	−3.9	−3.5	1.1
4.206	2.630.3	2.627.0	3.3	−1.4	−2.4
5.020	1.792.5	1.795.1	−2.6	−0.77	3.4
6.060	1.186.3	1.185.2	1.1	−.44	−2.5
6.977	852.60	853.10	−0.50	−.29	1.7
8.066	596.36	596.29	.07	−.19	−0.4
8.989	451.44	451.34	.10	−.13	−.8
9.889	351.63	351.60	.03	−.093	−.3
10.901	272.27	272.32	−.05	−.065	.8
12.018	211.53	211.55	−.02	−.045	.4
12.962	174.68	174.77	−.09	−.034	2.6
14.036	143.80	143.78	.02	−.025	−0.8
14.993	122.98	122.98	.0	−.019	−.0
16.050	105.21	105.20	.01	−.015	−.7
16.970	92.96	92.94	.02	−.012	−1.7
18.004	81.743	81.785	−.042	−.0097	4.3
18.940	73.469	73.494	−.025	−.0080	3.1
20.054	65.351	65.341	.010	−.0066	−1.5

[a] T_{data} and R_{data} refer to calibration quantities, temperature and resistance.
[b] R_{gen} is the resistance, at the temperature T_{data}, obtained by generating resistance as a function of temperature from the evaluated polynomial coefficients A_n.
[c] $\frac{dR}{dT}$ is generated from the evaluated coefficients A_n.
[d] ΔT is obtained by dividing $(R_{data}-R_{gen})$ by $\frac{dR}{dT}$.

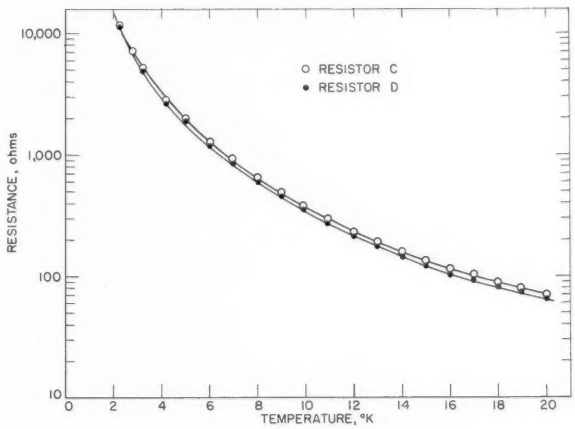

FIGURE 1. *A plot of resistance as a function of temperature:* o, *Resistor C;* ● *Resistor D.*

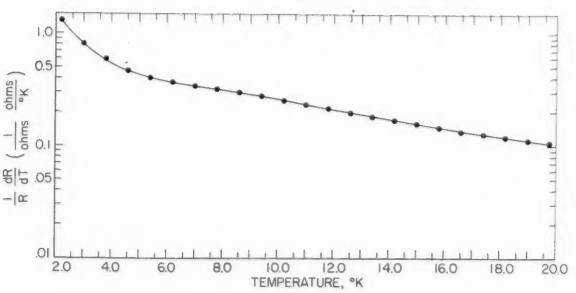

FIGURE 2. *Resistance-temperature sensitivity,* $\frac{1}{R}\frac{dR}{dT}\left(\frac{1}{°K}\right)$, *as a function of temperature* (°K).
The plot is applicable to both C and D since their temperature sensitivities do not differ more than one percent.

While resistors C and D are the basis for present calibrations from 2 to 20 °K at the National Bureau of Standards, several other resistors exist that have been similarly treated; additionally, resistors A and B are still intact within the acoustical thermometer. Resistor D, prior to its mounting in the acoustical thermometer, had been calibrated at the National Bureau of Standards against the NBS (1955) scale below 20 °K. It was one of the two thermometers that afforded a comparison, (which has been reported previously [1, 2]) between values of acoustically determined temperatures and the NBS (1955) scale.

3. Calibrator[5]

3.1. General Design Considerations of Calibrator

Central to apparatus which we have constructed is a solid copper cylinder. It is required, during the course of calibration measurements, that the copper mass and its contained resistors be maintained at accurately controllable temperatures at approximately every degree from 2 to 20 °K. To achieve this temperature regulation the system must be quasi-thermally isolated from its surroundings. The copper mass and imbedded thermometers are shown in figure 3. In operation (the smaller can having been soldered in place) the copper mass and small can are included in the large can. If a vacuum is maintained within the larger can, then the small can and its contents are partially isolated, thermally, from the environment that contains the large can.

[5] Certain commercial materials and equipment are identified in this section in order to adequately specify the experimental procedure. In no case does such identification imply recommendation or endorsement by the National Bureau of Standards, nor does it imply that the material or equipment identified is necessarily the best available for the purpose.

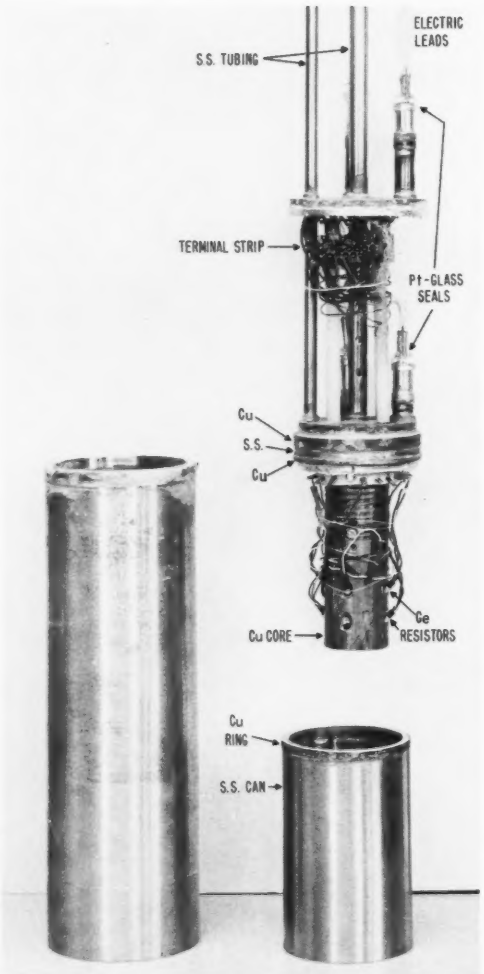

FIGURE 3. *Closeup photograph of the calibrator that is used in the temperature calibration of germanium resistors.*

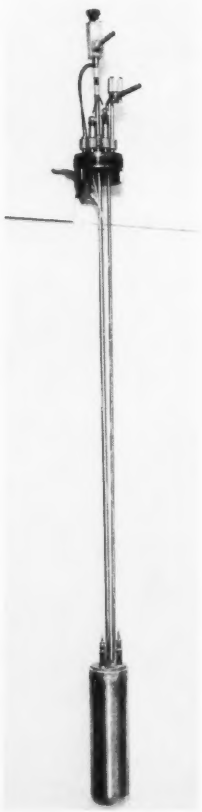

FIGURE 4. *Assembled calibrator.*

Within the vacuum enclosure heat transfer by gas conduction and convection is essentially eliminated, and the small can will reduce radiant heat flow between the thermometers and the outer vacuum can. There remains, however, a thermal connection between the inner assembly and the outer can via electrical leads and mechanically supporting members, i.e., the two stainless steel tubes. The inner assembly is thermally floated at temperatures that exceed the environmental temperature of the outer can, with a resultant temperature gradient along the electrical lead wires and stainless steel tubes.

A more complete view of the calibrator is depicted in figure 4. Uppermost is the Dewar cap, which affords ingress of electrical leads and the stainless steel tubings. Because the lower portion is in a liquid helium bath during calibrations any heat from ambient temperatures that is conducted downward along the leads and tubings is dissipated in the refrigerant. Thus it is evident that under steady state conditions, the interesting heat flow occurs from the inner assembly toward the top of the outer vacuum can. The dimensions of the supporting tubes and electrical leads have been selected so that accurate temperature control of the copper core and resistors is attained through a reasonable expenditure of electrical heating to the copper core.

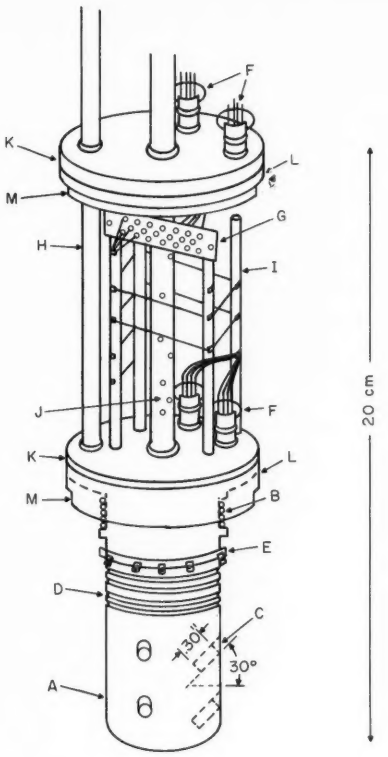

A Cu Core
B HEATER COIL
C CAVITIES FOR THERMOMETERS
D .05" DIA. GROOVES FOR WIRES
E ANNULAR TERMINAL STRIP
F PLATINUM GLASS SEALS
G TERMINAL STRIP
H PUMPING LINE (INNER CAN)
I NYLON
J OUTER CAN PUMPING LINE
K Cu CAPS OF CANS
L STAINLESS STEEL RING
M Cu RING

FIGURE 5. *Detailed drawing of the calibrator low-temperature components.*

3.2. Main Copper Core

The main core (A) of the isothermal system in figure 5 was constructed of 58.93 mm (diameter) copper rod. Cavities 3.58 mm (diameter) drilled at 60° angles to its axis serve as receptacles for the germanium thermometers. Also machined in the core was a spool-like section (B) upon which the heater coil was wound. Directly above the coil form is the cap (K) for the inner chamber. Silver soldered to the cap's perimeter is a stainless steel tubing sleeve (L) 0.30 mm thick, 12.70 mm long. Soldered on the lower end of the tubing is a copper ring (M) with a tongued edge to receive the groove of the small vacuum can of figure 3. In the cap (K) two 9.53 mm holes were drilled for the platinum glass seals, a 6.35 mm hole for an evacuation tube (H), a 9.53 mm opening for the supporting tubing (J), and four screw threads were tapped for the nylon rods (I). On the copper core below the coil form a spiral groove (D), 1.27 mm deep, three threads per cm, was routed from the core's perimeter to serve as a channel for thermally anchoring the lead-in wires that return upwards to the terminal ring (E).

The terminal ring was fabricated from Teflon tubing and contains terminal lugs made of 0.76 mm platinum wire. The wire has been flattened on one extremity and cut to extend 9.53 mm beyond the Teflon ring. Holes 0.50 mm were drilled at the end of the platinum lugs to secure the thermometer electrical leads prior to their soldering. Two set screws attached the ring to the copper core.

3.3. Vacuum Chambers

For thermal isolation the above components were encased within a vacuum tight cannister. The vacuum can was constructed of stainless steel tubing 58.93 mm diam, 114.30 mm long and 0.30 mm thick with one capped end of 0.50 mm thickness. A copper ring was silver soldered to the open end of the can; the ring was grooved to receive the tongued edge (M) of the can top.

The outer can top was also made of copper and holes, similar to those of the inner can, were drilled for the insertion of seals and evacuation lines. There also, a stainless steel sleeve that terminates in a tongued copper ring was soldered to the cap's circumference. The reason for using the stainless steel sleeves in both vacuum systems may not be obvious. In assembling the apparatus, heating is required to solder the

vacuum cans to the flanges (M). If the heat were sufficiently great, electrical lead insulation might be damaged in regions where the insulation is in contact with copper (the spiral groove (D) and the vacuum can tops). Additionally, heating of the large copper core would elevate the temperature of the germanium thermometers to such an extent that they might be damaged. Precautions have been taken to avoid such heating. (a) Wood's metal solder is used for assembly because its melting point is relatively low. (b) The stainless steel paths (L) provide a sufficiently large thermal resistance that the solder joints can be made with only a slightly perceptible temperature rise in the vacuum can tops and the copper mass (A). A similar design has been employed in mounting the platinum glass seals (F) to simplify their replacement.

3.4. Electrical Seals and Wiring

Glass-metal type electrical lead-in seals were used exclusively in the construction of the isothermal calibrating system. For ambient conditions, Kovar-glass type capillary-tubing seals were utilized. At temperatures where components are immersed in cryogenic liquids, our experience has shown the necessity for using platinum-glass type seals. The NBS glass shop made the 9-capillary platinum-glass seals [6] that were incorporated in the system.

At ambient temperatures where electrical leads entered the Dewar system, eighteen #38 AWG double nylon, enamel coated copper wires were fed through and soldered to individual capillaries of two 9-capillary Kovar-glass seals that were located on the Dewar cap. The wires continued from the ambient seals, were strung through and soldered to individual capillaries of two platinum-glass seals (F) of the outer can, and terminated at the 20-pin rectangular terminal strip (G).

From the terminal strip, 1.54 m lengths of Evanohm wire were spiraled around the notched nylon supporting rods (I) in six windings and the remaining lengths of wire were passed through and soldered at the individual capillaries of the two platinum-glass seals that are mounted on the top of the inner vacuum can. The remaining lengths of wire within the inner can region were then snugly wound into the spiral groove (D) of the main copper core (A) and terminated at the nylon ring (E). The strands of Evanohm wire were wound around the nylon rods to lengthen the thermal resistance path along the lead wires, in effect, to reduce the temperature gradient along the electrical leads, since the temperature difference between the isothermal system and its heat sink (cryogenic bath) can differ by as much as 18° during a calibration run. The enamel coated Evanohm lead wires were placed in physical contact with the copper core to enhance thermal equilibrium between resistance thermometers, electrical leads and the environment within the calibrating unit. Evanohm wire was used because its resistance-temperature coefficient is quite low.[7] The heater coil was noninductively wound on spool (B) of figure 5, with 61.5 m of the above wire. The wire diameter is 0.10 mm and the wire has a resistance of 1.65 Ω/cm.

4. Germanium Thermometers

4.1. General Description

The bridge-shaped encapsulated germanium thermometer, shown in figure 6 with current contacts external to the potential contacts, has advantages not found in some other types. The germanium element is mounted in a relatively strain-free manner within its encapsulation to reduce piezoresistance [20, 22] that is exhibited by germanium at low temperatures. Effects of contact resistances and possible thermal strains in the contacts are relatively unimportant because measurements are made potentiometrically and temporal changes in contacts do not necessarily change the thermometer calibration [20]. Encapsulation of the thermometer element in helium exchange gas aids the germanium element in achieving thermal equilibrium with its metallic capsule.

4.2. Mounting of Thermometers

Leads of the germanium thermometers are soldered with Wood's metal to the platinum lugs of the nylon terminal ring (E) using a low-powered soldering iron to minimize overheating of the germanium element through heat conduction. A very dilute solution of Baker's Flux (aqueous solution of the chlorides of Zn and NH_4) is used and upon completion of the soldering, the terminal junctions are flushed with a swab and hot water to remove traces of flux.

The casings of the thermometers are placed within the copper cavities. A primary consideration in the calibrator design is the attainment of thermal equilibrium between the resistors (the sensor, secondary standards, and those to be calibrated). Since the resistors are generally encapsulated, one must be concerned with the thermal equilibrium between each resistor and its encapsulation, as well as between all

[6] The seals were thermally cycled from ambient to liquid helium temperatures at least three times and leak tested on a mass spectrometer type helium leak detector prior to their use in the calibrator.

[7] At 20 and 273 °K, its resistivity is 132.5 and 133.3 μΩ cm, respectively [23].

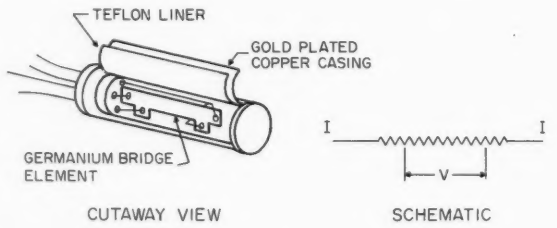

FIGURE 6. *Schematic portrayal of a typical germanium resistor encapsulation.*

encapsulations. After the germanium thermometers are wired into the circuit and continuity and shorting checks made, the inner-most vacuum can is soldered into place with Wood's metal, using a modified soldering gun that possesses an annular copper heater element for uniform heating. Then the outer vacuum can is soldered into place using a gas-air torch of fine orifice. Both vacuum systems are leak detected, and again checks are made to assure circuit continuity and adequate electrical insulation between the d-c electrical circuits and "ground." Insulation resistances of 10 MΩ – the limit of a portable Wheatstone bridge – are commonly measured.

5. Temperature Measurements and Control

5.1. Refrigerant Reservoir

For temperature-calibration measurements 5 to 20 °K or above, the helium bath into which the calibrator is immersed, is vented to atmospheric pressures. The bath at this temperature provides an adequate heat sink for dissipating the energy emitted from the calibrator. For temperature measurements 2 to 5 °K, the bath pressure is reduced to achieve a bath temperature of 1.8 °K or less. A requirement for temperature stability within the calibrator is that there should be a current flow to the heater coil at all times, and experience has shown that the minimum power output of the heater should be 6.25 μW (25 μA through the 10,000 Ω heater coil), otherwise the required stability and reproducibility of temperatures is not possible.

5.2. Temperature Control

Temperature control is attained through the use of bridge and amplifier circuits and a three-action control unit with recorder. The temperature sensor (one leg of a Wheatstone bridge) is a germanium resistor that has been repeatedly cycled from ambient to liquid helium temperatures to determine its stability and reproducibility. The unbalance of the bridge circuit is detected and fed into a servo-control unit, which possesses the controlling actions of proportional band, rate time and reset – the servo-unit's controlled current output is fed directly to the calibrator's heater coil. Current to the Wheatstone bridge circuit is supplied by a voltage divider circuit to permit a variation of current through the germanium sensor. This variable control is essential since, for sensitive temperature control the apparatus, the same currents cannot be applied at all temperatures. Because of the low specific heats and extremely high values of sensor resistance at low temperatures, too large a sensor current can cause: (a) excessive Joule heating of the sensor; and (b) a dissipation of heat (from the sensor into the calibrator) that is large compared with the heat output of the controlling heater coil. At the high calibration temperatures larger sensor currents are required, than at low temperatures, to obtain sufficient sensor sensitivity. In general, the temperature is controlled by the above method to about 0.0001 °K.

5.3. Resistance Measurements

Potential and current measurements are made on a double-bank six-dial potentiometer equipped with an external reversing switch. The advantage of the double-bank unit is that it relieves the necessity of repositioning dials when transferring from potential to current measurements. One bank of the potentiometer is used for measuring current. An external standard resistor is connected in series with the resistors to be calibrated and thus, from a measurement of the potential across the standard resistor $\left(I=\frac{E}{R}\right)$, a value is obtained for the current through the total external circuit. The external reversing switch permits reversal of currents within the potentiometer and the external circuit, which includes the germanium thermometers. The measuring circuit is shown in figure 7. With this arrangement the thermal emf's may be detected and their effect on the measurements eliminated.

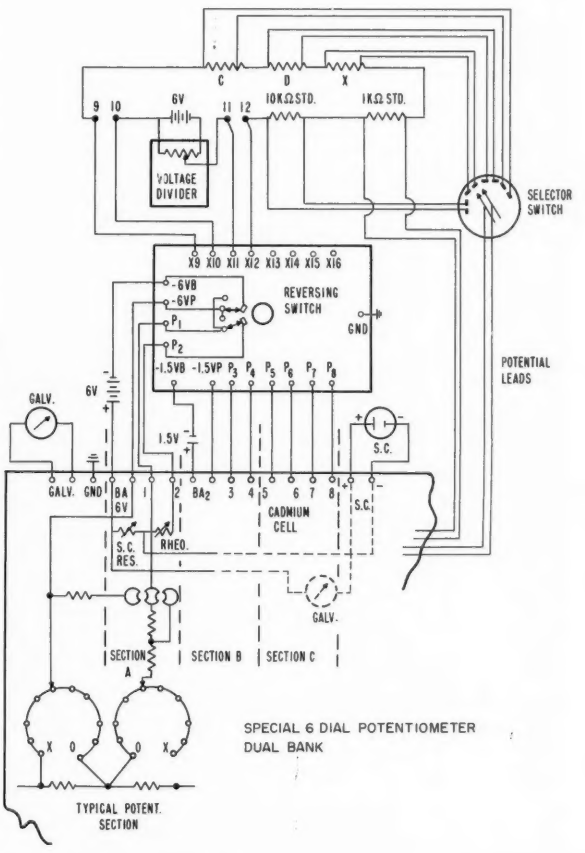

FIGURE 7. *Schematic of the d-c resistance measurement circuit.* This potentiometer actually consists of 3 potentiometer units in series (A, B, and C). Two sets of switches are connected to each decade to provide the "dual bank" feature.

5.4. Calibration Techniques

For many germanium thermometers, the resistor is a four-lead element, as shown in figure 6; two leads are for the current source and two for potential measurements. In the calibrator the current leads of the uncalibrated resistors are connected in series with the current leads of the calibrated thermometers to the current source at the terminal ring (E) of figure 5. The potential leads are wired individually to the platinum lugs which have electrical lead lines communicating to the potentiometer. The calibrated thermometers C and D are controlling parameters for determining the point-by-point resistance-temperature relation of the uncalibrated thermometers. Since an approximate temperature-resistance calibration of the sensor resistor is available, we are able to dial (for each calibration point) a particular value for this resistance on the Wheatstone bridge and then make final adjustments after comparing the two calibrated thermometer resistance-measurements with their previous values, i.e., temperature-resistance relation from the acoustical thermometer measurements. After the temperature constancy of the desired calibration point is clearly demonstrated, several series of potential measurements are made to determine the resistance of both the calibrated reference standards (C and D) and the submitted unknowns.

The complete calibration of submitted resistors is performed twice, covering the range 2 to 20 °K; in general, the temperature of a calibration point (column 1 of tables 3 through 5) must be within a few millidegrees of the calibration temperatures associated with resistors C and D (column 1 of tables 1 and 2); the differences of indicated temperatures between the standards C and D cannot exceed ±0.001 °K; and, if possible, the two separate calibrations of the submitted resistors should be consistent within ±0.002 °K.

TABLE 3. *Resistor X*

T_{data} [a]	R_{data} [a]	R_{gen} [b]	$\frac{R_{data}-R_{gen}}{\Delta R}$	dR/dT [c] (Ohms/0.001 °K)	ΔT [d] (0.001 °K)
°K	*Ohms*	*Ohms*	*Ohms*		
2.321	12,473.	12,473.6	−1.0	−15.0	.1
2.805	7,584.2	7,580.8	3.4	−6.74	−0.5
3.207	5,458.2	5,462.6	−4.4	−4.5	1.1
4.206	2,944.3	2,940.5	3.8	−1.54	−2.5
5.020	1,991.5	1,994.6	−3.1	−0.87	3.5
6.060	1,307.5	1,306.0	1.5	−.50	−3.0
6.977	932.73	933.39	−0.66	−.33	2.0
8.065	647.37	647.17	.20	−.21	−1.0
8.989	486.30	486.32	−.02	−.14	.1
9.889	376.44	376.40	.04	−.103	−.4
10.905	289.37	289.26	.11	−.071	−1.6
12.018	223.35	223.44	−.09	−.049	1.8
12.963	183.57	183.64	−.07	−.036	1.9
14.036	150.42	150.41	.01	−.026	−0.4
14.994	128.21	128.18	.03	−.020	−1.5
16.050	109.35	109.33	.02	−.016	−1.3
16.970	96.422	96.376	.046	−.013	−3.5
18.004	84.619	84.657	−.038	−.010	3.8
18.938	75.967	75.981	−.014	−.0085	1.7
20.048	67.490				

[a] T_{data} and R_{data} refer to calibration quantities, temperature and resistance.
[b] R_{gen} is the resistance, at the temperature T_{data}, obtained by generating resistance as a function of temperature from the evaluated polynomial coefficients A_n.
[c] $\frac{dR}{dT}$ is generated from the evaluated coefficients A_n.
[d] ΔT is obtained by dividing $(R_{data}-R_{gen})$ by $\frac{dR}{dT}$.

TABLE 4. *Resistor Y*

T_{data} [a]	R_{data} [a]	R_{gen} [b]	$\frac{R_{data}-R_{gen}}{\Delta R}$	dR/dT [c] (Ohms/0.001 °K)	ΔT [d] (0.001 °K)
°K	*Ohms*	*Ohms*	*Ohms*		
2.322	71,352.	71,441.	−89.0	−180.	0.5
2.807	22,038.	21,946.	92.0	−50.	−1.8
3.208	9,273.	9,311.3	−38.	−18.2	2.1
4.208	1,921.0	1,919.5	1.5	−2.4	−0.6
5.019	826.04	828.27	−2.23	−0.71	3.1
6.060	400.48	398.17	2.31	−.23	−10.0
6.976	253.51	253.44	0.07	−.107	−0.7
8.066	169.44	169.70	−.26	−.054	4.8
8.990	129.30	129.70	−.40	−.034	11.8
9.887	103.81	103.98	−.17	−.024	7.0
10.901	83.627	83.623	.004	−.017	−0.2
12.017	67.719	67.607	.112	−.012	−9.3
12.962	57.492	57.388	.104	−.0096	−10.8
14.048	48.274	48.201	.073	−.0075	−9.7
14.993	41.852	41.820	.0321	−.0061	−5.2
16.051	35.977	35.996	−.019	−.0050	3.8
16.969	31.781	31.816	−.035	−.0042	8.3
18.006	27.805	27.859	−.054	−.0035	15.4
18.940	24.820	24.852	−.032	−.0030	10.7
20.049	21.880	21.831	.049	−.0025	−19.6

[a] T_{data} and R_{data} refer to calibration quantities, temperature and resistance.
[b] R_{gen} is the resistance, at the temperature T_{data}, obtained by generating resistance as a function of temperature from the evaluated polynomial coefficients A_n.
[c] $\frac{dR}{dT}$ is generated from the evaluated coefficients A_n.
[d] ΔT is obtained by dividing $(R_{data}-R_{gen})$ by $\frac{dR}{dT}$.

TABLE 5. *Resistor Z*

T_{data} [a]	R_{data} [a]	R_{gen} [b]	$\frac{R_{data}-R_{gen}}{\Delta R}$	dR/dT [c] (Ohms/0.001 °K)	ΔT [d] (0.001 °K)
°K	*Ohms*	*Ohms*	*Ohms*		
2.319	1,918.8	1,918.9	−0.1	−1.45	0.07
2.806	1,404.7	1,404.5	.2	−0.76	−.3
3.208	1,156.3	1,156.6	−.3	−.50	.6
4.203	829.83	829.54	.29	−.21	−1.4
5.018	695.22	695.42	−.20	−.13	1.5
6.059	596.69	596.58	.11	−.071	−1.5
6.977	543.81	543.93	−.12	−.046	2.6
8.068	504.17	504.17	.00	−.029	0.0
8.988	482.13	482.07	.06	−.020	−3.0
9.889	466.52	466.45	.07	−.015	−4.7
10.901	452.99	452.97	.02	−.012	−1.7
12.018	440.23	440.30	−.07	−.011	6.4
12.962	429.69	429.78	−.09	−.011	8.2
14.048	416.56	416.59	−.03	−.013	2.3
14.993	403.63	403.60	.03	−.015	−2.0
16.049	387.11	387.05	.06	−.017	−3.5
16.970	370.98	370.89	.09	−.018	−5.0
18.004	351.02	351.08	−.06	−.020	3.0
18.940	331.84	331.96	−.12	−.021	5.7
20.048	308.51	308.45	.06	−.021	−2.9

[a] T_{data} and R_{data} refer to calibration quantities, temperature and resistance.
[b] R_{gen} is the resistance, at the temperature T_{data}, obtained by generating resistance as a function of temperature from the evaluated polynomial coefficients A_n.
[c] $\frac{dR}{dT}$ is generated from the evaluated coefficients A_n.
[d] ΔT is obtained by dividing $(R_{data}-R_{gen})$ by $\frac{dR}{dT}$.

Periodically during calibrations, when the extent of Joule heating in a submitted resistor is not known, power tests are performed. This is to insure that the resistor current is sufficiently low that Joule heating effects are well below 1 mdeg.

Certain features of the calibration apparatus merit mentioning. A high vacuum is maintained within the inner can; the resistors are mounted (within the copper core) in a stopcock grease medium; the region of the copper core, which contains the spiralled leads, has been covered with a suitable varnish to enhance thermal equilibrium between the core and leads; the heater coil has been varnished onto its containing form; and the current leads from each resistor are thermally anchored to the copper core. These features aid in

promoting thermal equilibrium (between the germanium resistors) to such an extent that a thermal gradient has not been detected—even though the heater has been operated at powers that have varied by an order of magnitude. (The power variance occurs, during measurements at a constant temperature, as the vacuum in the outer can [figure 3] is allowed to change.)

6. Results and Conclusions

The calibration data for three resistors that have been calibrated against resistor C and D are presented in figure 8 and in columns 1 and 2 of tables 3, 4, and 5. The resistors are from three different commercial sources and may, perhaps, be considered typical of available resistors. The resistors are labeled as X, Y, and Z and their calibration data have been treated on the computer in a manner paralleling that previously described in this paper for resistors C and D. We have attempted to fit the data for each resistor to a polynomial of the form

$$\log_{10} R = \sum_{n=0}^{m} A_n (\log_{10} T)^n$$

Resistors X and Z appeared to be reasonably represented by an eighth order polynomial; for Y, the significance of the polynomial coefficients became doubtful for the seventh and eighth orders. Generations for X, Y, and Z, based upon 9, 7, and 9 coefficients, respectively, were performed to obtain the quantities

$$R, \frac{dR}{dT}, \frac{d^2R}{dT^2} \text{ and } \frac{1}{R}\frac{dR}{dT}$$

as a function of temperature. Since the columns of tables 3, 4, and 5 correspond to those of tables 1 and 2, columns 6 indicate how well the calibrations of resistors X, Y, and Z are represented by the fitted polynomials. For these resistors also, elimination of the data at the lowest temperature will generally result in a more accurate functional fit at lower polynomial orders.

It is to be noted, for resistor Z in figure 8 that the R–T relationship is not characterized by a monotonically decreasing derivative $\frac{dR}{dT}$. Indeed the generation of the second derivative $\frac{d^2R}{dT^2}$ clearly exhibits a change in sign between 12.060 and 12.070 °K, and also between 20.480 and 20.490 °K. (The change in sign is not significant at the higher temperatures, since 20.480 °K exceeds the range of the calibration data.) Such a condition indicates that caution must be exercised in attempting to use our functional relationship for interpolating temperatures and resistances that are intermediate to the calibration points of resistor Z. Perhaps a better approach for interpolation would result from functionally fitting selected segments of the calibration data.

To repeat, columns 6 of tables 3, 4, and 5 demonstrate that the functional representations for resistors X and Z are more accurate than is indicated for resistor Y. While this can possibly be partially attributed to Y's low values of $\frac{dR}{dT}$ at the highest temperatures, one must note that the polynomial fit for resistor Y covers a much larger range of resistance than is the case for resistors X and Z. However, it is probably more significant to note that Y is basically a two lead resistor while X and Z involve four lead contacts. As has been described earlier in this paper, the electrical measurements of resistance are made by a direct-current, potentiometric technique. In the case of resistors X and Z, current connections to the germanium crystal are distinctly separate from the potential

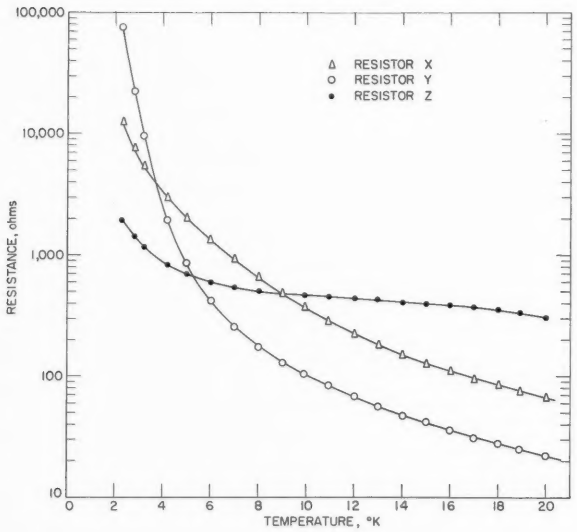

FIGURE 8. *Plot of resistance as a function of temperature: Δ, resistor X; o, resistor Y; and ●, resistor Z.*

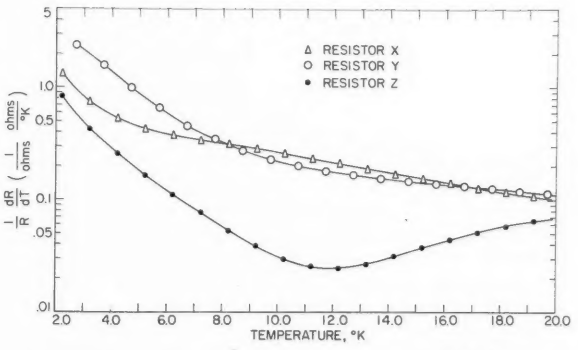

FIGURE 9. *Resistance-temperature sensitivity,* $\frac{1}{R}\frac{dR}{dT}\left(\frac{1}{°K}\right)$, *as a function of temperature (°K): Δ, resistor X; o, resistor Y; and ●, resistor Z.*

leads. For resistor Y, a current and potential lead are connected to each of the two leads that lead to the germanium resistor. It is possible that lead or contact resistances introduce additional uncertainties in the determination of Y's resistance.

Figure 9 indicates resistor sensitivities. The sensitivity is the fractional change of resistance per °K as a function of the absolute temperature. Quite obviously, depending upon the user's requirements, selection of a particular type of resistor is important since the sensitivities, $\frac{1}{R}\frac{dR}{dT}$, as well as the absolute magnitude of resistance, R, are variable—depending upon the concentration of impurities that have been added to the germanium.

Calibration certificates for submitted resistors are issued for calibrations at approximately the temperatures indicated in column 1 of table 1 or table 2; it is expected that these values of temperature are reproduced within ± 0.002 °K; and the measuring current at each temperature is specified. For the user's information we attempt to fit the calibration data with a polynomial and include the results as part of the calibration service.

7. References

[1] H. H. Plumb and G. Cataland, J. Res. NBS **69A** (Phys. and Chem.) No. 4,375 (1965); Technical News Release, May 1965–Str–3198.

[2] H. H. Plumb and G. Cataland, Science **150,** 3693 (1965) p. 155.

[3] F. G. Brickwedde, H. van Dijk, M. Durieux, J. R. Clement, and J. K. Logan, The 1958 He^4 Scale of Temperature, J. Res. NBS **64A** (Phys. and Chem) No. 1, 1 (1960).

[4] H. J. Hoge and F. G. Brickwedde, The Establishment of a Temperature Scale for the Calibration of Thermometers between 14° and 83 °K, J. Res. NBS **22,** 351 (1939) RP1188.

[5] J. R. Clement and E. H. Quinnell, Rev. Sci. Instr. **23,** 213 (1952).

[6] A. Brown, M. W. Zemansky and H. A. Boorse, Phys. Rev. **84,** 1050 (1951).

[7] M. H. Edlow and H. H. Plumb, Temperature, Its Measurement and Control in Science and Industry (Reinhold, New York 1963), Vol. **3,** C. M. Herzfeld ed., Part 1, F. G. Brickwedde ed., p. 407.

[8] P. Lindenfeld, Rev. Sci. Instr. **32,** 1 (1961).

[9] T. M. Dauphinee and H. Preston-Thomas, Rev. Sci. Instr. **25,** 9 (1954).

[10] H. van Dijk, Comité International des Poids et Mesures, Comité Consultatif de Thermométrie, 6e Session-1962, Annexe 25, p. 151.

[11] R. J. Corruccini, Advances in Cryogenic Engineering, Vol. **8,** p. 315 (Plenum Press, New York, 1963).

[12] T. M. Flynn, H. Hinnah, and D. E. Newell, Advances in Cryogenic Engineering, Vol. **8,** p. 334 (Plenum Press, New York, 1963).

[13] G. K. White and S. B. Woods, Rev. Sci. Instr. **28,** 8 (1957).

[14] I. Estermann, Phys. Rev. **78,** 83 (1950).

[15] S. A. Friedberg, Phys. Rev. **82,** 764 (1951); S. A. Friedberg, Temperature, Its Measurement and Control in Science and Industry (Reinhold, New York, 1955) Vol. 2, H. C. Wolfe, ed., p. 359.

[16] T. H. Geballe, F. J. Morin, and J. P. Marta, Conférence de Physique des Basses Températures, Paris (1955) p. 87.

[17] J. E. Kunzler, T. H. Geballe, and G. W. Hill, Rev. Sci. Instr. **28,** 96 (1957).

[18] J. S. Blakemore, Rev. Sci. Instr. **33,** 106 (1962).

[19] F. J. Low, Advances in Cryogenic Engineering, Vol. **7,** p. 514 (Plenum Press, New York, 1962).

[20] J. S. Blakemore, J. W. Schultz, and J. G. Myers, Rev. Sci. Instr. **33,** 545 (1962).

[21] M. H. Edlow and H. H. Plumb. (Being edited at NBS).

[22] H. Fritzsche, Phys. Rev. **119,** 1899 (1960).

[23] R. B. Scott, Cryogenic Engineering, p. 337 (D. van Nostrand Co., Inc., Princeton, New Jersey, 1959).

(Paper 70A3–400)

JOURNAL OF RESEARCH of the National Bureau of Standards—A. Physics and Chemistry
Vol. 70A, No. 3, May-June 1966

Dissociation Pressure of Aluminum Carbide Using a Rotating Knudsen Cell

E. R. Plante and C. H. Schreyer

Institute for Materials Research, National Bureau of Standards, Washington, D.C.

(February 17, 1966)

An attempt was made to eliminate surface depletion effects in the vaporization of aluminum carbide (Al_4C_3) by carrying out measurements in a Knudsen cell rotating at an angle of 45 deg from the vertical. Results showed that the surface depletion effects encountered with this material are due to formation of layers of graphite over individual particles of aluminum carbide rather than to formation of a macroscopic layer of graphite over the sample. In order to achieve near-equilibrium pressures, vaporization experiments were carried out in which the sample was ground prior to each experiment and the amount of aluminum vaporized during each experiment minimized. Third law treatment of these data yielded $\Delta H°(298)$ of 91.6 kcal mol^{-1} (383.3 kJ mol^{-1}) for the decomposition of $\frac{1}{4}Al_4C_3$ to form Al(g) and $\frac{3}{4}C$(C), in good agreement with data based on calorimetric studies.

Key Words: Aluminum carbide, dissociation pressure, heat of decomposition, rotating Knudsen cell, surface depletion.

1. Introduction

The Knudsen method is widely used in obtaining vapor pressure data and heats and entropies of vaporization of inorganic materials. The equilibrium vapor pressure of a univariant system is a function of temperature [1] only; however, since the Knudsen effusion method is a dynamic process, departure from equilibrium is possible.

The inorganic materials which undergo univariant vaporization can be divided into two classes, those which vaporize congruently and those which vaporize incongruently. Frequently, it is difficult to achieve equilibrium or near-equilibrium conditions with those materials which vaporize incongruently.

The pressure versus time curve for such materials at constant temperature typically shows an initial region in which the pressure decreases rapidly by a factor of 2 to 4, followed by a region in which the pressure appears to have achieved a constant value within experimental error. Among the examples of incongruent vaporization reactions for which this type of vaporization behavior has been reported are

(a) the decomposition of Mo_3Ge to Mo(c) and Ge(g) reported by Peavler and Searcy [1],[2]

(b) the decomposition of TiC to Ti(g) + C(c) and Cr_3C_2 to Cr(g) + C(c) reported by Fujishiro and Gokcen [2, 3],

(c) the decomposition of $Mg(OH)_2$ reported by Gregory and Kay [4]; and

(d) the decomposition of Al_4C_3, and SiC reported by Meschi and Searcy [5] and Davis, Anthrop, and Searcy [6].

Various explanations have been advanced to account for the pressure variation with time. Among these are that the vaporizing species has a low evaporation coefficient on the surface in question, i.e., that the rate of evaporation is much slower than the rate at which molecules collide with the surface under the equilibrium pressure, or that the formation of a nonvolatile surface layer (the solid decomposition product) impedes the rate of transfer of vapor from the evaporant to the effusion space sufficiently so that near-equilibrium pressures cannot be maintained. In the event that surface depletion effects are important, one can distinguish between two cases. In one case, a macroscopic layer of the nonvolatile decomposition product can be formed over the surface of the sample in the Knudsen cell and the transfer of material through this layer is rate determining. In the second case, the nonvolatile decomposition product can form a layer over each particle of the vaporizing material. In conformance with the previous usage of Davis, Anthrop, and Searcy [6], these two types of surface depletion will be referred to as macrolayering and microlayering effects, respectively. In the event that macrolayer effects are responsible for the decrease in pressure with time, rotation of a crucible making an angle of about 45° from the vertical during the measurements should prevent formation of macrolayers and enable one to obtain near-equilibrium pressures.

[1] All temperatures in this paper are based on the 1948 IPTS.

[2] Figures in brackets indicate the literature references at the end of this paper.

2. Experimental Method

Measurements were carried out in a conventional oil-pumped vacuum system. A graphite Knudsen cell was attached to a 1.27 cm O.D. stainless steel center shaft by three 0.16 cm diam tungsten legs. The center shaft was mounted on two precision stainless steel ball bearing assemblies which fitted snugly ingo the vacuum housing. A commercially available rotary feedthrough, modified for this work and using a magnetic coupling through the vacuum wall was connected to the center shaft by a pair of beveled gears and allowed the center shaft to be rotated at approximately 7 rpm. A rotatable flange connected the part of the vacuum system containing the rotation axis to the trap and diffusion pump. For experiments in which the crucible was rotated, this flange was rotated to about 45° from the vertical. It was concluded from visual inspection of a rotating lidless Knudsen cell containing an aluminum carbide sample at room temperature that sufficient mixing of the sample would take place to prevent the formation of macrolayers of graphite over the aluminum carbide sample.

The vacuum system could be used with a conventional Vycor effusion apparatus utilizing collection of a known fraction of the vapor on fused silica or platinum targets. This technique allows one to obtain pressure-time data without opening the system to the atmosphere and is advantageous in the case of aluminum carbide because it is hydrolyzed by moist air. However, preliminary data indicated that rotation of the crucible failed to prevent a decrease in the volatility with time and because of the relatively poor precision obtained by this method when target weight gains were determined on a microbalance, this method was abandoned and further experiments carried out using the weight loss method. In these latter experiments, a conventional water cooled Vycor condenser connected to the vacuum system by a ground glass to stainless steel joint sealed with Apiezon W sealant completed the system.

The Knudsen cell was fabricated from a special grade of graphite obtained from Chance-Vought Corporation. The cell was 2.5 cm high by 1.9 cm O.D. with 0.32 cm thick sidewalls and an effusion hole and assumed blackbody hole of 0.1 cm diameter. The blackbody hole had a depth of 0.6 cm. Heating was accomplished by induction at 450 kHz. Temperatures as measured with an NBS calibrated optical pyrometer sighted on the blackbody hole corrected for reflection of light by a window and mirror were accepted.

No radiation shields were used on the crucible. Temperature uniformity of the crucible could be achieved by careful positioning of the induction coil which was mounted on a rigid Plexiglas frame. The position of the work coil was reproduced relative to that of the crucible within a few mm. Good temperature uniformity was inferred from the observation that in a typical experimental series, the crucible lid, which constituted about 40 percent of the internal surface area of the crucible, gained about 3 mg and the crucible bottom gained 2 mg, while 106 mg of Al was vaporized.

Choice of aluminum carbide as a test substance for the rotating effusion cell apparatus was made because measurements, since published, were in progress to determine reliable heat of formation [7] and heat capacity data [8] at NBS. In addition, mass spectrometric data [9] indicated that within the temperature range of interest, the vapor is almost pure Al(g) and previous effusion measurements [5] indicated that nonequilibrium effects might be due to the formation of a graphite macrolayer over the Al_4C_3 within the Knudsen cell.

The aluminum carbide sample used in this work was a portion of that previously used at NBS by King and Armstrong for combustion experiments [7] and by Furukawa et al. [8], for heat capacity measurements. The results of chemical analysis of portions of this material have previously been reported in detail [7, 8]. These data showed major impurities to be approximately 1 percent free Al, 1 percent free C, 1.3 percent AlN and 2.0 percent Al_2O_3. It was assumed that nitrogen determined by the Kehldahl method was present as AlN and that aluminum not accounted for as Al, Al_4C_3, or AlN was present as Al_2O_3. X-ray analysis carried out during the course of the present work showed that the sample as received contained minor phases of C(gr) and Al(c) besides Al_4C_3. After vaporization of about 30 percent of the aluminum in a sample the Al peak disappeared as expected. Failure to detect either Al_2O_3 or AlN in the x-ray patterns may indicate that oxygen and nitrogen were present in the sample in solid solution or as complicated carbonitrides [10] or oxycarbides [11]. However, the amounts of these materials present in the sample would be close to the limits of detection and it was not possible to establish the nature of the oxygen or nitrogen impurities on the basis of the x-ray data. On the basis of previous data [12], one would expect the CO pressure above an aluminum oxycarbide or Al_2O_3-C mixture to be sufficiently high so that oxygen would be preferentially lost from the Knudsen cell as CO during the vacuum vaporization measurements while any AlN or carbonitride would be concentrated in the condensed phase.

The procedure followed in obtaining pressure data consisted of slowly heating the crucible to a temperature of about 1500 °K, allowing the background pressure to decrease to about 10^{-5} torr then rapidly increasing the power to the predetermined setting. The duration of the experiment was measured from the time the predetermined power level was reached to the time the oscillator was turned off. Hence, the initial deficiency in vaporized aluminum caused by the fact that the Knudsen cell is not at temperature at $t=0$ is approximately compensated by the excess of aluminum vaporized after the oscillator is turned off.

Weight changes were determined by weighing the crucible to the nearest 0.1 mg before and after an experiment. During exposure to the atmosphere

while in the Knudsen cell, the specimen gained weight initially at the rate of approximately 0.6 mg per hour. Weight pick up during grinding was undoubtedly greater than this but no simple method of correcting for this effect could be made. Total time exposure to air during experiments where grinding was necessary was 10 to 15 min and shorter for other experiments. Leakage between the lid and crucible junction was judged to be negligible on the basis of visual inspection of the Vycor condenser surrounding the crucible.

3. Data and Thermodynamic Treatment

Vapor pressures were calculated using the equation[3]:

$$P=\frac{m}{kat}\left(\frac{2\pi RT}{M}\right)^{1/2}$$

where m is the mass of aluminum vaporized, t is the duration of the experiment, a is the area of the effusion hole, k is the Clausing correction, T is the absolute temperature, R is the gas constant, and M is the atomic weight of the vaporizing species, Al(g). The area of the effusion hole calculated from its measured diameter was increased by 2 percent to correct for thermal expansion.

The Clausing factor k corrects for the fact that the orifice has finite depth and was taken from the tabulation in Dushman [13]. For our crucible the length to radius ratio was 3.14 and $k=0.410$.

The heat and entropy change for the reaction

$$1/4\,Al_4C_3(c)=Al(g)+3/4\,C(c) \qquad (1)$$

were evaluated by the least squares solution of the approximate integrated form of the Clausius-Clapeyron equation

$$\ln P(\text{atm})=-\frac{\Delta H^\circ}{RT}+\frac{\Delta S^\circ}{R} \qquad (2)$$

where ΔH° and ΔS° are the heat and entropy changes for reaction (1) at the average temperature.

In addition, third law heats for reaction (1) were calculated using the equation

$$\Delta H^\circ_{298}=T\left[\left(\frac{G^\circ_T-H^\circ_{298}}{T}\right)_R-\left(\frac{G^\circ_T-H^\circ_{298}}{T}\right)_P-R\ln P(\text{atm})\right]$$

where $\left(\frac{G^\circ_T-H^\circ_{298}}{T}\right)$ is the free energy function and the subscripts R and P refer to reactants and products. Since free energy functions for $Al_4C_3(c)$, Al(g), and C(c) are well established, the average third law heat of sublimation is more reliable than the second law heat provided dissociation pressures close to equilibrium have been obtained.

4. Results

Experimental results of two types were obtained in this study. In the first type of experiment, apparent pressures versus time or fraction of aluminum vaporized were obtained to try to determine the shape of these curves and the extent of departure from equilibrium pressures based on thermochemical data.

These experiments showed that rotation of the crucible had no detectable effect on the apparent vapor pressure which continually decreased as the fraction of aluminum vaporized from the sample increased. Figure 1 shows some typical volatility data expressed as weight loss/unit time versus fraction of Al vaporized from the sample. As is usual with this type of experiment, an initially rapid decrease in volatility is followed by a region in which the volatility appears to be essentially constant. This behavior is illustrated by the first six data points of the IV-62 data obtained at about 1870 °K shown in figure 1. On raising the temperature to 1970 °K, the same type of behavior is observed for the next seven points and when the temperature is again lowered to 1870 °K with about 0.49 of the available aluminum vaporized from the sample, the volatility is found to be only about 1/4 of its previous "steady-state" value at this temperature. After grinding the sample, the last three points of the IV–62 data were obtained at about 1870 °K. These points show the same type of behavior as those obtained at the beginning of the series except that the rate of decrease of volatility is slower than was observed initially. This is probably due to the smaller particle sizes present in the latter measurements. Although the IV–62 data are entirely consistent with the idea that the volatility of aluminum carbide decreased continually with the fraction vaporized, the series V–44 data were taken in order to study this process at a constant temperature. This series of data clearly shows that at about 1915 °K, no steady state pressure is ever achieved.

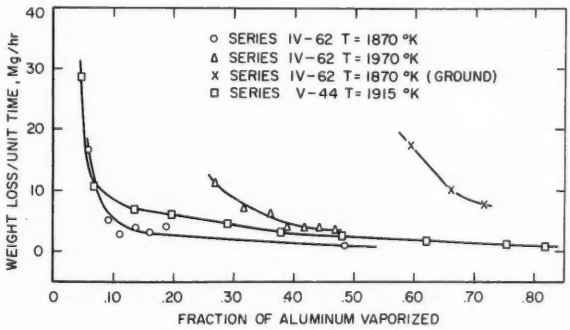

FIGURE 1. *Volatility as a function of fraction of aluminum vaporized from* Al_4C_3.
(a) Original sample weights were 198 mg for series IV–62 and 134 mg for series V–44.

[3] Values of constants used in the calculations were $R=8.3143\ J\ mol^{-1}\ °K^{-1}$ or 1.98717 cal $mol^{-1}\ °K^{-1}$; atomic weight of aluminum 26.98; one standard atmosphere = 101,325 $N\ m^{-2}$.

On the basis of these measurements, we conclude that in order to obtain apparent pressures anywhere near equilibrium one must take advantage of every possible factor which increases the degree of saturation within the Knudsen cell. These factors require that the sample be ground before each experiment to break up the graphite on the sample particles, and that the amount of aluminum vaporized from the sample during any experiment be kept as small as possible.

TABLE 1. *Decomposition pressures and heats of decomposition of aluminum carbide*[a]

Temp.	Duration of run	Weight loss[b]	Decomposition pressure	$\Delta H°(298)$
°K	*sec*	*mg*	atm × 10^4	kcal/mol Al(g)
1705	9600	6.3	0.341	92.5
1706	9600	3.1	.168	94.9[c]
1924	600	12.6	11.6	90.6
1889	900	10.2	6.20	91.3
1835	1800	8.8	2.64	91.9
1783	3600	8.6	1.27	92.0
1810	2400	9.0	2.01	91.7
1651	14400	4.9	0.174	91.8
1757	3600	5.8	.850	92.1
1730	5400	6.8	.659	91.5
1863	14400	13.3	5.02	90.9
1676	8100	4.1	0.261	91.8
Mean $\Delta H°(298)$ and standard error..... 91.6 ± 0.2 kcal/mol Al				
Estimated overall uncertainty..... 0.6 kcal/mol Al				

[a] In experimental sequence.
[b] Orifice area at room temperature = 8.25×10^{-3} cm^{-2}, clausing factor = 0.410, initial sample weight = 301 mg.
[c] This point was not included in the analysis.

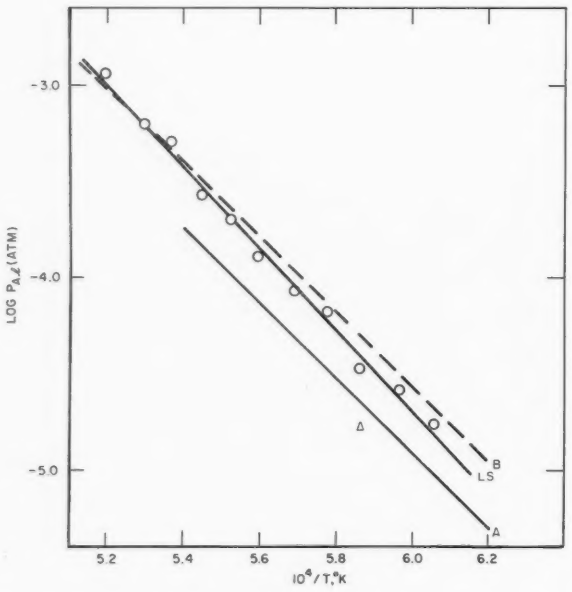

FIGURE 2. *Clausius-Clapeyron plot of aluminum carbide dissociation pressure data.*
(a) Triangular point was omitted from the least squares analysis. All points shown were obtained in this work.
(b) *LS* is least squares line of our data.
(c) *A* is least squares curve reported by Searcy and Meschi.
(d) *B* is the vapor pressure curve based on the heat of formation reported by King and Armstrong [7], and thermal data reported by JANAF.

Measurements carried out in this way in an attempt to obtain equilibrium pressures are listed in table 1 and shown in figure 2. These data yield a third law heat of decomposition, using JANAF [14] free energy functions, of $\Delta H°$ (298) for reaction (1) of 91.6 kcal mol^{-1} (383.3 kJ mol^{-1}) of Al and a standard error of 0.17 kcal mol^{-1} (0.71 kJ mol^{-1}). Second law treatment of the same data gives a $\Delta H°(298)$ of 99.1 kcal mol^{-1} (414.6 kJ mol^{-1}) and a standard error of 2.5 kcal mol^{-1} (10.5 kJ mol^{-1}) of Al. These values are compared in table 2 with the values obtained from the data of Searcy and Meschi who studied the decomposition of Al_4C_3 by both the torque-Knudsen and weight loss method and with the most recent thermochemical data. Since Searcy and Meschi did not report their data in detail, the value listed in table 2 was based on their reported average pressure of 4.2×10^{-6} atm at 1600 °K.

TABLE 2. *Heat of decomposition of* $1/4Al_4C_3$

Investigator	$\Delta H°(298)$ 3d Law kcal/mol Al (kJ/mol Al)	Overall uncertainty kcal/mol Al (kJ/mol Al)	$\Delta H°(298)$ 2d Law kcal/mol Al (kJ/mol Al)	Standard error kcal/mol Al (kJ/mol Al)
This work	91.6 (383.3)	0.6 (2.5)	99.1 (414.6)	2.5 (10.5)
Meschi and Searcy	93.7 (392.0)	3.0[a] (12.6)[a]	90.9 (380.3)	3.0[a] (12.6)[a]
King and Armstrong	90.4[b] (378.2)[b]	1.5[c] (6.3)[c]		
Mah	91.4[b] (382.4)[b]	1.4[c] (5.9)[c]		

[a] These errors, reported by the authors, appear to be overall uncertainty estimates.
[b] Derived from heat of formation of Al_4C_3 reported by these authors and heat of formation of Al(g) at 298 °K of 78.0 kcal mol^{-1}.
[c] For description of the derivation of these uncertainty estimates, see text.

The overall uncertainty in the third law heat for the decomposition reaction was estimated as the sum of the squares of the uncertainties resulting from random errors (0.51 kcal), pyrometer calibration uncertainty (0.20 kcal), and window and prism uncertainty (0.15 kcal). These errors are based on three standard errors except for the pyrometer calibration uncertainty which was estimated from the uncertainties quoted on the NBS calibration certificate. It is not possible to make a reliable estimate of the error arising from nonequilibrium effects. Hopefully, part of this error will cancel because of vaporization of impurities or excess loss of vapor from the joint between the bottom and top of the crucible. The difference between the second law heat and the third law heat of about 7 kcal may be due to a progressively greater evaporation of impurities at the higher temperatures although other sources of systematic error are also possible.

The heat for the decomposition of Al_4C_3 can also be calculated on the basis of the recent combustion studies of King and Armstrong [7] who reported $\Delta H_f°(298.15) = -49.7 \pm 1.2$ kcal and Mah [15] who reported $\Delta H_f°(298.15) = -53.4 \pm 2.0$ kcal. These

values lead to the heats of decomposition shown in table 2 when combined with the heat of sublimation of Al of 78.0 ±0.4 kcal tabulated by JANAF. However, the errors quoted by JANAF and King and Armstrong were multiplied by 3 and that reported by Mah multiplied by 3/2 in order that all the uncertainties would be based on three standard deviations in the mean. These results indicate that the measured decomposition pressures of Al_4C_3 are consistent with the decomposition pressures predicted on the basis of heats of combustion and heat content data.

5. Discussion

One of the principal differences between our work and the results reported by Searcy and Meschi is that at no time did we observe any segregation within the crucible into macrolayers of graphite and aluminum carbide. Our results indicate that for the Al_4C_3-C system, the formation of graphite over individual particles is responsible for the decrease in volatility as the sample is vaporized. It is possible, however, that macrolayering effects might become important if the sample depth is sufficiently great.

At 1700 °K, our average dissociation pressure of aluminum carbide is about 60 percent greater than the average pressure at 1700 °K reported by Meschi and Searcy. This is consistent with the observation that the volatility of Al_4C_3 decreased with the fraction of the sample vaporized (provided the sample is not disturbed by grinding) and is taken to indicate that Meschi and Searcy obtained pressure data after having vaporized a larger fraction of the sample than we had in the present study. It is also consistent with the fact that Meschi and Searcy were able to obtain pressures in torsion experiments as high as those obtained in weight loss experiments despite a less favorable ratio of orifice area to sample surface area. The approximate pressure of Al over Al_4C_3 (6×10^{-4} at 2100 °K) reported by Chupka et al. [9], lower than the estimated equilibrium Al pressure by about a factor of ten is also consistent with these observations.

For the type of vaporization process under consideration here at least three different regions of a volatility-time plot can be imagined. In the initial region, the surface area of the material undergoing decomposition might be sufficiently large so that equilibrium pressures are obtained, in the second region the volatility will decrease as the decomposing surface area decreases, and in the third region the rate of vaporization will be diffusion controlled.

For any particular study, the importance of these three regions will depend on the sample size, the average particle size, the sample surface area and the amount of material which has vaporized from the Knudsen cell, although for most studies the first two regions will probably be traversed so quickly that they will be of no experimental significance. Hole size correlations based on Motzfeldt's [16] or similar relations will be subject to indefinite error because of the variation in the pressure with time. In general, one can expect that the rate of decrease of volatility with fraction of sample vaporized will depend on temperature although for the limited temperature ranges used in most high temperature studies, such an effect may be of only secondary importance. One additional complicating factor is that rupture or opening of fissures in individual particles of the sample may take place because of the difference in densities of the solid product and the reactant.

In view of these many complexities, development of a method to eliminate various kinetic effects is desirable and rotation of the Knudsen cell has been our first attempt in this direction. This study has shown that microlayering is an important cause of decrease in the volatility of aluminum carbide. Work on other carbides is in progress to determine if this is a general property of carbides and if so, to attempt to develop a means of preventing formation of microlayering. Mechanically grinding the specimen within the Knudsen cell while experiments are in progress is a possibility which may hold promise if sufficient grinding can be obtained and the material problem is not too great.

6. References

[1] R. J. Peavler and A. W. Searcy, J. Am. Chem. Soc. **78,** 2076 (1956).
[2] S. Fujishiro and N. A. Gokcen, J. Phys. Chem. **65,** 161 (1961).
[3] S. Fujishiro and N. A. Gokcen, Trans. Metal. Soc. AIME **221,** 275 (1961).
[4] E. Kay and N. W. Gregory, J. Phys. Chem. **62,** 1079 (1958).
[5] D. J. Meschi and A. W. Searcy, J. Phys. Chem. **63,** 1175 (1959).
[6] S. G. Davis, D. F. Anthrop, and A. W. Searcy, J. Chem. Phys. **34,** 659 (1961).
[7] R. C. King and G. T. Armstrong, J. Res. NBS **68A** (Phys. and Chem.) No. 6, 661 (1964).
[8] G. T. Furukawa, T. B. Douglas, W. G. Saba, and A. C. Victor, J. Res. NBS **69A** (Phys. and Chem.) No. 5, 423 (1965).
[9] W. A. Chupka, J. Berkowitz, C. F. Giese, and M. G. Inghram, J. Phys. Chem. **62,** 611 (1958).
[10] G. A. Jeffrey and V. W. Wu, Acta Cryst. **16,** 559 (1963).
[11] L. M. Foster, G. Long, and M. S. Hunter, J. Am. Ceram. Soc. **39,** 1 (1956).
[12] J. H. Cox and L. M. Pidgeon, Can. J. Chem. **41,** 671 (1963).
[13] S. Dushman, Scientific Foundations of Vacuum Technique, 2d edition, J. M. Lafferty, ed., p. 94 (John Wiley & Sons, Inc., New York, London, 1962).
[14] JANAF Thermochemical Tables, Dow Chemical Co., Midland, Michigan (1961) Al(g) + C(c) tables dated March 31, 1961, Al_4C_3 table dated June 30, 1963.
[15] A. D. Mah, Heat of Formation of Aluminum Carbide, U.S. Bureau of Mines, Report of Investigations 6415 (1964).
[16] K. Motzfeldt, J. Phys. Chem. **59,** 139 (1955).

(Paper 70A3-401)

JOURNAL OF RESEARCH of the National Bureau of Standards—A. Physics and Chemistry
Vol. 70A, No. 3, May-June 1966

Determination of Intermolecular Potential Functions From Macroscopic Measurements*

Max Klein

Institute for Basic Standards, National Bureau of Standards, Washington, D.C.

(February 11, 1966)

The second virial, adiabatic Joule-Thomson, viscosity, and diffusion coefficients predicted for a number of potentials are compared with those predicted for the (12, 6) potential. A quantitative picture, as a function of temperature, is obtained of the ability of each property to act as a probe of the potential function. The transport properties are found to be the most sensitive probes, the Joule-Thomson coefficient next, and the second virial coefficient least, the last property being essentially useless in the range $2.0 < T^* < 8.0$ on the (12, 6) reduced temperature scale.

Key Words: Potential function, second virial, viscosity, diffusion coefficient, Joule-Thomson, potential parameters.

1. Introduction

Statistical mechanics provides a molecular foundation for thermodynamics. This results in the expression of thermodynamic properties as functionals of the intermolecular potential functions of the constituent molecules. In principle, given the potential function appropriate to a given system one can calculate all of the thermodynamic properties of that system merely by turning the computational crank. In practice, matters are not so simple both because the relationships to be evaluated are enormously complicated and because the potential functions are not known with sufficient accuracy.

The most accurate of the statistical mechanical expressions contain N-body potential functions ($N \sim 10^{23}$) which are impossibly difficult to calculate. Simplifying assumptions can be made which often, as in the virial expansion, result in a power series in some parameter (e.g., the density) whose coefficients depend on lower order N-body potentials ($N=2, 3, \ldots$). Since even the three-body potential is exceedingly difficult to calculate, the assumption of pairwise potential additivity must generally be included. With this assumption, the thermodynamic properties, in the statistical mechanical expressions, can be made to depend on only the pair potential function. Most theories for the further simplification of the complicated expressions proceed from this point on the assumption that the pair potential function is known. These theories result in simpler, but generally still complicated, relationships between the thermodynamic properties and the potential function. The evaluation of such theories can be a formidable task. All too often their final evaluation is obscured [1][1] considerably by the fact that pair potential functions are, in practice, only imperfectly known.

The intermolecular potential function together with a sufficiently accurate theory can be used to extrapolate far beyond the bounds of available experimental data [2], something which is not possible using completely empirical methods. Such extrapolations are very strongly dependent on the potential function and can be considerably in error when the wrong potential function is used.

Clearly the determination of accurate intermolecular potential functions is of some importance. In this work we have sought to understand some of the methods generally used to determine such functions, particularly with respect to the question of the uniqueness of the potentials obtained. A lack of uniqueness exists when a set of experimental data for a given property can be correlated equally well using the appropriate theory and any of two or more potential functions. Where a lack of uniqueness exists, it becomes necessary to attempt to determine if there is a lack of sensitivity inherent in the theoretical quantity itself or if it is lack of experimental precision which makes it possible to fit the data equally well with two or more theoretical curves. These are equivalent to the following two questions. First, how well can the property of interest, in principle, distinguish among potential functions and, second, how well can it distinguish among such functions at the present time, given present day experimental precision. The answer to the first question is a perma-

*Supported, in part, by the Air Force Systems Command, Arnold Engineering Development Center, Tullahoma, Tenn., Delivery Order Number (40-600) 66-22 Program Element 61445014, AF Project 8951.

[1] Figures in brackets indicate the literature references at the end of this paper.

nent one while the answer to the second one changes as experimental technique is refined, approaching the first answer in the limit of zero experimental error. We have restricted ourselves to the first question and discuss the second one only in passing mainly to place our results in a practical light. The answer to the first question is of considerable practical importance since it points out where refined experimental techniques will not produce more information about the potential function.

In principle the pair potential functions can be calculated in an a priori fashion using quantum mechanics by calculating the potential energy of two molecules as a function of nuclear spearation. Since one needs to consider all the electrons in each molecule, this is also an intractable N-body problem, N now being the total number of electrons involved. This leaves one no alternative but to turn the problem around and determine the potential, in some manner, from experiment. In practice, the procedure is reduced to a semiempirical one. A functional form is assumed for the potential whose choice is based, in part, on theoretical arguments. In this form are included parameters whose values (and hence the detailed potential) are to be determined from experiment. The parameter determination is made by substituting the potential into statistical mechanical expressions for some macroscopic property and comparing the result with experiment [3]. Best results are to be expected when the theory is one whose dependence on the pair potential is strongly based as is the case, for example, in the low density limit of certain theories.

In this paper we shall discuss the use of the zero-density viscosity, diffusion, and adiabatic Joule-Thomson coefficients and the second virial coefficient as ways of obtaining the potential parameters. For each of these, the pair potential appears in the integrand of an expression for the macroscopic property. This suggests that, given enough experimental data of sufficient accuracy, one might be able to invert the theoretical expressions and determine the potential as a unique functional of the experimental data. For the second virial coefficient, however, Le Fevre and Keller and Zumino [4] have shown that the potential is not determined uniquely by the data, even in principle. In this work we demonstrate this lack of uniqueness quantitatively for particular potentials. We show there exists a lack of uniqueness for each of the macroscopic properties considered, although it is somewhat less pronounced for the transport properties than for the equilibrium properties. For each property, the lack of uniqueness is found to be more pronounced in one temperature range than in another. Strong positive statements can then be made about the temperatures at which experiments designed largely to determine potential functions should not be performed for particular substances. We are also able to show the simultaneous fit of certain of these properties to be sensitive to differences in the potential function.

2. Computational Method

Because of its relative simplicity, we shall use the second virial coefficient to illustrate the details of the computation. The other properties are handled in essentially the same manner. We shall restrict the discussion to two parameter potentials. This is no real restriction since a three-parameter potential can be treated as a family of two parameter potentials one for each value of the third parameter.

The second virial coefficient is related to the potential function, φ, by the relation [3]

$$B(T)=b_0B^*(T^*)=-b_0\int_0^\infty\left[\exp\left(-\frac{\varphi^*(r^*)}{T^*}\right)-1\right]r^{*2}dr^* \tag{1}$$

where $b_0=\frac{2\pi N\sigma^3}{3}$, $T^*=kT/\epsilon$, $\varphi^*=\varphi/\epsilon$, and $r^*=r/\sigma$. Here, as usual, σ is a characteristic length related to φ and ϵ is the depth of the potential well. N is Avogadro's number. For a given potential, a given T, and in the left-hand side, a given experimental value of B at that T, (1) contains only the two unknowns σ and ϵ. In this work, in place of experimental $B(T)$ values, we supply to the left-hand member of (1) the second virial coefficient for a potential function other than the one appearing in the right-hand side. Thus, if the subscripts 1 and 2 refer to the two potentials, (1) becomes

$$B(T)=(b_0)_1B_1^*(T_1^*)=(b_0)_2B_2^*(T_2^*)$$

or

$$B_1^*(T_1^*)=\frac{(b_0)_2}{(b_0)_1}\int_0^\infty\left\{\exp\left(-\frac{\varphi_2^*(r^*)}{T_2^*}\right)-1\right\}r^{*2}dr^*$$

where $B_1^*(T_1^*)$ is a functional of $\varphi_1^*(r^*)$. Now $T_1^*=kT/\epsilon_1$ and $T_2^*=kT/\epsilon_2$ hence, for a given T, $T_2^*=\frac{\epsilon_1}{\epsilon_2}T_1^*$ so that

$$B_1^*(T_1^*)=\frac{(b_0)_2}{(b_0)_1}\int^\infty\left\{\exp\left(-\frac{\varphi_2^*(r^*)\epsilon_2}{T_1^*\epsilon_1}\right)-1\right\}r^{*2}dr^*. \tag{2}$$

This is an equation containing two unknowns, namely, the ratios ϵ_2/ϵ_1 and $(b_0)_2/(b_0)_1$. These ratios are completely determined, given another equation connecting some other functional of the potential for the two potentials. We have taken, for this second functional, the first derivative of B with respect to the logarithm of T [5]. We thus determine, *at each temperature*, that pair of ratios, ϵ_2/ϵ_1 and $(b_0)_2/(b_0)_1$ which results in the equality, for the two potentials, of both the second virial coefficient and its first derivative with respect to the logarithm of the temperature. Ordinarily, the ratios are different at different temperatures, hence we shall actually determine their temperature depend-

ence. By dividing the equation which represents the requirement of equality of the first derivatives by that representing the equality of the second virial coefficients themselves, one obtains a single equation for the equality of the logarithmic derivatives. The working equation becomes

$$\frac{d \ln B_1^*(T_1^*)}{d \ln T_1^*} = \frac{d \ln B_2^*(T_2^*)}{d \ln T_2^*}. \tag{3}$$

This is a single implicit equation in the ratio ϵ_2/ϵ_1, the dependence on $(b_0)_2/(b_0)_1$ being removed in the process of differentiating the logarithm.

On the substitution of the set of values $B_1^*(T_1^*)$ in the left-hand member, (2) becomes a family of curves for the ratio ϵ_2/ϵ_1, as a function of the ratio $(b_0)_2/(b_0)_1$, one curve for each value of T_1^* [7]. These can also be used for obtaining information about the potential function [8], although the results so obtained cannot be easily presented in a manner suitable for our purposes. We have therefore used a different approach. We have computed, for each of a number of potentials, B^* and $B'^* = T^* \left(\frac{dB^*}{dT^*}\right)$ and from these

$$S = \frac{T^*}{B^*}\frac{dB^*}{dT^*} = \frac{B'^*}{B^*} = \frac{d \ln B^*}{d \ln T^*}.$$

These are used to solve (3) in the following way. Each value of T_2^* has associated with it a value S_2. Using inverse interpolation, the value of T_1^* is found for which $S_1 = S_2$. The ratios ϵ_2/ϵ_1 and $(b_0)_2/(b_0)_1$ are then computed simply from

$$\frac{\epsilon_2}{\epsilon_1} = \frac{T_1^*}{T_2^*} \text{ and } \qquad \frac{(b_0)_2}{(b_0)_1} = \frac{B_2^*(T_2^*)}{B_1^*(T_1^*)}.$$

This procedure can be illustrated graphically with the help of figures 1 and 2. These contain plots of S for the second virial coefficient [9] versus the logarithm of the reduced temperature for several representative potential functions. Temperatures below the Boyle temperature appear in figure 1, those above that temperature in figure 2. Note that the S values for each potential are plotted against the logarithm of the reduced temperature *for that potential*. Equation (3) is solved graphically at each T_1^* by measuring the horizontal distance between the ordinate associated with T_1^* on curve 1 and the same ordinate on curve 2. This distance is then just

$$\log T_2^* - \log T_1^* = \log (T_2^*/T_1^*) = \log (\epsilon_1/\epsilon_2).$$

It should be noted that where there are values of S_2 greater than the maximum S_1 value, solution of (3) is impossible. This occurs (see fig. 1) for the (9,6) potential compared to the (12,6).

Note that both the value and slope of B_1^* are fit by B_2^* at T_1^*. It follows, therefore, that B_2^* will actually produce a relatively good fit to B_1^* in a small neighborhood

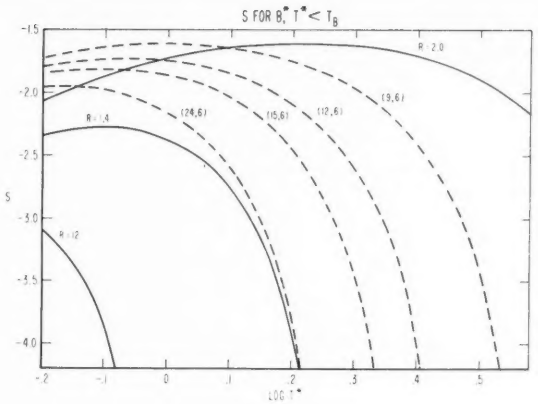

FIGURE 1. S *for the second virial coefficient of several potentials,* T* *less than the Boyle temperature.*

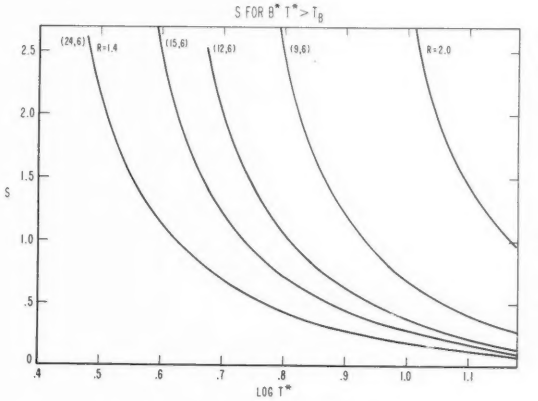

FIGURE 2. S *for the second virial coefficient of several potentials,* T* *greater than the Boyle temperature.*

around T_1^* for the parameter ratio obtained by solving (3) at T_1^*. Furthermore, when this ratio is found to be independent of T_1^* over a range of values of T_1^*, B_2^* provides an excellent fit to B_1^* over that range.

In this calculation, the Boyle temperature serves as a natural dividing point between two temperature ranges. Since B is zero at that temperature, the derivatives in (3) are not defined. Furthermore, since B changes sign while $\frac{dB}{dT}$ does not, S also changes sign. Hence, values of S taken from temperatures above the Boyle temperature for one potential cannot possibly be made to fit those taken from below it for the other potential. Therefore, we have treated these two ranges separately coming as close to the Boyle temperature as desired from either side.

As mentioned in the introduction, the zero density adiabatic Joule-Thomson, viscosity, and diffusion coefficients are also considered here. These are also treated as outlined above. The equation (3) for each

of these is replaced in turn by the requirement that the quantities $\frac{d\ln[\mu C_p^{(0)}]}{d\ln T^*}$ for the adiabatic Joule-Thomson coefficient, $\frac{d\ln \eta T^{*-1/2}}{d\ln T^*}$ for the viscosity, and $\frac{d\ln[\mathscr{D}T^{*-3/2}]}{d\ln T^*}$ for the diffusion coefficient be equal for the two potentials. Now [3] $\mu^* C_p^{(0)} = T^* \frac{dB^*}{dT^*} - B^* = B'^* - B^*$ so that the connection between this quantity and the potential function is essentially the same as between the second virial coefficient and the potential. From this last,

$$T^* \frac{d}{dT^*}[\mu C_p^{(0)}] = B''^* \qquad \text{and} \qquad \frac{d\ln[\mu C_p^{(0)}]}{d\ln T^*} = \frac{B''^*}{B'^* - B^*}$$

where $B''^* = T^{*2} \frac{d^2 B^*}{dT^{*2}}$. Here, as with the second virial coefficient, there is a temperature which divides the calculation into two parts. Now, however, the zero density inversion temperature (defined by $B'^* = B^*$) plays the role previously played by the Boyle temperature.

The connection between the viscosity and diffusion coefficients and the intermolecular potential function is contained in the so-called collision integrals [3]

$$\Omega^{(l,s)*}(T^*) \quad \frac{2}{(S+1)!\,T^{*(s+2)}} \int_0^\infty e^{-g^{*2}/T^*} g^{*(2s+3)} Q^{(l)*}(g^*)\, dg^*$$

where

$$Q^{(l)*}(g^*) = \frac{2}{1 - \frac{1}{2}\frac{1+(-1)^l}{1+l}} l \int_0^\infty (1 - \cos^l \chi) b^*\, db^*$$

with the intermolecular potential function being contained in the equation for the scattering angle

$$\chi(g^*, b^*) = \pi - 2b^* \int_{r_m^*}^\infty \frac{dr^*/r^*}{\sqrt{1 - b^{*2}/r^{*2} - \phi(r^*)/g^{*2}}}$$

r_m^* being the distance between a pair of molecules at the time of closest approach.

In terms of these, the zero density viscosity and diffusion coefficients can be written [3]

$$\eta T^{*-1/2} = \frac{C_a}{\Omega^{(2,2)*}(T^*)\sigma^2}, \qquad \mathscr{D} T^{*-3/2} = \frac{C_b}{\Omega^{(1,1)*}(T^*)},$$

where C_a and C_b are constants whose precise values are of no particular interest here. It can be easily shown that

$$\frac{d\ln \Omega^{(l,j)*}}{d\ln T^*} = (j+2)\frac{\Omega^{(l,j+1)*}}{\Omega^{(l,j)*}} - (j+2).$$

From this it follows that, for the viscosity, eq (3) is replaced by the requirement that $4\frac{\Omega^{(2,3)*}}{\Omega^{(2,2)*}} - 4$ be equal for the two potentials. For the diffusion coefficient, on the other hand, the quantity $3\frac{\Omega^{(1,2)*}}{\Omega^{(1,1)*}} - 3$ must be equal for the potentials. Since η and $\mathscr{D}$ are each nonzero, there is no dividing temperature analogous to the Boyle temperature for these properties. The S values corresponding to these properties are plotted in figures 3 and 4.

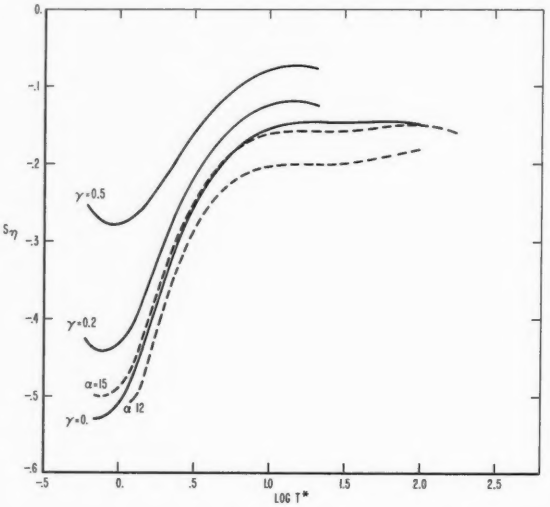

FIGURE 3. S *for the viscosity coefficient of several potentials.*

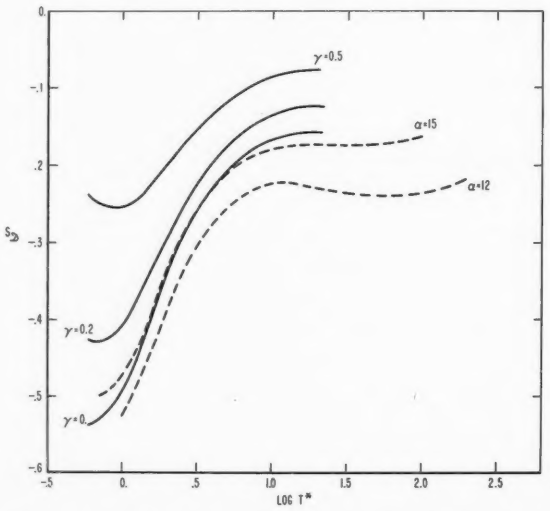

FIGURE 4. S *for the diffusion coefficient of several potentials.*

The macroscopic properties of most experimental systems have been correlated using the (12,6) potential function [10]. As a result ϵ/k values for that potential can be found in the literature for just about all possible systems of interest. Furthermore, it has been shown that, for very many substances, a very simple relationship exists between the ϵ/k value for the (12,6) potential and the temperatures for the critical and normal boiling points for that substance [3, 10, 11]. As a result, good first guesses for the ϵ/k values for the (12,6) potential can be made for any system for which either the critical temperature or normal boiling point is known. For these reasons we have chosen to compare each potential with the (12,6) function using the reduced temperature for the latter as the reference temperature T_1^*. The conversion to real experimental temperatures for any system merely requires multiplication by the (generally available) ϵ/k value of the (12,6) potential for that system.

3. Results

The Second Virial Coefficient. Our results for the second virial coefficient are given in figures 5 to 8 as plots of the ratios ϵ_2/ϵ_1 versus the Lennard-Jones (12,6) reduced temperature. Figure 11 contains plots of the ratio $(b_0)_2/(b_0)_1$. The potential functions considered are the following:

The (m, n):

$$\phi^*(r^*)=\frac{\phi(r)}{\epsilon}=\left\{\frac{1}{\left(\frac{n}{m}\right)^{\frac{m}{m-n}}-\left(\frac{n}{m}\right)^{\frac{n}{m-n}}}\right\}\left[\left(\frac{1}{r^*}\right)^m-\left(\frac{1}{r^*}\right)^n\right] \tag{1}$$

where $r^*=r/\sigma$, σ is that value of r for which $\varphi^*=0$.
The Kihara:

$$\phi^*(r^*)=\infty,\ r^*\leqslant\gamma^*$$
$$\phi^*(r^*)=4\left[\left(\frac{1}{r^*-\gamma^*}\right)^{12}-\left(\frac{1}{r^*-\gamma^*}\right)^6\right],\ r^*>\gamma^* \tag{2}$$

where $r^*=\dfrac{r}{\sigma-2a}$ and $\gamma^*=\dfrac{2a}{\sigma-2a}$, a being the core radius.

The Exp-6:

$$\phi^*(r^*)=\frac{1}{1-\frac{6}{\alpha}}\left[\frac{6}{\alpha}\exp\left(\alpha(1-r^*)\right)-\left(\frac{1}{r^*}\right)^6\right] \tag{3}$$

where $r^*=r/r_m$, r_m being that value of r for which $\varphi^*=-1$.

The Square Well:

$$\varphi^*(r^*)=\infty,\ r^*\leqslant 1$$
$$\varphi^*(r^*)=-1,\ 1\leqslant r^*\leqslant R^*$$
$$\varphi^*(r^*)=0,\ r^*\geqslant R^* \tag{4}$$

where $r^*=r/\sigma$.

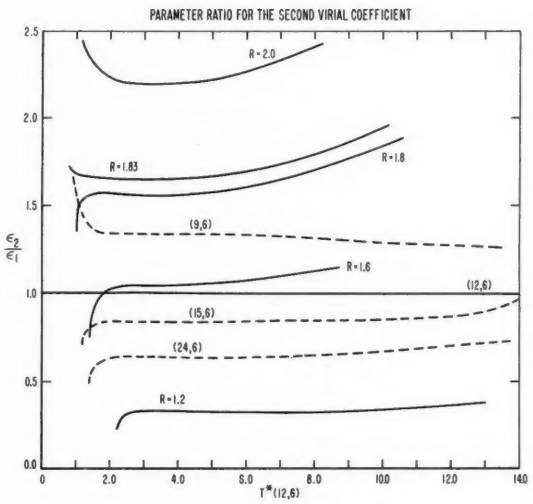

FIGURE 5. *The parameter ratios ϵ_2/ϵ_1 for the second virial coefficients of the* (m,6) *and square well potentials with respect to the (12,6) potential.*
Note particularly the flatness of the curves for the (*m*,6) potentials.

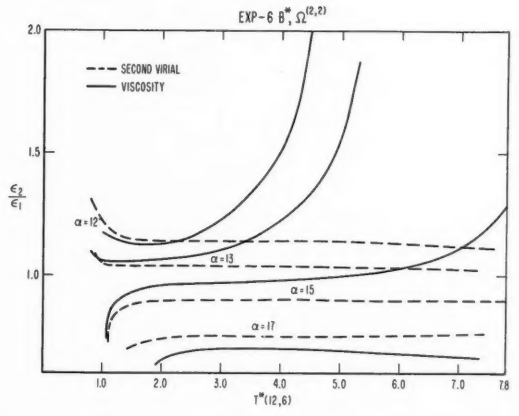

FIGURE 6. *The parameter ratios ϵ_2/ϵ_1 for both the second virial and viscosity coefficients of the exp-6 potential with respect to the (12,6) potential.*
Note that the former are flat while the latter are not flat.

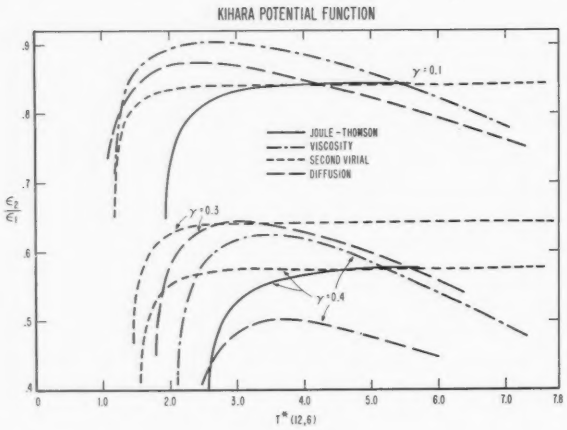

FIGURE 7. *The parameter ratios ϵ_2/ϵ_1 for all four properties for the Kihara potential with respect to the (12,6) potential.*
Note the absence of any single ratio for which both the equilibrium and transport properties are flat.

Figure 5 contains results for the (m,6) and square well potentials, while results for the exp-6 and Kihara potentials are contained in figures 6 and 7. Results for the (12,n) appear in figure 8. Each curve represents the comparison between a potential and the (12,6) potential, the subscript 2 always referring to the former potential. For each curve there is a smooth transition through the Boyle temperature indicating that the singularity in S at that temperature presents no problem. There exists, for each potential, a temperature range around the Boyle point such that in that range ϵ_2/ϵ_1 is essentially independent of T^*. This means that, for temperatures in that range, the (12,6) and the potential with which it is compared are equivalent [12]. In fact, each curve is flat to such an extent in this range that a choice cannot be made between the (12,6) potential and the one with which it is compared based on experimental second virial coefficient data taken entirely within the range, even when these data are obtained with an impossibly high precision. What is particularly striking is that there is a single temperature range in which all the curves are flat. This range becomes exceedingly large if one does not include the square well potential in the comparisons. Obviously, there is a reduced temperature regime in which the second virial coefficient is particularly useless as a probe of the potential function. What these results show specifically is that the second virial coefficient cannot be used in this range to distinguish among any of the members of the (m,6), exp-6, Kihara, (12,n) and square well families of potentials. The list would presumably have been broadened had we considered other classes of functions.

Of considerable interest are the results obtained when the (12,n) potentials are compared with the (12,6). The curves obtained for these are essentially the same as those for the (m,6) emphasizing the fact that the second virial coefficient cannot be used to determine the exponent of the attractive part of the potential. The requirement that the attractive exponent be 6 is, rather, a restriction placed on the potential based on a priori information, at least for the second virial coefficient. Thus, we see that the second virial coefficient is determined by the general shape of the potential and not necessarily by its details. This has previously been demonstrated formally by Le Fevre [4] and by Keller and Zumino [4]. They showed

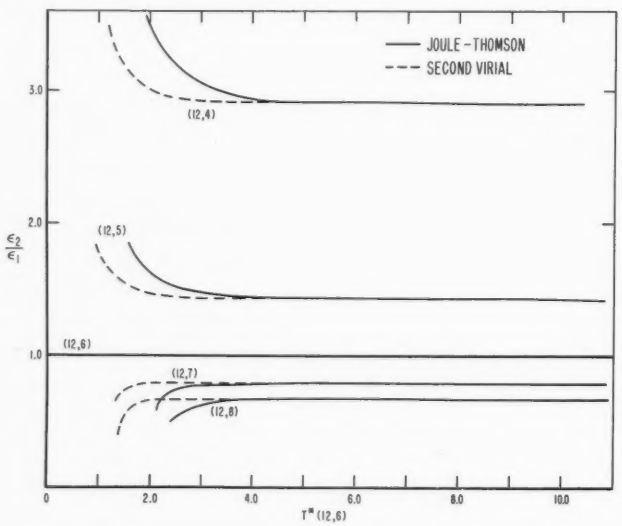

FIGURE 8. *The parameter ratios ϵ_2/ϵ_1 for both the second virial and Joule-Thomson coefficients for the* (12,n) *potential with respect to the (12,6) potential.*
Note that for temperatures above the Boyle point all curves are flat making it impossible to select a value of n at such temperatures.

that all potentials for which the sum of a certain pair of integrals, one over the repulsive part and one over the attractive part, were equal yielded the same second virial coefficient. A special case of their result is that all potentials with the same repulsive part and whose attractive parts have the same width as a function of depth (i.e., but whose bowls are possibly displaced laterally) yield the same second virial coefficient.

At temperatures outside the flat portion, the ratio ϵ_2/ϵ_1 is no longer constant. Below $T^*=2.0$ a particularly rapid variation is indicated. The origin of this rapid variation can be seen in figure 1 to be due to large differences in the slopes of the corresponding S curves for equal values of the ordinate. According to figure 1, there are also potentials for which there is a temperature range in which there are S values larger than the maximum S value of the (12, 6) potential. The (9,6) function is an example. In such cases, solution of (3) is impossible. In other words, no ratio ϵ_2/ϵ_1 exists by means of which one can obtain simultaneous equality of both B and $T\frac{dB}{dT}$ for the two potentials.

The existence of a rapid variation of ϵ_2/ϵ_1 with T^* at low temperatures would seem to indicate a very strong sensitivity, at such temperatures, to differences in the potential functions. Inability to solve (3) indicates an even stronger sensitivity to such differences. However, the sensitivity indicated applies strictly to exact data and the exact simultaneous fit of B and $T\frac{dB}{dT}$. As the requirement on the exactness of the fit is relaxed, the sharpness of the variation of ϵ_2/ϵ_1 with T^* is reduced. The introduction of these uncertainties in effect replaces each S curve of figure 1 by an area bounded by two S curves. One has then to compare two broadly defined S areas rather than two sharply defined S curves. This can make an overlap of ordinates possible near the maximum of the (12, 6) curve and hence make solution of (3) possible where it previously was not. Furthermore, in comparing the two S areas one has the possibility of choosing the two S curves, one within each area, whose slopes are most nearly alike. This could result in a reduction in the rapid variation of ϵ_2/ϵ_1 with T^* at low temperatures. For application to inherently imprecise experimental data, the low temperature region therefore becomes a much less sensitive probe of the potential than is indicated in figure 5. That is, an approximate fit to an accuracy compatible with experimental error might be possible where an exact fit, as indicated by figures 1 and 5, is impossible or, at best, difficult.

There is another, more fundamental reason why the rapid variation of ϵ_2/ϵ_1 with T^* at low temperatures does not necessarily mean a sensitivity to differences in the potential functions. In this calculation, we have required the equality of both the second virial coefficient and its slope for the two potentials. This applies a much more stringent condition on the functions than is required in the correlation of experimental data. In the latter case, it is asked only that the theoretical values of $B(T)$ come as close as possible to the experimental ones. Nothing is asked of the slope of the second virial coefficient. Clearly two functions may each fit the data within experimental precision, yet their slopes may disagree by considerably more than the precision of the present calculation.

On the other hand, the fact that we place such strong conditions on the potential enables us to make strong statements where the second virials and their first derivatives for the potentials are essentially indistinguishable from each other. Obviously where our calculations cannot distinguish between potentials, a correlation which makes use of experimental data will be able to distinguish between them to a much lesser extent. Clearly, therefore, experiments designed to measure the second virial coefficient for purposes of learning something about the potential function should never be carried out above $T^*=2.0$ on the (12,6) scale. In fact, existing data in that range should not be included in a determination of potential parameters since such data will supply experimental error without supplying any discrimination and so will reduce, for example, the ratios of the standard deviations obtained from fits of different potentials. This reduced temperature is easily converted to real temperatures for a particular substance given the ϵ/k value for the (12,6) potential for that substance. For example, for argon, the data must have been taken at $T<240$ °K while for xenon, the corresponding requirement is $T<450$ °K.

It is clear from figures 5 and 6 that in each class (i.e., square well, exp-6, etc.) there exists a potential for which the ratio ϵ_2/ϵ_1 is essentially independent of T^* even at low temperatures. For the exp-6 this occurs for α slightly larger than 13. For the square well, it occurs for R^* approximately equal to 1.82. One expects this also to be true for other classes of three parameter potential classes of which the (12,6) is not a member. That is, there will exist a member of each such class which is equivalent to the (12,6) in predicting the second virial coefficient over a large temperature range including low temperatures. Since the (12,6) potential function was chosen as the reference potential in an entirely arbitrary fashion, there is no need to restrict this result to it. Thus, one can actually state that given any potential function, it is possible to find in every three parameter family of functions of which it is not a member, a potential function with which one can obtain a classical second virial coefficient whose value and slope differ from those calculated with the given potential by an amount much less than the best available experimental precision over a temperature range starting at extremely low temperatures and extending to temperatures well above experimental conditions for almost all substances. In short, the second virial coefficient is seen to be at best a three parameter quantity with regard to the potential function and any attempt to use functions with more parameters necessarily leads

to redundancies. This is presumably what is behind the inability to obtain unique parameters in recent attempts to determine the potential function from second virial coefficient data using many parameter potential functions.

As expected, deviations from this can occur at high temperatures. That is, where the repulsive parts of the potentials differ sufficiently in character, the high temperature region can be used to choose among different classes. Thus a choice can be made between the extremely different (12,6) and square well potentials if the data covers a range above $T^* = 7.0$ on the (12,6) temperature scale. A choice between the somewhat less different exp-6 and (12,6) potentials, on the other hand, requires data at $T^* > 10.0$ on the same scale. These are very high temperatures for most substances. For argon this latter requirement is $T > 1200$ °K while for xenon it is $T > 2250$ °K.

The ratio $(b_0)_2/(b_0)_1$ for the second virial coefficient behaves in essentially the same way as does ϵ_2/ϵ_1. There is, therefore, no need to discuss its behavior separately.

Attempts to select, from several functions, a potential function for a particular system have sometimes been based on fits to second virial coefficient data which lie almost entirely within the flat portions of figures 5 to 8. Examples are the correlations of Whalley and Schneider [13] and of Mason and Rice [14]. In table 1 we have reproduced the standard deviations obtained by Whalley and Schneider for several potential functions. Note that only in the case of xenon, where half of the points lie outside the flat portions of figures 5 to 8, is there a strong discrimination among the potential functions. For the krypton data, one certainly has no basis for the selection of one potential over another while for argon the choice is, at best, a marginal one.

TABLE 1. *Standard deviations obtained by Whalley and Schneider* [a]

	(9,6)	(12,6)	$\alpha=12$	$\alpha=13$	$\alpha=14$	$\alpha=15$	Total number of isotherms	Number of isotherms $T^* < 2.0$ (12,6)
Argon	0.39	0.42				0.53	15	2
Krypton	.35	.36	0.46	0.47	0.41	.42	9	2
Xenon	1.20	.82	.88		.70	.62	12	6

[a] E. Whalley and W. G. Schneider, J. Chem. Phys. **23**, 1644 (1955).

From our results one can also see the futility of basing the choice of a potential function on the basis of the best fit of experimental data to a single two parameter function. To demonstrate this, let us take as an experimental system that system whose intermolecular potential function is exactly the (12,6) function. Figure 6 then represents an attempt to fit the "experimental" second virial coefficients to those predicted for the exp-6 potential. The best fit is obtained for that potential which gives the most nearly flat curve in figure 6. According to that figure, this best fit occurs for a value of α slightly greater than 13. The potential function defined by that value of α and the pair of parameters which give this best fit can then be associated with our "experimental" system and possibly used as such in other theories. Suppose now that instead of doing fits for a series of values of α we had just done the fit for a single value of α. Clearly, for every value of α, a pair of parameters exists which gives the best fit to the "experimental" data for that value of α. However, the potential represented by that value of α and this pair of parameters could not in general, be associated with the experimental system unless the application is to a theory only weakly dependent on the potential, since the second virial coefficient associated with that function does not properly represent the low temperature second virial coefficient data. It is clear from figure 6, therefore, that one must take the best fit of experimental data to a series of two parameter potentials (here the family of functions generated by varying the third parameter, α) before assigning a particular potential to the experimental system. Unfortunately, the literature is full of fits of data to single potential functions, particularly to the (12,6) potential. Quite often the resulting potential has been used as the intermolecular potential functions for particular systems in evaluations of theories [15]. According to our results one must be suspicious of conclusions as to the relation between the particular theory and experiment, based on such work, unless the theory is known to depend only weakly on the potential function.

4. Zero Density Adiabatic Joule-Thomson Coefficient

This quantity is obtained directly as the zero density limit of experimental free expansion data. To obtain the second virial coefficient, on the other hand, one must first, in some manner, differentiate the experimental P-V-T data with respect to the density and then take the zero density limit. As a result, given the same experimental precision, one obtains the latter with much less precision than the former. This is not a real advantage for the free expansion data at the present time, however, since such data can be obtained only with a precision orders of magnitude below that possible in P-V-T work, particularly at low densities.

The adiabatic Joule-Thomson coefficient depends both on the second virial coefficient and its first derivative. Clearly, where two second virial coefficients, one for each of two potentials, are indistinguishable over an extended temperature range, their first derivatives are also indistinguishable, at least for temperatures near the center of this range. Furthermore, this will be true for exactly the same parameter ratios. Differences which occur for the second virial coefficients near the edge of this temperature range necessarily appear as larger differences in their derivatives. Thus, one expects the range of equivalence for two potentials to be smaller for the zero density Joule-Thomson coefficient than it is for the second

virial coefficient. Results for this quantity are contained in figures 7 and 8. As expected, the range of equivalence of the potentials is shorter. It should be remembered that, since our method involves equating a property and its first derivative, equivalence here includes the second derivative of the second virial coefficient.

5. Zero Density Viscosity and Diffusion Coefficients

The ϵ_2/ϵ_1 ratios for the zero density viscosity and diffusion coefficients are contained in figures 6, 7, 9, and 10. The ratios $(b_0)_2/(b_0)_1$ for several potentials are presented in figure 11. In figure 7, for the Kihara potential, there is no curve for either of these properties which approaches that of the second virial coefficient in flatness. The ratio ϵ_2/ϵ_1, can be called independent of T^* only in a very narrow temperature region about the maximum of the curve. Figure 9 (which is drawn to a different scale) does indicate an increasing degree of flatness with increasing γ.

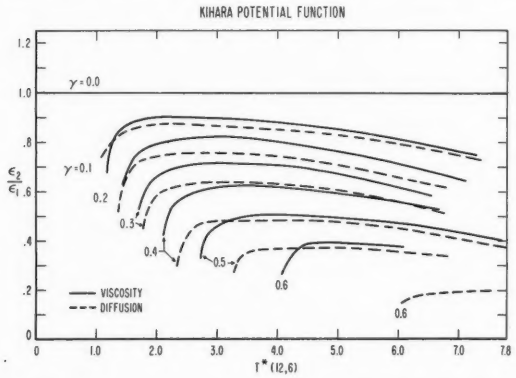

FIGURE 9. *The parameter ratios ϵ_2/ϵ_1 for the diffusion and viscosity coefficients for the Kihara potential function with respect to the (12,6).*
Notice the increasing flatness with increasing γ for T^* large.

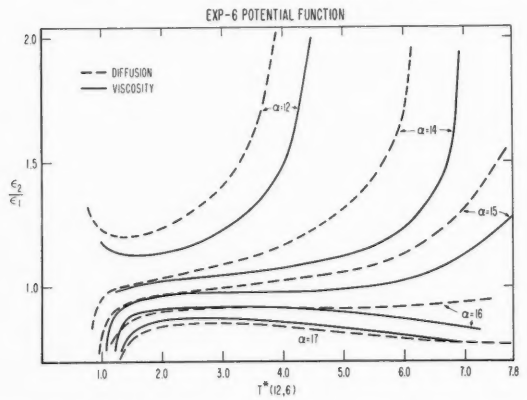

FIGURE 10. *The parameter ratios ϵ_2/ϵ_1 for the diffusion and viscosity coefficients for the exp-6 potential with respect to the (12,6) potential.*

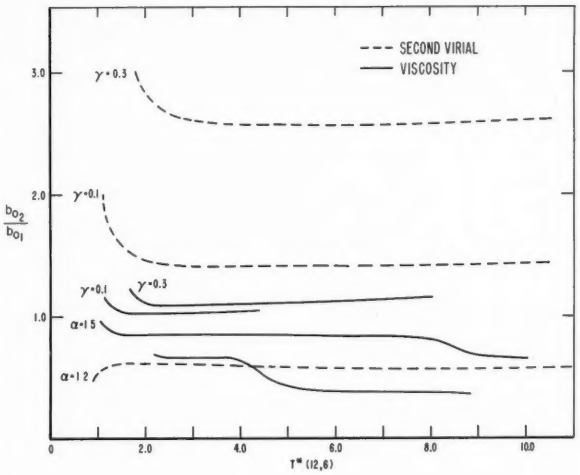

FIGURE 11. *The parameter ratios $(b_0)_2/(b_0)_1$ for the Kihara and exp-6 potentials with respect to the (12,6).*

This occurs for relatively high temperature, $T > T_B$, however. This demonstrates the strong role played by the bowl of the potential function in determining the transport properties. For any given potential function, there is a temperature above which the transport properties are entirely dependent on the repulsive part of the potential function. Now, for the Kihara potential function, the position of the hard sphere cutoff moves to larger values of r as γ increases. Therefore, the temperature at which the properties for the Kihara potential become those for a hard sphere should decrease with increasing γ. According to figure 9, this is compensated for by the changes produced by the modification of the bowl with increasing γ. The net result is a set of properties (e.g., for $\gamma=0.6$) more nearly like those for the $\gamma=0$, (i.e., (12,6)) potential at the highest temperatures of figure 9. Further proof of the strong effect produced by the bowl can be seen in the behavior at low temperatures. At such temperatures, the repulsive part has a very minor effect on the properties. Therefore, the rapid variation in the dependence of ϵ_2/ϵ_1, with T^* as a function of γ at low temperatures is an indication of the marked effect of the bowl on these properties.

The curves in figure 10 are most flat for T^* approximately equal to 2.0. It is interesting to note that there is a value of α for which the curve is quite flat at low temperatures as well. This occurs for α slightly larger than 13 for both properties. It should be noted that the corresponding ratio is very close to unity. Furthermore, for essentially the same value of α, a flat curve with essentially the same ordinate obtained down to low temperatures for the second virial coefficient. Note that, unlike the case of the second virial coefficient, for these properties the

curve for that value of α is not flat to very high temperatures. For these properties, a significant departure from unity occurs at $T^* = 5.0$, not an impossibly high temperature for many systems. There is a tendency for the curves to flatten out at high temperatures for a value of α larger than 15 under which conditions the curves show a marked deviation from flatness at quite low temperatures. This behavior shows that it may be possible to distinguish between the (12,6) potential and all members of the family of exp-6 functions given experimental transport data of sufficient accuracy which includes both the temperature ranges $T^* < 2.0$ and $T^* > 5.0$ on the (12,6) scale. For argon this requires that there be data for $T < 240$ °K and $T > 600$ °K while for xenon $T < 450$ °K and $T > 1225$ ° K. These conditions are met for argon but not for xenon, at the present time.

It is clear from these results that the diffusion and viscosity coefficients are potentially more sensitive probes of the potential function than either the second virial or Joule-Thomson coefficients given experimental data covering a sufficiently large temperature range. One might not have expected this since the latter properties are more simply related to the potential function than are the former. One might have expected a quantity like the second virial coefficient which is related to the potential function through a single integration to be much more sensitive to differences in that function than one like the transport properties which are connected by three integrations, particularly when the functional dependence in the integrand is also more indirect for the latter than it is for the former.

It must be remembered that the requirement here has been that both the value and slope of the properties be equal for the two potentials. It is possible that some of the apparent sensitivity found for the transport properties comes from the requirement on the slope. Whether or not this disappears when one asks only for a match to the property, as is done in a correlation, bears further study. Again one can state that a lack of uniqueness found in this calculation will not disappear on the application to experimental data. Therefore, one must have data present in the temperature ranges mentioned if one is even to have a chance to discriminate between potential functions.

The slope of the ϵ_2/ϵ_1 versus T^* curve, for a given potential, is essentially the same for both the viscosity and diffusion coefficients. On this basis, the two quantities are equally effective when used individually. As we shall see in the next section, however, there is a difference between them in sensitivity to changes in the potential function. That difference makes the simultaneous fit of the two properties potentially a sensitive tool for finding the potential function.

The ratios $(b_0)_2/(b_0)_1$ for these properties are less dependent on temperature than are the ratios ϵ_2/ϵ_1. A discussion of them would therefore not contribute anything new with regard to the sensitivity of these properties as probes of the potential function.

6. The Simultaneous Fit to More Than One Property

Figures 6, 7, 9, and 10 contain plots of the ratio ϵ_2/ϵ_1 for more than one property. With the help of these one can examine the effect the requirement of a simultaneous fit to two or more properties and their first derivatives has on the lack of uniqueness in the potential function. Figure 9 is particularly informative in this regard. Note that in that diagram, the curves for both the viscosity and diffusion coefficients for $\gamma = 0$ would be straight lines parallel to the abscissa at $\epsilon_2/\epsilon_1 = 1.0$. As γ deviates from zero, however, each curve begins to deviate from a straight line, particularly at low temperatures. Furthermore, the curves for the diffusion coefficient separate from those for the viscosity until, by $\gamma = 0.6$, the curves are quite widely separated. The lack of uniqueness associated with the flatness of the curves for the separate properties would be extended to the simultaneous fit to the pair of properties and their derivatives were the two curves essentially flat *at the same value of the ordinate.* However, the increase in the separation of the curves with γ (i.e., with increased deviation from the (12,6) reference potential) demonstrates a strong sensitivity of the simultaneous fit to changes in the potential function. This sensitivity is much stronger than that of the individual properties in the range $T^* > 4.0$. Whether or not it is more sensitive than the behavior for $T^* < 4.0$ would require an examination of detailed fits to data.

Figure 10 contains the same kind of information for the exp-6 function. Here the changes that occur at low and intermediate temperatures are much smaller while those at high temperatures are much more pronounced. There appears to be a value of α for which the curves both have a flat range and are essentially superimposed at high temperatures. However, for that value of α, the low temperature data still serves as a discriminant. In this case the simultaneous use of both properties and their derivatives does not appear to add any discrimination beyond that available with either property by itself. Note that the curves for the two properties exchange relative positions when one goes from $\alpha = 12$ to $\alpha = 17$. Increasing α beyond 17 would presumably result in further separation.

Figure 7 contains plots for all of the properties for the Kihara potential. These curves necessarily each form a straight line parallel to the abscissa with ordinate 1.0 for $\gamma = 0$. Increasing γ causes them to separate as in figure 9 for the two transport properties. It is interesting to note that the change in separation between the curves for diffusion and second virial coefficients at intermediate temperatures is not uniform. Thus, for $T^* \cong 3.0$, the diffusion curve for $\gamma = 0.1$ lies above that for the second virial coefficient, for $\gamma = 0.3$ they are superimposed in a small region around $T^* = 3.0$, while for $\gamma = 0.4$ the diffusion curve lies below. Thus, as γ is increased from 0. to 0.1, the second virial curve "moves" more rapidly while for $\gamma > 0.1$ the reverse is true.

7. Conclusions

We have investigated the use of the second virial coefficient as well as the zero density Joule-Thomson, viscosity, and diffusion coefficients as probes for the intermolecular potential function. We have found the second virial coefficient to be particularly poor in this regard in the temperature range $2.0 < T^* < 7.0$ on the Lennard-Jones (12,6) reduced temperature scale. The Joule-Thomson coefficient has been found to be somewhat better particularly in the lower part of this range. Considerably better were the transport coefficients, i.e., the viscosity and diffusion coefficients. It is clear from our results that these last coefficients can be sensitive probes of the potential function given experimental data covering a sufficiently large temperature range.

Further comparisons of this kind between the transport coefficients for the (12,6) potential function and those for other potential functions are clearly called for, particularly for classes of potentials of which the (12,6) is not a member. In particular, one would like to find such classes of functions as exist which contain a member whose transport properties can be fit to those of the (12,6) over an extensive temperature range. This will require the calculation of collision integrals for these various functions. In some cases tables do exist [16, 17] which, unfortunately, contain too few points in the temperature region of interest. It is hoped that these will be extended shortly.

These calculations will be extended to include the thermal diffusion ratio and, possibly, the quantum corrections to certain of these properties.

As regards the relationship between our results and experiment with present day precision, the fact that our results apply precisely to experiment only in the limit of very high precision actually strengthens our conclusions in regard to *lack* of uniqueness while conclusions regarding uniqueness are weakened. That is, where we did not find it possible to use a macroscopic property to distinguish between potential functions under our conditions, it certainly would not be possible to use this property for this purpose under less precise experimental conditions. On the other hand, our ability in other circumstances to distinguish among potentials (e.g., using second virial coefficient data for T^* (12,6, < 2.0) may be due in part, to the fact that we have required a precise fit, something not possible with experimental data. It may likewise be due to the inclusion here of a requirement that the first derivative of the property be equal for the two potentials. More precise statements in this latter case await the result of fits to actual data.

Early portions of this work were completed at the Weizmann Institute, Rehovoth, Israel. The author wishes particularly to thank the computer staff for their cooperation in the use of their CDC−1604 computer.

8. References and Notes

[1] M. Klein, J. Chem. Phys. **39,** 1367 (1963).
[2] J. Hilsenrath and M. Klein, Tables of Thermodynamic Properties of Air from 1500 °K to 15000 °K, Report AEDC TR−65−58 Arnold Engineering Development Center, Tullahoma, Tenn.
[3] J. O. Hirschfelder, C. F. Curtiss, and R. B. Bird, The Molecular Theory of Gases and Liquids (John Wiley & Sons, Inc., New York, N.Y., 1954).
[4] J. B. Keller, and B. Zumino, J. Chem. Phys. **30,** (1959); J. E. Le Fevre, Heat Division Paper 129 (1957), Mechanical Engineering Research Laboratory, East Kilbride, Glasgow, Scotland.
[5] Note that equating the second virial coefficients and their first derivatives is equivalent to equating, for the two potentials, the first density correction to PV/RT and simultaneously requiring the first density corrections to the internal energy, U/RT, to be equal for the same two potentials [6]. The author is indebted to Lester Haar for pointing this out.
[6] The requirement on the internal energy can be replaced by an equivalent requirement on the zero density Joule-Thomson coefficient.
[7] One can also associate each curve of the family of curves with T_2^* or, for that matter, with the experimental temperature T.
[8] M. Klein, Ph.D. thesis, 1962, University of Maryland.
[9] Note that S is dependent on T^* and contrary to the statement in J. O. Hirschfelder, C. F. Curtiss, and E. M. Spotz, Chem. Rev. **44,** 205 (1949), (see also p. 566 ref. 3) is not the exponent in the representation $B(T^*) = AT^{*t}$.
[10] e.g., R. A. Svehla, NASA−TRR−132 (1962); see also reference 2.
[11] C. J. G. Raw, J. South African Chemical Institute VII, 96 (1954).
[12] As regards the second virial coefficient and hence low density P-V-T data, this weakens considerably one of the restrictions of the law of corresponding states in this temperature range. Thus, at these temperatures, one needs to place only mild restrictions on the form of the potential function.
[13] E. Whalley and W. G. Schneider, J. Chem. Phys. **23,** 1644 (1955).
[14] E. A. Mason and W. E. Rice, Jr., J. Chem. Phys. **22,** 843 (1954).
[15] e.g., L. Verlet, and D. Levesque, Physica **38,** 1124 (1962); J. deBoer, J. M. H. van Leeuwen, and J. Groenevelt, Physica **30,** 2265 (1964); J. G. Kirkwood, V. A. Lewison, and B. J. Alder, J. Chem. Phys. **20,** 929 (1952); G. Casanova, and A. Levi, Physica **30,** 937 (1964).
[16] F. J. Smith and R. J. Munn, J. Chem. Phys. **41,** 3560 (1964).
[17] S. G. Brush and J. D. Lawrence, Report UCRL−7376 Lawrence Radiation Laboratory, Livermore, Calif.

(Paper 70A3−402)

JOURNAL OF RESEARCH of the National Bureau of Standards—A. Physics and Chemistry
Vol. 70A. No. 3, May-June 1966

Publications of the National Bureau of Standards*

Selected Abstracts

Chemical structures as information—representations, transformation, and calculations, S. J. Tauber, G. F. Fraction, and H. W. Hayward, *Book, Colloquium on Technical Preconditions for Retrieval Center Operations, Philadelphia, Pa., Apr. 24–25, 1964, ed. B. F. Cheydleur, pp. 73–101 (Spartan Books, Inc., Washington, D.C., 1965).*

Chemical structure is discussed as a specific example of information which can be represented completely and unambiguously in a storage and retrieval system. Complete representation of information is necessary if no information is to be lost upon entry into a storage and retrieval system. A beginning has been made toward handling chemical structural information as such. Interconversion, now becoming possible, makes reasonable the use of as many different structure representations as thought useful. It is similarly becoming possible to use computer operations to generate explicitly information which can be used for screening during searches. Substructure searches of a file of unambiguously represented compounds will permit computer-generated fragmentation indexes. Algorithms have been developed for some transformations among representations and for calculation of characteristics useful for screening.

Digital handling of chemical structures and associated information, S. J. Tauber, *Proc. 20th Natl. Conf. Association for Computing Machinery, pp. 206–216 (1965).*

Chemical information processing by digital computer is the basis for more effectively meeting information requirements than has been possible heretofore. Present work utilizes the versatility of computers to make feasible answers to types of technical questions not previously systematically accessible. The basic approach used is to represent information itself, not merely indexing terms, insofar as possible.

Chemical structures are represented in complete detail by strings of symbols constructed by either of two sets of specialized rules. The symbol strings can be used directly for some simple but common types of structure searches. The symbol strings are also transformed into conceptually two-dimensional connection tables of nodes and branches. The nodes are assigned values corresponding to chemical elements; the branches, to chemical bonds. Connection tables can also be entered directly into the computer.

Structures which represent entire classes of compounds occur commonly in chemical publications, as do structures which are intended to apply equally well to any of several compounds. Such generic and partially indeterminate structures must be entered into the same computer file as individual structures. Mixtures and compounds of unknown composition are two further types of materials which must be handled in the same file.

The information about any given material may be of several types: (a) precise representation of the material itself, i.e., structure; (b) dictionary and bibliographic information, e.g., name, location of description of preparation, isolation, or other mention; (c) numeric information, e.g., physical constants; and (d) descriptive information, e.g., commercial uses or biological effects. Information may also be about several materials simultaneously, e.g., types of chemical reactions or solubilities among compounds.

For efficient search among entries for several million different compounds, classes of compounds, and mixtures the master file would be subdivided into working subfiles, and screening information would be carried with the items. The several subfiles may either be constructed on the basis of a property that varies among substances, e.g., one subfile each for solids, liquids, and gases, or else may contain only a limited selection, e.g., commercially available insecticides. Screening information may be numeric, e.g., molecular formulae, or true/false, e.g., "Biological properties have been reported," or, "A naturally occurring substance."

Several distinct computer techniques exist for seeking types of chemical structures, including matching symbol substrings and node-by-node matching. Methods are being worked out for dealing with other types of chemical information.

The crystal and molecular structure of iodopentaborane-9, L. H. Hall, S. Block, and A. Perloff, *Acta Cryst.* **19,** *pt. 4, 658–661 (Oct. 1965).*

The compound formed by the direct attack of elemental iodine on pentaborane-9 in excess pentaborane-9 at 70 °C (Hall, Koski, and Subbana, 1964) has been shown to be 1-iodopentaborane-9; that is, the iodine is bonded to the apical boron of the tetragonal boron pyramid.

This work is the first reported single crystal structure determination of a halogen substituted boron hydride. Schaeffer, Shoolery, and Jones (1958) determined only the iodine positions but not boron positions in $B_{10}H_{12}I_2$ from projection data only and Ring, Donnay, and Koski (1962) determined the structure of BI_3 from powder data.

International weights and measures, C. H. Page (*ISA 20th Annual Conference and Exhibit, Los Angeles, Calif., Oct. 4–7, 1965), ISA Preprint 33.3–1–65 (1965).*

A brief survey of the background, organization, and operation of the International Bureau of Weights and Measures and related committees.

Measurement standards, A. G. McNish, *Intern. Sci. Tech. 58–66 (Conover-Mast. Publ., New York, N.Y., Nov. 1965).*

This article is a general discussion of the philosophic and historical basis of our measurement system and its current state of development.

Infrared and microwave spectra of ClCN, W. J. Lafferty, D. R. Lide, and R. A. Toth, J. Chem. Phys. **43,** No. 6, 2063–2070 (Sept. 15, 1965).

The microwave spectra of $Cl^{35}C^{12}N^{14}$ and $Cl^{37}C^{12}N^{14}$ have been obtained for molecules in the vibrational states ν_1, $2\nu_2^0$, and $2\nu_2^2$. In addition, high resolution infrared spectra have been obtained for the bands ν_3, $\nu_2^1+\nu_3$, $\nu_1+\nu_3$, and $2\nu_2^0+\nu_3$. Estimates for the frequencies of ν_1 and ν_2^1 have been made, and equilibrium and average bond distances have been calculated.

Ionization energies of the singly ionized rare earths, J. Sugar and J. Reader, *J. Opt. Soc. Am.* **55,** *No. 10, 1286–1290 (Oct. 1965).*

Values of the ionization energies of the singly-ionized rare earths have been obtained by means of a semi-empirical calculation. The results in eV are:

La II 11.06	Sm II 11.07	Ho II 11.80
Ce II 10.85	Eu II 11.25	Er II 11.93
Pr II 10.55	Tb II 11.52	Tm II 12.05
Nd II 10.73	Dy II 11.67	Yb II 12.17
Pm II 10.90		Lu II 13.8

The uncertainty is estimated to be ±0.08 eV, except for the case of Lu II, where the estimated uncertainty is ±0.3 eV.

Quantum statistics of fully ionized gases, W. T. Grandy and F. Mohling, *Ann. Phys.* **34,** *No. 3, 424–464 (Oct. 1965).*

A recently developed theory of the quantum statistical mechanics of multicomponent systems is applied to a fully ionized gas in thermal equilibrium, and the grand potential and equation of state are calculated through fifth order in the electronic charge. These results are valid in regions of moderately high temperature and moderately low density, and the equation of state has the form of a virial expansion. The following considerations are reflected in this latter expression: quantum mechanical interactions among the particles, quantum statistics, many-body self-energy parts, and the inclusion of radiative corrections to charged particle contributions.

Three important results of this work are (1) the observation that the master graph formulation of quantum statistics developed by Mohling is quite necessary for studying the general ionized gas, (2) the appearance of a new parameter which indicates that a quantum mechanical screening of the Coulomb interaction occurs in the ionized gas, over and above the classical Debye screening, and (3) the conclusion that the so-called electron gas is a very unphysical approximation.

Elastic stress-strain relations in perfect elastic fluids, B. Bernstein, E. Kearsley, and L. Zapas, *Trans. Soc. Rheol.* **9,** *pt. 1, 27–39 (1965).*
The theory of perfect elastic fluids deals with the nonequilibrium thermodynamics of finite visco-elastic deformation. The thermodynamics of finite elastic strain and of perfect elastic fluids are discussed. It is shown that the stress-strain relations for perfect elastic fluids may be written in a way which appears formally identical to those in elasticity theory, but the form of this dependence depends on past history.

Atomic lifetimes in neon I, J. Z. Klose, *Phys. Rev.* **141,** *No. 1, 181–188 (Jan. 7, 1966).*
Mean lives of a number of electronically excited atomic levels in Ne I have been determined using a method of delayed coincidence. Following a detailed description of the experimental procedure, the measured values of the mean lives of the $2p_1$ through $2p_9$, $3p_1$, $3p_{10}$, and $4d'_1$ (Paschen notation) levels in neutral neon are given. These lifetimes, determined from transitions with associated wavelengths extending from ≈ 3400 Å to ≈ 6400 Å, ranged in value from ≈ 14 nsec (10^{-9} sec) to ≈ 500 nsec. The lifetimes were estimated to contain possible systematic errors varying from 5 to 20 percent and are presented in comparison with corresponding results of other workers.

Infrasonic observations of the May 16, 1964, volcanic explosion on the island of Bali, V. H. Goerke, J. M. Young, and R. K. Cook, *J. Geophys. Res.* **70,** *No. 24, 6017–6022 (Dec. 15, 1965).*
The volcanic eruption of Mount Agung on the island of Bali reached explosive proportions on May 16, 1963. Perturbations generated in the atmosphere traveling at sonic velocities were recorded in Boulder, Colo., 14,700 km distant. The infrasonic event was seen both via the nominal great circle path and via the long great circle path around the world. The average transit velocity via the short path is 48 m/s faster than for the long path. This can be accounted for if wind directions are generally west to east at the time of the event.

Interaction of 350-keV polarized neutrons with oriented ^{165}Ho nuclei, R. Wagner, P. D. Miller, T. Tamura, and H. Marshak, *Phys. Rev.* **139,** *No. 1B, B29–B46 (July 12, 1965).*
The interaction of polarized and unpolarized 350 keV neutrons with oriented and unoriented ^{165}Ho nuclei was investigated in order to study the effect of nuclear deformation and to search for a possible spin-spin interaction. The differential cross section for unpolarized 350 keV neutrons elastically scattered from unoriented ^{165}Ho nuclei, as well as the total cross section was measured and successfully compared to the predictions of the optical model using the coupled channel formalism. To investigate the spin-spin interaction, measurements were made of the transmitted intensities with the target nuclei polarized alternately parallel and antiparallel to the direction of neutron polarization. Comparison of this result with that of the coupled channel calculation indicates that if the spin-spin interaction in the optical model potential is written as $-V_{ss}(\sigma{:}\mathrm{I})$ times a Saxon form factor, then V_{ss} lies between -130 and $+280$ keV. Since the ^{165}Ho nucleus is highly deformed, a transmission measurement was made to determine the change in cross section between a highly oriented and a nearly unoriented target. The transmission of the target decreased by (1.3 ± 0.4) percent for the higher orientation value, which corresponds to a cross section increase of 350 ± 100 mb (standard error). This deformation effect on the total cross section is also in good agreement with that derived from the coupled channel calculation. The deformation parameter, β, used in the optical model potential was $+0.3$, in agreement with other measurements.

Nonanalyticity of transport coefficients and the complete density expansion of momentum correlation functions, J. Weinstock, *Phys. Rev.* **140,** *No. 2A, A460–A465 (Oct. 18, 1965).*
The complete "formal" density expansion of any momentum autocorrelation function—at any frequency—is derived from the density expansion of the generalized master equation. (the sth term in this expansion is explicitly defined in terms of the time-displacement operator of $(s+1)$ particles and involves the dynamics of $(s+1)$ isolated particles.) The entire derivation consists of only a few algebraic steps, and is valid for noncentral (polar) pair forces as well as central forces.
It is then shown that the third and higher order terms in the *zero frequency* limit of the density expansion diverges—although the first two terms and the entire sum converge (the density expansion "breaks down"). This implies that transport coefficients are not analytic functions of the density. It is suggested that a partial re-summation (re-normalization)—analogous to that used in the electron gas problem—be used to calculate the nonanalytic behavior of transport coefficients.

On the use of thermopiles for absolute radiometry in the far ultraviolet, R. G. Johnston, and R. P. Madden, *Appl. Opt.* **4,** *No. 12, 1574–1580 (Dec. 1965).*
Thermopiles used for absolute radiometry in the far ultraviolet spectral region are generally calibrated with visible and near-infrared radiation. Three possibilities for the failure of the sensitivity of thermopiles to be independent of wavelength have been investigated. It was found that gold black typical of that used on thermopiles for far ultraviolet applications reflectively scattered 2–4 percent of the incident far ultraviolet radiation. Since the same gold black scattered a similar fraction of incident visible and near-infrared radiation, the correction for this effect was small. An analysis of surface sensitivity maps indicated that a thermopile of 0.04 sec time constant showed no wavelength variation of sensitivity when either d.c. detection or a.c. synchronous detection with 13 c/s chopping was used. The most significant wavelength-dependent phenomenon of importance was found to be the photoelectric effect. Ejected electrons carry a significant amount of energy away from gold blacked thermopiles in the spectral region below 1600Å. The maximum correction determined for a particular thermopile was 5.2 percent at 735Å.

Spectra of C_3 in solidified gases at 4° and 20 °K, R. L. Barger and H. P. Broida, *J. Chem. Phys.* **43,** *No. 7, 2364–2370 (Oct. 1, 1965).*
Wavelength, line width, and intensity measurements have been made from 3000 Å to 4500 Å of the spectra of triatomic carbon molecules trapped in solid matrices of Ar, Kr, Xe, O_2, N_2, CO_2, and SF_6 at 4 °K and 20 °K. The carbon source was a Knudsen cell, operated at temperatures up to 2900 °K, from which effused a molecular beam with known densities of C_3. Absorption transitions are assigned to vibrational levels of both upper and lower states of the $^1\Pi_u - X\,^1\Sigma_g^+$ 4050 Å group of C_3. The fundamental vibrational frequencies ν_1 and ν_2 for the upper $^1\Pi_u$ state, ν_2 for the ground $^1\Sigma_g^+$ state, and Renner constants for ν_2 of the $^1\Pi_u$ state in these matrices are given. Measurements of absorption intensities give an oscillator strength, averaged for all matrices, equal to 6×10^{-2} for the C_3 group. Little or no matrix effect on the intensities is found. However, experimentally determined corrections to the intensities are necessary for effects of diffusion of carbon in the matrices with the apparent formation of nonabsorbing carbon aggregates C_3 line widths vary with matrix from 40 cm^{-1} to 500 cm^{-1}, and C_3 line shifts vary from -410 cm^{-1} to 1065 cm^{-1}. All matrix shifts are to the red except in the case of the CO_2 matrix. No definite effect of temperature on line widths or shifts is found.

Thermal conductivity and viscosity of simple fluids, J. V. Sengers, Intern *J. Heat Mass Transfer* **8,** *1103–1116 (1965).*
The behavior of the thermal conductivity and viscosity coefficient of simple fluids as a function of pressure, density and temperature is surveyed. Particular attention is given to the behavior of the transport coefficients in the critical region. In a previous paper it was shown that the thermal conductivity coefficient exhibits a pronounced maximum in the critical region. Additional information confirming the existence of such a maximum is presented.

Theoretical predictions of the transport coefficients in dense systems are often based on the theory of Enskog. A survey is presented showing to what extent the theory of Enskog describes the density dependence of the transport coefficients in monatomic fluids. Finally, the transport mechanism leading to the anomalous rise of the thermal conductivity in the critical region is indicated.

Accuracy in electrical and radio measurements and calibrations, 1965, ed. R. C. Powell, *NBS Tech. Note 262–A, (June 15, 1965), 50 cents.*
NBS estimates of uncertainties associated with physical measurements, and with some NBS calibration services, are shown by 42 provisional "accuracy charts." Each chart is accompanied by a facing page giving a brief statement of the state of the art and tentative plans for NBS work in areas where improvement is needed.

Organic chemistry: Radioactive carbohydrates, sugars in solution, aldol condensations, molecular structure, synthesis of selected compounds, air pollution studies, reference materials (organic), July 1964 to June 1965, ed H. S. Isbell, *NBS Tech. Note 274 (Dec. 3, 1965), 60 cents.*
The report describes work in progress in the Organic Chemistry Section of the Analytical Chemistry Division at the National Bureau of Standards. It presents reviews of recent contributions of the Section on the following subjects: Synthesis of carbon-14- and tritium-labeled carbohydrates, isotope dilution and double-label methods of analysis, determination of kinetic isotope effects, use of solvent isotope-effects for studying pyranose-furanose interconversions, measurements of rates of primary enolization, rates of rearrangement of one sugar to another by bases, estimation of the relative stabilities of isomeric hexoses, reversible aldol condensations, mechanism for the formation of saccharinic acids, formation of branched-chain aldoses and linear ketoses by aldol condensations, stereochemistry of monoaminotetrahydroxycyclopentane derivatives, cyclic polyhydroxy ketones, phenylhydrazono-phenylazo tautomerism, acetamido-deoxyketoses, syntheses and properties of selected organic compounds, interaction of aromatic hydrocarbons with oxygen, oxidation of polycyclic, aromatic hydrocarbons on particulate matter, loss on filtration of aqueous solutions of polycyclic, aromatic hydrocarbons, oxidation products of pyrene, and preparation of 1-phenyl-1,3-butanedione chelates of chromium and iron for use as new metallo-organic standards.

Flux averaging devices for the infrared, S. T. Dunn, *NBS Tech. Note 279 (Dec. 9, 1965), 30 cents.*
The spatial and angular sensitivity of infrared detectors recently has been investigated. In order to eliminate this effect and obtain accurate measurements in the infrared, it is necessary to distribute the flux as uniformly as possible over the entire sensitive area of the detector. A solution to this problem is presented in the form of several averaging devices developed at the National Bureau of Standards. Among the devices investigated are roughened NaCl windows, diffusing light ducts, and spheres with different coatings. Each device was subjected to a series of tests to establish its averaging capability and useful wavelength range. Results of these tests indicate that the use of a small sulfur-coated hollow sphere over the detector increased the accuracy of most types of infrared reflectance measurements and, at the same time, decreased the requirement for precise optical alignment of the detector in the wavelength range of 1.5 to 8 microns. The use of the sulfur-coated sphere over a thermopile extends the usefulness of the multiple-reflection specular reflectometer to about 10 microns.

Other NBS Publications

J. Res. NBS 79B, (Math. and Math. Phys.) No. 1, (Jan.-Mar. 1966) 75 cents.
Invariant properties of the spheroidal potential of an oblate planet. J. P. Vinti.
Inclusion of the third zonal harmonic in an accurate reference orbit of an artificial satellite. J. P. Vinti.
On EPr and normal EPr matrices. I. J. Katz and M. H. Pearl.
The Bernstein form of a polynomial. G. T. Cargo and O. Shisha.
Remarks on measurable sets and functions. R. O. Davies.
The form factor for the Fermi model spatial distribution. L. C. Maximon and R. A. Schrack.
Tables for the evaluation of the Faxén approximation to the solution of the Lamm equation. M. Dishon and G. H. Weiss.

A table of radiation characteristics for uniformly spaced optimum endfire arrays with equal sidelobes, M. T. Ma and D. C. Hyovalti, NBS Mono. 95, (Dec. 10, 1965), 45 cents.
Safety rules for the installation and maintenance of electric supply and communication lines, Supplement 1 to NBS Handbook 81 (Dec. 15, 1965).
Standard Reference Materials: Analysis of uranium concentrates at the National Bureau of Standards, M. S. Richmond, NBS Misc. Publ. 260–8, (Dec. 1, 1965), 55 cents.
Standard Reference Materials: Homogeneity characterization of NBS spectrometric standard II: Cartridge brass and low-alloy steel, H. Yakowitz, D. L. Vieth, K. F. J. Heinrich, and R. E. Michaelis, NBS Misc. Publ. 260–10, (Dec. 14, 1965), 30 cents.
Voltage ratio detector for millivolt signals, J. R. Houghton, NBS Tech. Note 266, (Dec. 13, 1965), 15 cents.
A peak ac-dc voltage comparator for use in a standards laboratory, L. A. Marzetta, NBS Tech. Note 280 (Jan. 17, 1966), 25 cents.
Materials for PLACEBO V, W. C. Watt, NBS Tech. Note 281 (Jan. 17, 1966), 50 cents.
A method for obtaining the parameters of electron-density profiles from topside ionograms, R. S. Lawrence and M. Hallenbeck, NBS Tech. Note 315, (Aug. 3, 1965), 25 cents.
Numerical simulation of ionospheric wave interaction experiments, T. M. Georges, NBS Tech. Note 325 (Oct. 25, 1965), 30 cents.
Determination of hide substance in leather by the Kjeldahl method, S. Dahl, Book, The Chemistry and Technology of Leather IV, ch. 52, 45–70 (Reinhold Publ. Corp., New York, N.Y., 1965).
Determination of tellurium by cathode-ray polarography, E. J. Maienthal and J. K. Taylor, Anal. Chem. **37,** No. 12, 1516–1519 (Nov. 1965).
Electrodeposition of alloys, past, present, and future, A. Brenner, Plating **52,** No. 12, 1249–1257 (Dec. 1965).
Physical and mechanical properties of electrode-deposited copper. I. Literature survey, V. A. Lamb and D. R. Valentine, Plating **52,** No. 12, 1289–1311 (Dec. 1965).
Some experience with the Hayward linear notation system, H. W. Hayward, H. M. S. Sneed, J. H. Turnipseed, and S. J. Tauber, J. Chem. Doc. **5,** No. 3, 183–189 (Aug. 1965).
The use of visible and ultraviolet spectroscopy to identify carbonyl compounds in photodegraded plastics, V. E. Grady and J. R. Wright, Polymer Engr. Sci. **5,** No. 4, 284–290 (Oct. 1965).
Time-correlation functions and transport coefficients in statistical mechanics, R. Zwanzig, Ann. Rev. Phys. Chem. **16,** 67–102 (1965).
A theoretical model for predicting thermal stratification and self-pressurization of a fluid container, R. W. Arnett and D. R. Millhiser, Proc. Conf. Propellant Tank Pressurization and Stratification, Jan. 20–21, 1965, **II,** 1–16 (NASA, George C. Marshall Space Flight Center, Huntsville, Ala., 1965).
Calibration of peak A-C to D-C comparators, D. Flach and L. A. Marzetta (ISA 20th Annual Conference and Exhibit, Los Angeles, Calif., Oct. 4–7, 1965), ISA Preprint 14.2–3–65 (1965).
Cryogenics and space technology, R. B. Scott, Proc. XIth Intern. Congress of Refrigeration, Munich, Germany, 1963, pp. 105–114 (Pergamon Press, Inc., New York, N.Y., 1965).
Evidence for an electrochemical-mechanical stress corrosion fracture in a stainless steel, H. L. Logan, M. J. McBee, and D. J. Kahan, Corrosion Sci. **5,** 729–730 (1965).
Preparation of copper crystals with low electrical resistivity, J. J. Gniewek and A. F. Clark, J. Appl. Phys. **36,** No. 10, 3358–3359 (Oct. 1965).
The world of cryogenics. III. Cryogenics at the National Bureau of Standards Boulder Laboratories, B. W. Birmingham, Cryogenics **5,** No. 3, 121–128 (June 1965).
AXLE: An axiomatic language for string transformations, K. Cohen and J. H. Wegstein, Commun. Assoc. Compt. Mach. **8,** No. 11, 657–661 (Nov. 1965).
Morphological classification in the National Bureau of Standards mechanical translation system, L. F. Meyer, J. Assoc. Compt. Mach. **12,** No. 4, 437–472 (Oct. 1965).

Cesium beam atomic time and frequency standards, R. E. Beehler, R. C. Mockler, and J. M. Richardson, Metrologia **1,** No. 3, 114–131 (July 1965).

Of time and the atom, G. E. Hudson, Phys. Today **18,** No. 8, 34–38 (Aug. 1965).

A new speculation of terrestrial helium loss, E. E. Ferguson, F. C. Fehsenfeld, and A. L. Schmeltekopf, Planet. Space Sci. **13,** 925–928 (1965).

Breadth of decay quanta in gas lasers, J. A. White, J. Opt. Soc. Am. **55,** No. 11, 1436–1442 (Nov. 1965).

Classical diagram technique for calculating thermostatic properties of solids; application to dielectric susceptibility of paraelectrics, R. M. Wilcox, Phys. Rev. **139,** No. 4A, A1281–A1291 (Aug. 16, 1965).

Conformation of polystyrene adsorbed at the θ-temperature, R. R. Stromberg, D. J. Tutas, and E. Passaglia, J. Phys. Chem. **69,** No. 11, 3955–3963 (Nov. 1965).

Critical-point phenomena, M. S. Green, Science **150,** No. 3693, 229–236 (Oct. 8, 1965).

Density expansion of the viscosity of a moderately dense gas, J. V. Sengers, Phys. Rev. Letters **15,** No. 12, 515–517 (Sept. 20, 1965).

Differences in the characteristic electron energy-loss spectra of solid and liquid bismuth, C. J. Powell, Phys. Rev. Letters **15,** No. 22, 852–854 (Nov. 29, 1965).

Dipole moment of PCl_4F from the nonresonant microwave absorption of the vapor, A. A. Maryott and S. J. Kryder, J. Chem. Phys. **43,** No. 7, 2556–2557 (Oct. 1, 1965).

Investigation of the anomaly in the response of silicon semiconductor radiation detectors at low temperatures, W. R. Dodge, S. R. Domen, A. T. Hirshfeld, and D. D. Hoppes, IEEE Trans. Nuclear Sci. **NS-12,** No. 1, 295–303 (1965).

Microwave spectrum and barrier to internal rotation in methylsilylacetylene, W. H. Kirchhoff and D. R. Lide, Jr., J. Chem. Phys. **43,** No. 7, 2203–2213 (Oct. 1, 1965).

Modes of propagation in a bounded compressible plasma, J. R. Wait, Electronics Letters **1,** 193–194 (Sept. 1965).

Philosophical influences on radiation protection standards, L. S. Taylor, Health Phys. **11,** 859–864 (1965).

Precision refractometry of small lens-shaped objects, J. R. Meyer-Arendt, Lab. Invest. **13,** No. 5, 529–532 (1965).

Resonance in the light scattered from a plasma, J. Weinstock, Physics Letters **18,** No. 1, 21–22 (Aug. 1, 1965).

The direction of the force on a dislocation and the sign of the Burgers vector, R. DeWit, Acta Met. **13,** No. 11, 1210–1211 (1965).

Ultrasonic determination of crystalline resonances and sound velocities, using NMR techniques, R. J. Mahler, and W. H. Tanttila, J. Acoust. Soc. Am. **38,** No. 3, 429–432 (Sept. 1965).

Another method of synthesizing nonuniformly spaced arrays, M. T. Ma, IEEE Trans. Ant. Prop. **AP-13,** No. 5, 833–834 (Sept. 1965).

On the relation between auroral radio absorption and very low frequency emissions, W. L. Ecklund, J. K. Hargreaves, and J. H. Pope, J. Geophys. Res. **70,** No. 17, 4285–4292 (Sept. 1, 1965).

The effect of ion-drag on the neutral air in the ionospheric *F*-region, H. Rishbeth and L. R. Megill, Ann. Geophys. **21,** No. 2, 235–244 (Apr.-June 1965).

Deuterium isotope effect in vacuum-ultraviolet absorption coefficients of water and methane, A. H. Laufer and J. R. McNesby, Can. J. Chem. **43,** No. 12, 3487–3490 (Dec. 1965).

Electrochemical methods, J. K. Taylor, E. J. Maienthal, and G. Marinenko, Book, Trace Analysis: Physical Methods, ed. G. H. Morrison, ch. 10, pp. 377–433 (Interscience Publ. Inc., New York, N.Y., 1965).

Interaction of oxygen with platinum, A. J. Melmed, J. Appl. Phys. **36,** No. 11, 3691–3692 (Nov. 1965).

Proton transfer reactions occurring in the gas-phase radiolysis, P. Ausloos and S. G. Lias, Discussions Faraday Soc. **39,** 36–44 (1964).

Restoration of complete dentures inadvertently warped by the patient: Report of case, J. B. Woefel and G. C. Paffenbarger, J. Am. Dental Assoc. **71,** 866–870 (Oct. 1965).

Solid-vapor equilibrium in the system hydrogen-methane, M. J. Hiza and R. N. Herring (Proc. 1964 Cryogenic Engineering Conf., Philadelphia, Pa., Aug. 17–21, 1964), Book, International Advances in Cryogenic Engineering, ed. K. D. Timmerhaus, 10, Sec. Q, pp. 182 (Plenum Press, Inc., New York, N.Y., 1965).

Spectrophotometric determination of bromine and hydrogen bromide, E. C. Creitz, Anal. Chem. **37,** 1690–1692 (Dec. 1965).

Comment on obscurities of oscillator noise, L. Fey, W. R. Atkinson, and J. Newman, Proc. IEEE Letter **52,** 104–105 (Jan. 1964).

Cryogenic fluid, two-phase critical flow studies related to reactor systems, R. V. Smith, H. S. Isbin, H. K. Fauske, M. Petrick, C. H. Robbins, and F. R. Zuludek, Proc. 3rd United Nations Intern. Conf. Peaceful Uses of Atomic Energy, Geneva, Switzerland, Aug. 31-Sept. 9, 1964.

Field strength calibration techniques at the NBS, H. E. Taggart, IEEE Trans. Electromag. Compatability **EC-7,** No. 2, 163–169 (June 1965).

Field-strength measurements in a multipath field, C. C. Watterson, Proc. 4th Natl. IEEE Symp. Radio Frequency Interference, San Francisco, Calif., June 28–29, 1962.

Gearing errors as related to alignment techniques of the rotary-vane attenuator, W. Larson, 19th Annual IEEE Conference and Exhibit on Instrumentation and Measurements, New York, N.Y., Oct. 12–15, 1964, Preprint No. 12–5–2–64 (Sept. 1965); IEEE Instr. Meas. **IM-14,** No. 3, 117–123 (Sept. 1965).

Optical instrumentation for the biologist, J. R. Meyer-Arendt, Appl. Opt. **4,** No. 1, 1–9 (Jan. 1965).

The NBS cryogenic data center, Proc. XI Intern. Congress Refrigeration, Munich, Germany, Aug. 28, 1963, pp. 110–114 (1965).

Timing and space navigation with an existing ground based system, G. Hefley, R. F. Linfield, and R. H. Doherty, AGARD Navigation Systems for Aircraft and Space Vehicles, pp. 490–506 (Pergamon Press, Inc., New York, N.Y., 1962).

22 ISCC–NBS centroid colors of maximum contrast, K. L. Kelly, Color Engr. **3,** No. 6, 26–27 (Nov.-Dec. 1965).

A bounded automorphic form of dimension zero is constant, M. I. Knopp, J. Lehner, and M. Newman, Duke Math. J. **32,** No. 3, 457–460 (Sept. 1965).

Density distribution of polymer segments in the vicinity of an absorbing interface, C. A. J. Hoeve, J. Chem. Phys. **43,** No. 9, 3007–3008 (Nov. 1, 1965).

Error bounds for asymptotic solutions of second-order differential equations having an irregular singularity of arbitrary rank, F. W. J. Olver and F. Stenger, J. SIAM, Ser. B. **2,** No. 2, 244–249 (1965).

Estimation of the parameters of the Hyper-Poisson distributions, E. L. Crow and C. E. Bardwell, (Proc. Symp. Classical and Contagious Discrete Distribution, Montreal, Canada, Aug. 15–20, 1963), ch. V, pp. 127–140 (Statistical Publ. Soc., Calcutta, India, 1965).

Generalized functions of symmetric matrices, M. Marcus and M. Newman, Proc. Am. Math. Soc. **16,** No. 4, 826–830 (Aug. 1965).

Inequalities for permanents and permanental minors, R. A. Brualdi and M. Newman, Proc. Camb. Phil. Soc. **61,** 741–746 (Jan. 1966).

Normal subgroups of the modular group which are not congruence subgroups, M. Newman, Proc. Am. Math. Soc. **16,** No. 4, 831–832 (Aug. 1965).

On the asymptotic solutions of second-order differential equations having an irregular singularity of rank one, with an application to Whittaker functions, F. W. J. Olver, J. SIAM, Ser. B. **2,** No. 2, 225–243 (1965).

Real two-dimensional representations of the modular group and related groups, J. Lehner and M. Newman, Am. J. Math. **87,** No. 4, 945–954 (Oct. 1965).

The fundamental solution and Huygens' principle for decomposable differential operators, J. E. Lagnese, Archive Rat. Mech. Anal. **19,** No. 4, 299–307 (Jan. 22, 1965).

A stable arc source of high ultraviolet radiance, C. R. Yokley, Proc. Symp. Solar Radiation Simulation, Los Angeles, Calif., Jan. 18–20, 1965, pp. 107–110 (1965).

A latitude survey of the night airglow, T. N. Davis and L. L. Smith, J. Geophys. Res. **70,** No. 5, 1127–1138 (Mar. 1965).

A theoretical study of the Martian and Cynthetian ionospheres, R. B. Norton, Natl. Aeronautic. Space Admin. Tech. Note TN D–2333 (1964).

Coherent Raman effect in the off-axis Raman resonator, D. A. Jennings and H. Takuma, Appl. Phys. Letters 4, No. 11, 185–186 (June 1964).

Comment on the "Difference between a non-LTE, and a pure absorption, model for the line-blanketing effect," R. N. Thomas, Astrophys. J. **141,** No. 1, 333–335 (Jan. 1965).

Flare importance ratings—some hope for improvement, C. S. Warwick, Proc. Natl. Aeronautic. Space Admin. Flare Conf. The Physics of Solar Flares, pp. 27–28 (1964).

Generalized master equation for arbitrary initial states, J. Weinstock, Phys. Rev. **140,** No. 1A, A98–A99 (Oct. 4, 1965).

Generalized variational principles for electromagnetic junctions. Vibrations: application to the theory of waveguide, Proc. Symp. Electromagnetic Theory and Antennas, Copenhagen, Denmark, June 1962, ed. E. C. Jordan, pp. 253–260 (Pergamon Press Inc., New York, N.Y., 1963).

Non-linear ambipolar diffusion across a magnetic field, K. B. Persson and E. R. Mosburg, Phys. Fluids **7,** No. 11, 1829–1833 (Nov. 1964).

Nuclear size determination by neutral-pion photoproduction, R. A. Schrack, Phys. Rev. **140,** No. 4B, B987–B904 (Nov. 22, 1965).

Phonon induced nuclear dipole transitions, R. J. Mahler (Proc. XIIIth Colloque and Relaxation in Solids), Book, Nuclear Magnetic Resonance and Relaxation in Solids, ed. L. V. Gerven, pp. 202–209 (North Holland Publ. Co., Amsterdam, The Netherlands, 1965).

Remarks on a paper by T. Makino "On the cosimic-ray cut-off rigidities and the earth's magnetic Field," H. H. Sauer, Report of Ionosphere and Space Research in Japan **19,** No. 1, 54–55 (1965).

Solute nuclear magnetic resonances in primary lead alloys, L. H. Bennett, R. M. Cotts, and R. J. Snodgrass (Proc. XIIIth Colloque and Relaxation in Solids), Book, Nuclear Magnetic Resonance and Relaxation in Solids, ed. L. V. Gerven, pp. 171–180 (North-Holland Publ. Co., Amsterdam, The Netherlands, 1965).

Spectra of C_2 in solidified gases at 4° and 20 °K, R. L. Barger and H. P. Broida, J. Chem. Phys. **43,** No. 7, 2371–2376 (Oct. 1, 1965).

Spectrum of stationary homogeneous magnetohydrodynamic turbulence, C. M. Tchen, Phys. Fluid **8,** No. 9, 1659–1667 (Sept. 1965).

Suppression at high temperature of effects due to statistics in the second virial coefficient of a real gas, S. Y. Larsen, J. E. Kilpatrick, E. H. Keb, and H. F. Jordan, Phys. Rev. **140,** No. 1A, A129–A130 (Oct. 1965).

The brush cathode plasma—a well behaved plasma, K-B. Persson, J. Appl. Phys. **36,** No. 10, 3086 (Oct. 1965).

The realization and use of the international practical temperature scale of 1948, J. P. Evans, ISA 20th Annual Conference and Exhibit, Los Angeles, Calif., Oct. 4–7, 1965), ISA Preprint 14.3–1–65 (1965).

The relationship of a.-c. resonant probes to resonant scattering, W. M. Leavens, Physics Letters **19,** No. 2, 118–120 (Oct. 1, 1965).

A study of auroral absorption events at the south pole: 2. Conjugate properties, J. K. Hargreaves and H. J. A. Chivers, J. Geophys. Res. **70,** No. 5, 1093–1102 (Mar. 1965).

Characteristic variations in the antarctic ionosphere, V. L. Peterson, G. Stonehocker, and J. W. Wright, Antarctic Research Series, Am. Geophys. Union, Geomagnetism and Aeronomy **4,** 47–75 (1965).

International comparison on dielectric measurements, E. Rushton, G. Russell, B. W. Petley, H. E. Bussey, J. E. Gray, E. C. Bamberger, and D. Morris, IEEE Trans. Instr. Meas. **IM-13,** No. 4, 305–311 (Dec. 1964).

Interrelations of sporadic *E* and ionospheric currents, S. Matsushita, Book, Ionospheric Sporadic-*E*, ed. E. K. Smith and S. Matsushita, ch. II, pt. C, No. 5, 344–375 (Pergamon Press Inc., New York, N.Y., 1962).

Lightning characteristics as derived from sferics, W. L. Taylor, (Proc. 3d Intern. Conf. Atmospheric and Space Electricity, Montreus, Switzerland, May 1963), Book, Problems of Atmospheric and Space Electricity, ed. S. C. Coroniti, pp. 388–404 (Elsevier Publ. Corp., Amsterdam, The Netherlands, 1965).

Long term characteristics for air-ground propagation in band nine, R. S. Kirby, IEEE Antenna Propagation Intern. Symp. Digest, pp. 43–47 (July 9–11, 1963).

On the continuity equation for electron density in the ionosphere, T. Shimazaki, J. Atmospheric Terrest. Phys. **27,** 593–604 (1965).

Studies of Alouette observations at the CRPL, W. Calvert, H. Rishbeth, and T. Van Zandt, Trans. American Geophysical Union, IG Bull. **45,** No. 2, 398–401 (June 1964).

Topside sounding as a tool for global ionosphere studies, R. W. Knecht, IEEE Trans. Ant. Prop. Programs Digest, pp. 21–23 (1963).

**Publications for which a price is indicated are available by purchase from the Superintendent of Documents, U.S. Government Printing Office, Washington, D.C., 20402 (foreign postage, one-fourth additional). Reprints from outside journals and the NBS Journal of Research may often be obtained directly from the authors.*

U.S. GOVERNMENT PRINTING OFFICE : 1966 O—210-682

UNIVERSITY MICROFILMS INC
SERIALS SECTION
313 NORTH FIRST ST
ANN ARBOR MICH

UNITED STATES
GOVERNMENT PRINTING OFFICE
DIVISION OF PUBLIC DOCUMENTS
WASHINGTON, D.C. 20402

OFFICIAL BUSINESS

POSTAGE AND FEES PAID
U.S. GOVERNMENT PRINTING OFFICE

JOURNAL OF RESEARCH of the National Bureau of Standards
A. Physics and Chemistry

Vol. 70A, No. 3 May–June 1966

Contents

Page

Thermal relaxation and Brillouin scattering in liquids. Raymond D. Mountain. 207

Denstity of polyethylene crystals grown from solution. Gordon M. Martin and Elio Passaglia. 221

Mechanical relaxation in polyethylene crystallized with various degrees of lamellar orientation. John M. Crissman and Elio Passaglia. 225

Pentafluorophenyl alkyl and vinyl ethers. Walter J. Pummer and Leo A. Wall. 233

Calibration of germanium resistors at low temperatures (2–20° Kelvin). G. Cataland and H. H. Plumb. 243

Dissociation pressure of aluminum carbide using a rotating Knudsen cell. E. R. Plante and C. H. Schreyer. 253

Determination of intermolecular potential functions from macroscopic measurements. Max Klein. 259

Publications of the National Bureau of Standards. 271

Library of Congress Catalog Card Number: 62–37059

For sale by the Superintendent of Documents, U.S. Government Printing Office, Washington, D.C., 20402. Price $1.00 (single copy)
Subscription price: $5 a year; $1.00 additional for foreign mailing.
UNITED STATES GOVERNMENT PRINTING OFFICE, WASHINGTON : 1966